

ASSESSMENT OF ARCHAEOLOGICAL DEPOSITS AND DEPOSITIONAL HISTORY OF  
SEDIMENT STRATIGRAPHIC UNITS USING GRAIN SIZE ANALYSES, GPR, XRD, AND  
ABSOLUTE DATING: NORTHERN SKIDAWAY ISLAND, GEORGIA

by

ERIN SUSAN SMITH

(Under the Direction of Ervan G. Garrison)

ABSTRACT

Skidaway Island is a Pleistocene-aged barrier island located along the northern coast of Georgia upon which more recent sediments have been deposited throughout the Holocene. Although past studies have analyzed various aspects of Skidaway Island, the study presented here represents the first direct comparison of soils, sediments, geomorphology and archaeological resources from the northern part of the island. Ground penetrating radar and analyses of grain size, mineralogy, and age are performed on sediments collected using a Giddings hydraulic corer. The first chronometric ages for sediments from the northern portion of Skidaway Island are reported and discussed. Using these dates in concert with other analyses reported herein, this thesis provides a geological context for the origin and subsequent development of the island along with a discussion of archaeological resources encountered at the study locations.

INDEX WORDS: Geoarchaeology, Skidaway Island, Barrier Island

ASSESSMENT OF ARCHAEOLOGICAL DEPOSITS AND DEPOSITIONAL HISTORY OF  
SEDIMENT STRATIGRAPHIC UNITS USING GRAIN SIZE ANALYSES, GPR, XRD, AND  
ABSOLUTE DATING: NORTHERN SKIDAWAY ISLAND, GEORGIA

by

ERIN SUSAN SMITH

B.S., College of Charleston, 2006

B.S., College of Charleston, 2006

A Thesis Submitted to the Graduate Faculty of The University of Georgia in Partial Fulfillment  
of the Requirements for the Degree

MASTER OF SCIENCE

ATHENS, GEORGIA

2013

© 2013

Erin Susan Smith

All Rights Reserved

ASSESSMENT OF ARCHAEOLOGICAL DEPOSITS AND DEPOSITIONAL HISTORY OF  
SEDIMENT STRATIGRAPHIC UNITS USING GRAIN SIZE ANALYSES, GPR, XRD, AND  
ABSOLUTE DATING: NORTHERN SKIDAWAY ISLAND, GEORGIA

by

ERIN SUSAN SMITH

Major Professor: Ervan G. Garrison  
Committee: Paul A. Schroeder  
Mark Williams

Electronic Version Approved:

Maureen Grasso  
Dean of the Graduate School  
The University of Georgia  
May 2013

**For Dave**

## ACKNOWLEDGEMENTS

Many thanks to my advisor, Erv Garrison, and committee members Paul Schroeder and Mark Williams for their support throughout this process. Thank you, Sandra Wyld, for critiquing a preliminary written assessment of the research. The expertise and guidance of Bill Miller and David Leigh regarding sediment classification and grain size statistics are much appreciated.

Thank you to the UGA Department of Crop & Soil Sciences for use of their truck-mounted Giddings probe. A million thanks to all of the people on Skidaway Island who provided guidance, support, and company while I was in the field; these include Clark Alexander, Mike Robinson, C.J. Jackson, Bob Allen, Chuck Hartman, and a great many people who helped without even knowing it.

The analyses performed in this study could not have been completed without the aid of numerous experts and helping hands. Thank you to George and Fong Brook for determining the OSL dates for my sediments. Thank you to Shannon Lowman and Katherine Addison for obtaining the AMS dates for my wood samples, and many thanks to Alex Cherkinsky for guiding them through the procedure. I cannot express the depth of my gratitude to the geoarch interns who spent countless hours processing my grain size analyses, among other tasks related to my research; THANK YOU Anna Jolley, Sydney Jokinen, Sarah Manavian, and McKee Gray!!!

Also, thanks to my colleague Sean Cameron, who led me to the SedLog graphing program, which made using Adobe Illustrator much less daunting. Thank you to Jessica Cook Hale for navigating GPR-SLICE for me. Many thanks to my fellow graduate students, who helped me through this process and made me smile along the way.

Funding for this research was provided by Watts Wheeler, Levy, and Berg Awards; thank you to the fund contributors and the committees overseeing fund management for your support.

Finally, special thanks to my parents and Dave Cuddeback; I would not have successfully navigated this process without your physical, mental, and emotional support!

## TABLE OF CONTENTS

ACKNOWLEDGEMENTS.....	v
CHAPTER	
1 INTRODUCTION.....	1
Geological History of Skidaway Island.....	3
Anthropological History of Skidaway Island.....	7
2 METHODS.....	11
Site Selection and Sample Collection.....	11
Macroanalyses.....	15
Mineralogical Analyses: X-ray Diffraction (XRD) .....	15
Grain Size Analyses.....	17
Ground Penetrating Radar (GPR) .....	20
Geochronology.....	23
3 RESULTS.....	25
Cores collected on UGA’s Marine Extension Campus (UGA Cores) .....	25
Cores collected near the Bluff (B Cores) .....	41
Cores collected near the Grove’s Creek site (GCF Cores) .....	53
GPR .....	69
Geochronology.....	75

4	DISCUSSION.....	77
	Geological Interpretations.....	77
	Archaeological Interpretations.....	88
	Methodological Implications.....	101
5	CONCLUSIONS.....	106
	Summary of Findings.....	106
	Recommendations for Future Research.....	108
	REFERENCES.....	111
	APPENDIX A.....	119
	APPENDIX B.....	133

## **CHAPTER 1 INTRODUCTION**

Skidaway Island is a Pleistocene barrier island located on the coast of Georgia that includes a sequence of older to younger strata deposited throughout the late Pleistocene and the Holocene during periods of sea level fluctuation (Fig. 1.1). Archaeological surveys have discovered many archaeological sites on Skidaway Island, although few comprehensive excavations have been conducted there (Pluckhahn, 1995a; Elliott and Holland, 2006), with the exception of the site of Grove's Creek (9CH71) (Keene, 2002; Keene, 2004; Garrison, 2007). Previous studies conducted on Skidaway Island have focused on archaeological resources, delineating the Late Holocene paleoshoreface, soil pedogenesis, and soil mapping (e.g., Pluckhahn, 1995c; Vanags, 2000; Keene, 2002; Keene, 2004; Garrison, 2007; White et al., 2010; Keene and Garrison, 2013).

Although Skidaway has long been identified as a Pleistocene-aged barrier island upon which sediments have continued to be deposited throughout the Holocene (Huddleston, 1988; Weems and Edwards, 2001), no study has undertaken an integrated analysis of the island's deposition with regard to human history. Thus, the study presented here will be the first to undertake a direct comparison of soils, sediments, geomorphology, and archaeological resources from different portions of the island. To facilitate detailed analysis, this project focused on three previously unstudied areas located on northern Skidaway Island; two of these areas are located on the eastern side of the island, and one site is located on the western side of the island. Ground

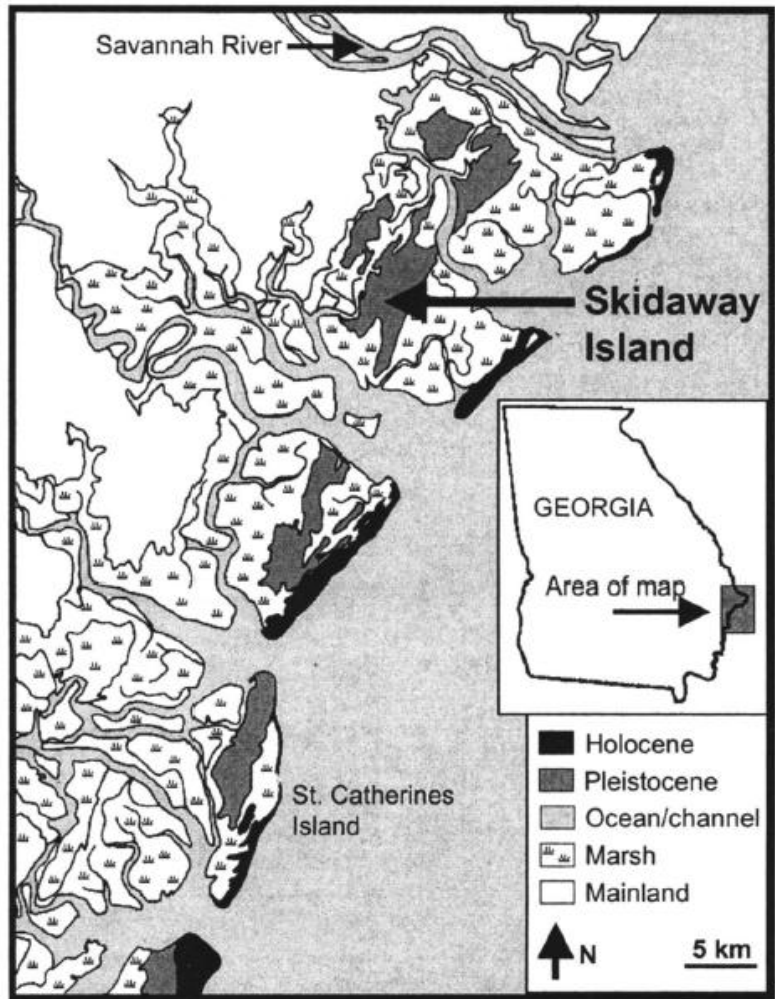


**Fig. 1.1** The location of the Pleistocene sediments that form the core of Skidaway Island. The modern barrier island composed of Holocene sediments located east of Skidaway Island is Wassaw Island (from Booth et al., 2003).

penetrating radar (GPR), grain size, mineralogical, and dating analyses were undertaken: (1) to determine if there is an age difference between the sediments on either side of the island; (2) to characterize differences and similarities between these deposits and the environments that formed them; and (3) to evaluate potential archaeological resources located at each study location.

The evaluation of the depositional history of the sediments that form Skidaway Island could be useful for future archaeological studies. An understanding of the island's architecture and where sediments of different ages can be expected to be located on the island will contribute to the development of a predictive model that can be applied to locating additional subsurface archaeological resources on this barrier island and other Georgia barrier islands (Vento and Stahlman, 2011). Indeed, over the course of this study, such a finding was realized.

### **Geological History of Skidaway Island**

Skidaway Island is located on the northern coast of Georgia in the Coastal Plain physiographic province (Fig. 1.1). The eastern Coastal Plain region of Georgia is composed of a succession of at least seven marine terraces formed by fluctuating sea level throughout the Late Pliocene to present (Figs. 1.2, 1.3) (Hoyt and Hails, 1974; Huddleston, 1988). These terraces originally formed as coastal sand dunes that were large enough to withstand submergence as sea level rose. With slow sea level rise, over time the area behind the sand dunes become submerged and eventually formed a marsh directly behind the subaerially exposed sandy sediments (Hoyt, 1967; Hoyt, 1968; NPS, 2005). As sea level rose further, the sand dunes were pushed back on top of the marsh sediments, which then served as a barrier platform that stabilized the sandy former dune sediments and supported barrier island formation (Oertel, 1985). Repetition of these

processes as sea level fluctuated over time led to the development of Georgia's Coastal Plain terraces, which become progressively younger closer to the modern coastline (Fig. 1.2).

The youngest, eastern-most terrace contains Georgia's current barrier islands, which were deposited during the Holocene. West of the current barrier islands are a series of Pleistocene-aged relict barrier islands that form what is commonly known as the Silver Bluff terrace (Figs. 1.1, 1.3). Together, these two sets of islands form the Holocene-Silver Bluff marine terrace complex that make up Georgia's welded barrier islands south of the Savannah River (Oertel, 1975; Huddleston, 1988). Near the Savannah River, however, high sediment supply from the river has facilitated deposition of Holocene sediments to form younger individual islands seaward of the relict Pleistocene islands (Fig. 1.1) (Oertel, 1975). In this area, the relict barrier islands (located well behind the modern coastline) are welded from ridges of sediment commonly identified as the Pleistocene-aged Silver Bluff terrace and older Pleistocene-aged Princess Anne terrace (Fig. 1.3) (Hoyt and Hails, 1974).

Thus, while eastern Skidaway Island is primarily composed of sediments associated with the Late Pleistocene Silver Bluff terrace, the western part of the island is composed of sediments associated with the Late Pleistocene Princess Anne terrace (Fig. 1.3) (Hoyt and Hails, 1974; Booth et al., 2003). The aforementioned terraces are built upon the Satilla Formation, which consists of fossil-poor sand, silt, and clay deposits of varying colors and is assumed to have been deposited simultaneously with terrace formation during the Pleistocene (Huddleston, 1988; Markewich et al., 1992; Weems and Edwards, 2001; Garrison et al., 2008). These sediments created the core of Skidaway Island and formed Georgia's oceanfront coastline until sea level began to regress well before the Last Glacial Maximum (LGM) (Hoyt and Henry, 1967; Schoettle, 2001; Garrison et al., 2008).

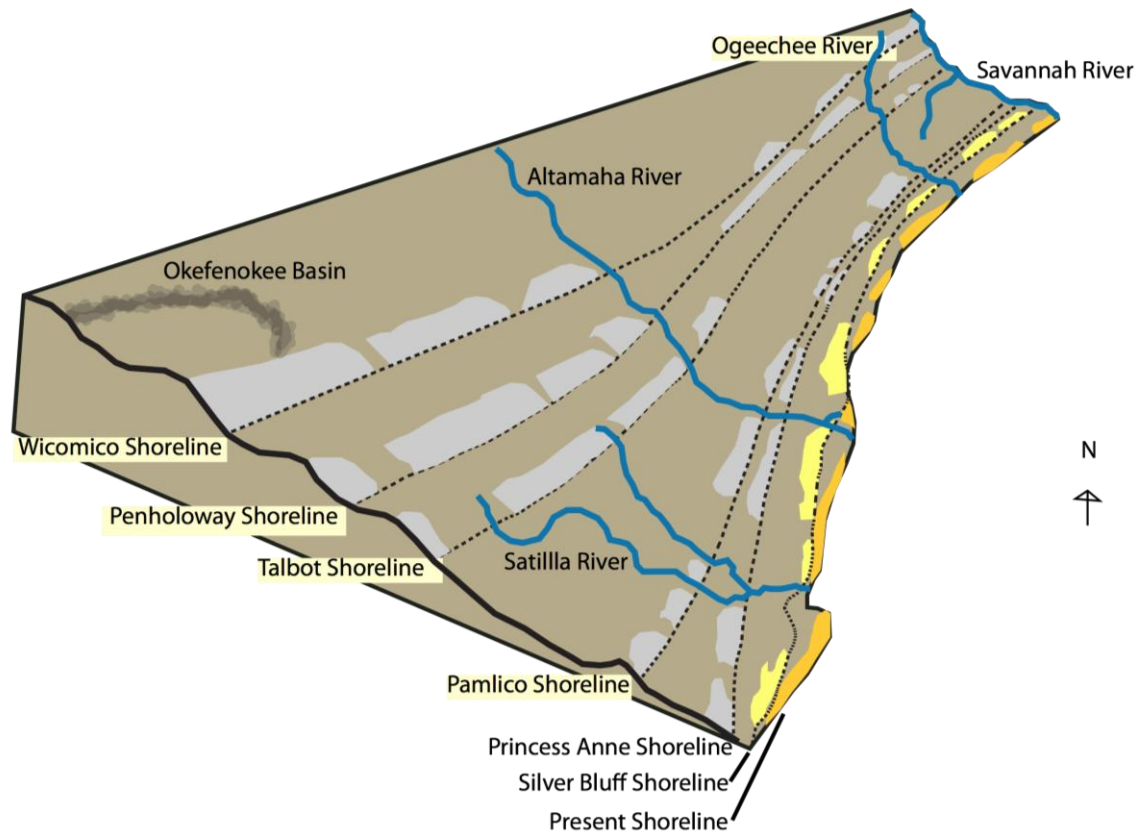


**Fig. 1.2** The shorelines associated with each of Georgia's coastal marine terraces. Gray indicates ancient shorelines. Although not explicitly designated as such in this diagram, western Skidaway Island is part of the Princess Anne shoreline. The Silver Bluff shoreline, of which eastern Skidaway Island is a part, is light yellow. The present shoreline is highlighted in dark yellow and is located directly east of the Silver Bluff shoreline (modified from Booth et al., 1999 [from Rich and Pirkle (1994) as modified from the Georgia Department of Natural Resources, 1976]).

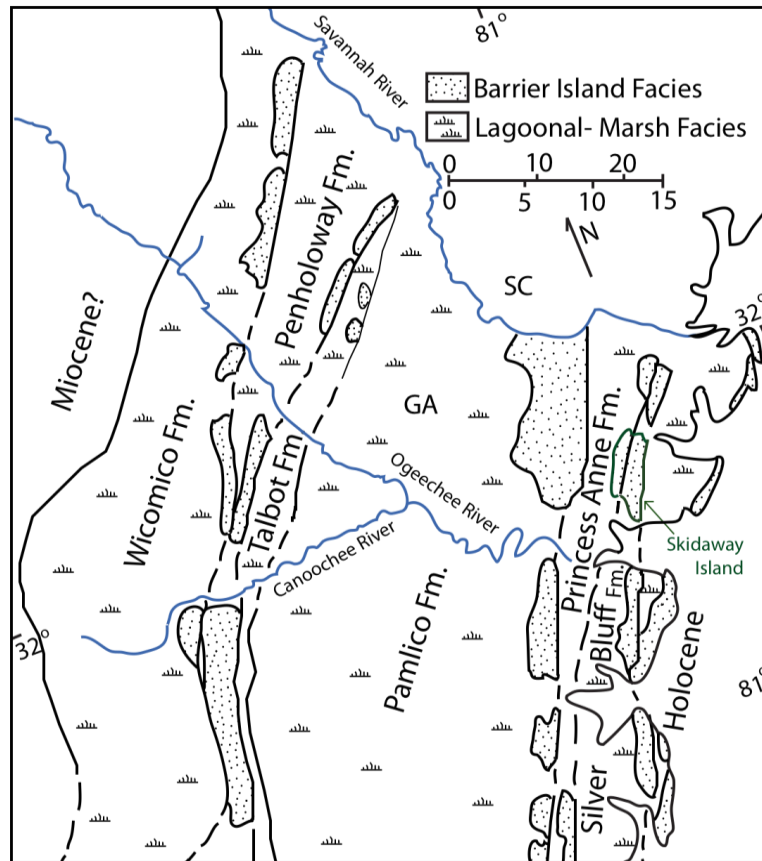


**Fig. 1.3** The terraces that form the core of Skidaway Island relative to other Coastal Plain terraces (modified from Hoyt and Hails, 1974).

During the LGM, the sediments of Skidaway Island stabilized and pedogenesis and erosion began (Vanags, 2000). Around 4,500 BP, Holocene sea level transgression caused reoccupation of older terraces and marshes, which resulted in addition of Holocene-aged sediments to the Pleistocene-aged barrier substrate (DePratter and Howard, 1977; Oertel, 1979; Huddleston, 1988). Thus, Skidaway Island represents a Pleistocene barrier island upon which Holocene-aged sediments have been and are currently being added.

Deposition during the Holocene also formed Wassaw Island, an active barrier island, on the seaward side of Skidaway Island (Fig. 1.1) (Schoettle, 2001). Coastal progradation from ~1700 BP to ~500 BP (Alexander et al., 2011), influenced by sediment input from the nearby Savannah River (Oertel, 1975), led to formation of ~7 km of marsh between Wassaw Island and Skidaway Island. OSL dates obtained from sediments ~1 meter below the surface (mbs) in the marsh date from  $1,556 \pm 220$  BP nearer Skidaway Island to  $528 \pm 50$  BP just inland of Wassaw Island (Turck and Alexander, 2013), with sediments becoming progressively younger seaward. Following this trend, OSL dates obtained from ~1 mbs on Wassaw Island date to  $389 \pm 60$  BP or younger (Turck and Alexander, 2013), which suggests that the modern shoreline stabilized around 500 BP (Alexander et al., 2011).

### **Anthropological History of Skidaway Island**

Archaeological surveys have located over 100 sites on Skidaway Island dating from the Late Archaic St. Simon phase (4500-3100 BP) into the Mississippian Irene phase (700-450 BP), but detailed excavations have been limited (DePratter, 1978; Pluckhahn, 1995c; Kelly, 2003; Elliott and Holland, 2006). Shell middens dated to 4300 BP correspond to the earliest known occupations of Skidaway Island and represent a phase, lasting until about 3000 BP, wherein shellfish seem to have comprised an important part of the local diet (DePratter, 1977; Elliott and Holland, 2006).

This earliest phase of occupation was followed by the Woodland period, which lasted from 3100 BP to 1000 BP (Pluckhahn, 1995c) and includes the Refuge, Deptford, and Wilmington phases (Caldwell and Waring, 1939; Pluckhahn, 1995b). Fewer sites are known from the Early and Middle Woodland Refuge and Deptford phases, although the population of

Skidaway Island appears to have increased by the Late Woodland Wilmington phase (DePratter, 1975) and Early Mississippian St. Catherine's phase (Pluckhahn, 1995c). This increase in the number of (known) sites appears to have been accompanied by expansion of the population from the eastern shoreline to the island interior; DePratter (1978) suggests this movement was associated with the early development of horticulture on the island.

Relative to the Late Woodland and Early Mississippian periods, fewer sites are known on Skidaway Island that date to the Middle Mississippian period (DePratter, 1975; Pluckhahn, 1995c). The Mississippian culture period began around 1000 BP and lasted until the historic period (shortly after 500 BP (1500 CE)), and includes the St. Catherine's, Savannah, and Irene phases (Pluckhahn, 1995b; Elliott and Holland, 2006). Abundant archaeological evidence of occupations on Skidaway Island exists for the Late Mississippian Irene phase (Pluckhahn, 1995c). One relatively well-researched Mississippian site dating to the Irene phase is the Grove's Creek site (9CH71). At the Grove's Creek site, multiple excavations have revealed one of only five known structure-containing sites dated to the Irene phase on the Georgia coast (Keene, 2002; Keene, 2004; Garrison, 2007; Keene and Garrison, 2013).

No Native American sites dating to the early historic period (ca. 500 BP (1500 CE)) have been located thus far on Skidaway Island (Elliott and Holland, 2006). In 1734 (CE), settlement of Skidaway Island by members of the Georgia colony began with the establishment of a defensive outpost, whose exact location remains unknown, on the northern end of the island (McGowan and DePratter, 1980). Occupation of this outpost was accompanied by eventual establishment of a village and several farms on the island. However, by 1740 difficult living conditions caused settlers to completely abandon the island, which remained uninhabited until the 1750s (Historic Services, Inc., 1971 as cited in Weinland, 1981; Pluckhahn, 1995c).

During the 1750s through the 1760s, the distribution of crown grants instigated reoccupation of the island (Historic Services, Inc., 1971 as cited in Weinland, 1981). Large land tracts that include the area of interest for this study were given to two individuals: John Milledge and James Deveaux (Pluckhahn, 1995c; Kelly, 2003). By the late 1700s, and into the 1840s, the Milledge plantation on Skidaway produced cotton, corn, oranges, cattle, sheep, hogs, horses, and even grew mulberry trees in hopes of producing silk (McGowan, 1983; Pluckhahn, 1995b; Kelly, 2003). It remains unknown whether Deveaux developed his Skidaway property (Pluckhahn, 1995c). Few archeological materials remain from this time, although plantation agriculture (i.e., plowing) may have impacted soil development in the study area (Pluckhahn, 1995b).

Throughout the 19th century, numerous properties on Skidaway Island were foreclosed upon, suggesting limited and/or unsuccessful productivity (Pluckhahn, 1995c; Kelly, 2003). After the Civil War, a colony for freed slaves was briefly established on Skidaway Island, and the population remained predominantly African American until the early 20th century. Small farms characterized the land use during this time (Sherrill, 1987 as cited in Pluckhahn, 1995c).

Towards the end of the century, in 1896, the island was visited by a party of explorers led by C. B. Moore. Moore and his crew, aboard his steamship *Gopher*, traveled the coastal waterways seeking and excavating archaeological sites, especially mound sites. On Skidaway Island, Moore and his crew excavated three mounds (Moore, 1897); this work represents the first semi-professional archaeological study conducted on the island.

By the early 20th century, nonresident landowners owned most of Skidaway Island. One exception was John Milledge's former property, where the Roebling family operated a cattle farm from the 1930s until 1954 (McGowan, 1983; Pluckhahn, 1995c; Kelly, 2003). Structures and pastures established by the Roeblings still remain on the property today.

In 1967, the University System was granted control of 700 acres including the Roebing land, which is now used primarily for research (McGowan, 1983). Multiple structures associated with the Skidaway Institute for Oceanography (SkIO) (now owned by the University of Georgia) are located on the northern portion of the island. The remainder of Skidaway Island currently includes gated residential communities, Skidaway Island State Park, and a village center consisting of various businesses. Archaeological surveys prior to the development of these late 20th century communities identified numerous archaeological sites across the island (e.g., DePratter, 1974; DePratter, 1975; DePratter, 1978; Weinland, 1981; Johnson, 1990; Pluckhahn, 1995a,b,c; Elliott and Holland, 2006).

## **CHAPTER 2 METHODS**

### **Site Selection and Sample Collection**

Sediment coring has a long history in the study of pedology and sedimentology (Lewis and McConchie, 1994). Due to its proven value in obtaining sediments and soils for characterization, sediment coring was chosen for use in this study. Using a truck-mounted Giddings hydraulic soil coring system, eight sediment cores were collected across three sites located on northern Skidaway Island (Fig. 2.1, 2.2; Table 2.1). Sample locations were chosen that met two criteria. First, the location must contain a cleared 50 to 100 m long transect accessible by the Giddings truck. The 50 to 100 m cleared transects were sought so that sediment cores could be collected at 50 m intervals, and GPR transects could later be collected directly along these lines. Second, locations must be located near areas of interest and provide a representative sampling of different locations on northern Skidaway Island. Areas of interest included: the relatively well-studied archaeological Grove's Creek site (9CH71) located on the eastern side of the island; a field that contains archaeological site 9CH127 and is located adjacent to a bluff, also on the eastern side of the island, where erosion exposes strata, and; locations as close as possible to the Skidaway River on the western-most side of the island. Therefore, three cores (GCF 0m, GCF 50m, and GCF 100m) were collected every 50 m along a 100 m transect in a field located near the Grove's Creek site (Fig. 2.2). Due to time constraints, only two cores (B 0m and B 100m) were collected from each end of a 100 m transect in a field adjacent to the

bluff (Fig. 2.2). Finally, one core (UGA P) was collected as close as possible to the Skidaway River, and two cores (UGA 0m and UGA 50m) were collected from an open field near the location of core UGA P (Fig. 2.2). The UGA 0m and UGA 50m cores could not be collected directly along a transect with the UGA P core because the surrounding area was occupied by a basketball court and underground utility lines associated with the University of Georgia's Marine Extension Campus and Aquarium.



**Fig. 2.1** The truck-mounted Giddings hydraulic soil coring system used to collect sediment cores.



**Fig. 2.2** Location of core sample sites, all of which are located on SkIO property on northwestern Skidaway Island (Modified from Google Earth, 2013).

**Table 2.1** Core Location Information

<b>Core Name</b>	<b>Latitude Longitude</b>	<b>Accuracy of Coordinates</b>	<b>Brief Description of Location</b>
<b>UGA P</b>	N 31.98840 W 081.02548	~ 4 cm	Closest to northwestern edge of island; On UGA Marine Extension Campus
<b>UGA 0m</b>	N 31.98713 W 081.02560	3.5 m	On northwestern side of island; Inland from core UGA P; On UGA Marine Extension Campus
<b>UGA 50m</b>	N 31.98689 W 081.02498	~ 6 m	On northwestern side of island; 50 m inland from core UGA 0m; On UGA Marine Extension Campus
<b>B 0m</b>	N 31.97394 W 081.02534	~ 5 m	Closest to northeastern edge of island; On bluff adjacent to Grove's Creek
<b>B 100m</b>	N 31.97471 W 081.02592	~ 4 cm	On northeastern side of island; 100 m inland from core B 0m
<b>GCF 0m</b>	N 31.96854 W 081.03053	~ 5.8 m	Near northeastern edge of island; Adjacent to Grove's Creek site
<b>GCF 50m</b>	N 31.96874 W 081.03091	~ 8 m	On northeastern side of island; 50 m inland from core GCF 0m
<b>GCF 100m</b>	N 31.96910 W 081.03139	~ 6 m	On northeastern side of island; 100 m inland from core GCF 50m

At these sites, soil cores were collected to depths of roughly 2 to 4 m. In an attempt to reach the maximum depth possible, each core was collected until a depth was reached at which the core collection became compromised or refusal was met. "Refusal" is the term describing no or little-to-no penetration by the corer. The most common reasons core collection was stopped were: subsurface clay layers threatening to permanently suction the Giddings apparatus into the ground; resistant subsurface layers causing tilting of the Giddings mast head, and; the water table causing slumpage into the core such that successive cores were contaminated. Contamination occurred because the Giddings hydraulic coring system requires a repetitive process of collecting a length of core, raising the apparatus, extruding the core, and then sending the apparatus back

down the open hole to collect the next section of core. Thus, slump deposits from up-hole, especially after the water table was reached, could cause core contamination.

### **Macroanalyses**

Preliminary macroanalyses of the sediments required no sample preparation or treatment. Each sample's moist color was determined using a Munsell Color book (Munsell Color, 1994). Qualitative differences between sample color, grain size, and composition that could be observed in hand samples using the unaided eye were noted. A magnet was passed over the untreated sample to check for the presence of magnetite. Core sediments were then subsampled to undergo further analyses, including x-ray diffraction (XRD), grain size analyses, and grain size statistics.

### **Mineralogical Analyses: X-ray Diffraction (XRD)**

To survey the mineralogic content of the cores, representative bulk samples were analyzed using XRD. The number of bulk samples analyzed from each core varied from four to eight samples, depending upon total core depth and apparent variation of strata within the core (i.e., variation in color or grain size). To prepare the samples for XRD analyses, 2 g of each sample were agitated for 10 minutes in a McCrone Micronizing Mill filled with corundum or agate pellets and half full of deionized water. During the first round of XRD analyses, samples were prepared using corundum pellets; however, after observation of corundum artifacts in all "first round" diffractograms (Fig. A.1), all later samples were prepared using agate pellets. After agitation, the slurry containing the pulverized sample was poured into a watch glass and dried in an oven set at 100°C.

For comparison with the bulk samples, the clay fraction of selected samples from each core was analyzed using XRD. The clay fraction was obtained during grain size analysis (via the pipette method) by pipetting some of the clay fraction in suspension from a graduated cylinder onto a petrographic slide (Moore and Reynolds, 1997). The suspension was then allowed to dry at room temperature, leaving behind the clay particles on the slide.

Prior to being analyzed in the diffractometer, the powdered bulk samples for each horizon were pressed into XRD mounts for 1 minute at a pressure of 400 psi using a Wabash hydraulic press. Clay fraction petrographic slides fit directly into the XRD machine mount after trimming the slides' corners. A Bruker D8 Advance diffractometer using Co K $\alpha$  radiation ( $\lambda = 1.7902 \text{ \AA}$ ) at 1.8 kW was used to collect data. Data were collected from 2 to 70  $2\theta$  at a step increment of 0.02 degrees and scan speed of 10 degrees per minute. XRD data were collected and saved using DIFFRAC<sup>plus</sup> XRD Commander software by Bruker AXS.

To test for the presence of mixed-layered clays containing smectite in the clay slide samples, these samples were placed in a bell jar containing ethylene glycol overnight and then re-run in the diffractometer. If smectite is present, mixed layered clay peaks should shift to a noticeably lower angle ( $2\theta$ ) (Moore and Reynolds, 1997). Data were collected using the same parameters as the previous scans, except that data were only collected from 2 to 10  $2\theta$ , since the peak shift attributable to ethylene glycol-solvated smectite occurs in this region. Finally, the resulting diffractograms were compared to the original diffractograms collected for each sample.

Prior to interpretation, raw diffractograms were processed using the DIFFRAC<sup>plus</sup> EVA software by Bruker AXS. K $\alpha$ 2 peaks were stripped, background noise was corrected, and threshold sensitivity was adjusted prior to performing a peak search to identify the major peaks

in the diffractogram. Any significant peaks missed by the automated peak search were manually selected and added to the diffractogram record. Finally, potential mineral matches for each peak were identified using the search/match tool in the EVA software. Suspected minerals not found by the automated search were checked by conducting manual EVA searches for individual minerals.  $2\theta$ , d-spacing, and peak intensity were used to identify the most likely mineral(s) responsible for each peak. The  $2\theta$  and d-spacing of suspected mineral matches were compared to known index values, and thereby verified or disqualified as a match, using Powder Diffraction Database Search software provided by the International Centre for Diffraction Data (ICDD).

### **Grain Size Analyses**

After cores were collected, samples were collected every 25 cm along the core to undergo grain size analyses. Also, samples were collected from cores on either side of soil horizon contacts, which were preliminarily identified by a change in sediment color and/or texture. Finally, additional samples were collected from areas of interest in the cores (e.g., locations of heavy mineral accumulation, humate accumulation, or texture change). For grain size analyses, these samples were processed in two groups: sand-dominated samples and clay-rich samples.

Sand-dominated samples were dried in an oven set at 100°C. Next, 15 g of sample were isolated for grain size analyses following the procedure described by Folk (1974). Sediments were dry sieved through 500, 250, 125, and 63 micron screens for 30 minutes using a Gilson Sieve Shaker. Each grain size fraction was weighed, and the resultant weights were used to calculate the percent coarse, medium, fine, and very fine sand along with the percent silt and clay in the sample. Since sand-dominated samples typically contained very little silt and clay, and

because dry sieving could not separate silt-sized particles from clay-sized particles, the total percent silt plus clay was calculated for sand-dominated samples.

For samples that were too clay-rich to undergo dry sediment sieving, samples were air-dried overnight. Following the procedure described by Folk (1974), 10 g of sample was isolated for pipette analysis. The sand fraction was collected using a 75  $\mu\text{m}$  screen, which may introduce a small margin of error since some very fine sand will pass through the screen. The sand fraction was dried in an oven set at 100°C and weighed, whereas the remaining silt and clay were separated using Folk's (1974) pipette analysis method. This method requires mixing the silt and clay fractions in a graduated cylinder, allowing these fractions to settle in the water for a given amount of time, and using Stoke's Law to calculate the settling depth of the clay particles. Using a pipette, a subsample of the clay fraction suspended in water is removed, dried in an oven at 100°C, and weighed. Along with the weight of the dried sand fraction, the weight of the clay fraction is used to calculate the percent clay, silt, and sand in the sample.

### *Grain Size Statistics*

All grain size statistics were obtained using Dr. Simon J. Blott's GRADISTAT program, version 8.0 (November 2010) which can be downloaded without charge from <http://www.kpal.co.uk/gradistat.html>. The user enters the screen aperture size and the weight percent sediment in each screen (obtained during grain size analysis), and GRADISTAT provides both quantitative and qualitative data regarding grain size statistics. GRADISTAT uses the method of moments "to calculate statistics arithmetically [...], geometrically [...], and logarithmically" and then uses values "extracted from the cumulative percentage curve [...] to calculate Folk and Ward parameters logarithmically [...] and geometrically" (Blott and Pye,

2001, p.1242). Output includes calculations of mean, mode, sorting (standard deviation), skewness, kurtosis, and numerous percentile values for an input dataset. These values are then used by GRADISTAT to qualitatively classify sediments' textural class (e.g., muddy sand) and degree of sorting, skewness, and kurtosis following the categorizations of Folk (1954) and Folk and Ward (1957), respectively (Blott and Pye, 2001).

In this study, GRADISTAT was used to obtain grain size statistics for both the dry sieved and wet processed (pipette analyzed) grain size data. For dry sieved data, weight percents for only the sand size fractions were entered into GRADISTAT because including bulk pan fractions (silt + clay) introduces error into the grain size statistics for this program. However, for nearly all dry sieved sediments, the omission of silt and clay should not significantly affect grain size statistics, since most dry sieved samples contained < 5% silt and clay (Blott and Pye, 2001). The grain size statistics for the few dry sieved samples that contained > 5% silt and clay likely contain significant error; thus, these samples are noted uniquely in the Results section.

For wet processed (pipette analyzed) grain size data, weight percents for all size fractions were entered into GRADISTAT because wet processing facilitated differentiation of silt versus clay weight percents. Since GRADISTAT requires the aperture size of the screens to be entered, but wet processing does not separate the silt from the clay fraction using screens, a value of 3.9  $\mu\text{m}$  (the lowest size fraction limit for silt) was entered for the silt "screen" and a value of 0.01  $\mu\text{m}$  (a value approaching 0  $\mu\text{m}$ ) was entered for the clay "screen." These approximations may introduce error into the grain size statistic calculations, and thus samples analyzed via wet processing are noted uniquely in the Results section.

After the user enters the screen aperture size and the weight percent sediment in each screen, GRADISTAT provides a plethora of grain size statistical data, as aforementioned. In this

study, only the Folk and Ward geometric results are presented for two reasons beyond the need to limit study focus to a single statistical dataset. First, Folk and Ward grain size statistical measures have been found to provide more reliable results (Blott and Pye, 2001; Wachecka-Kotkowska and Kotkowski, 2011). Finally, the Folk and Ward geometric ( $\mu\text{m}$ ) results rather than the Folk and Ward logarithmic ( $\phi$ ) results were selected to maintain metric unit consistency.

### **Ground Penetrating Radar (GPR)**

Ground Penetrating Radar (GPR) transects were collected *directly along* the 50 m to 100 m lines where sediment cores were collected. Since no cores were obtained in direct alignment with core UGA P, a transect was collected starting at core UGA P and running 50 m southeast towards the island interior (Fig. 2.3). In all transects, high quality subsurface imaging was expected due to low attenuation of GPR signal when moving through sand, especially in contrast to the higher attenuation that will occur within more clay-rich materials (Vanags, 2000; Bristow and Jol, 2003; Leckebusch, 2003; Vance et al., 2011). A GSSI SIR-2 100 MHz antenna was used to facilitate deep ( $> 5$  m) penetration into the sandy subsurface. The range was 500 ns and gains were set manually. Lines were manually marked every 10 m.



**Fig. 2.3** Location of GPR transects relative to core sample locations, all of which are located on SkIO property on northwestern Skidaway Island (Modified from Google Earth, 2013).

All transects were post-processed in RADAN® version 6.5. First, new start markers were inserted at the true start of each transect to cut off stationary data collected at the start of each transect when the antenna was collecting data but not yet moving along the transect. These stationary data were deleted and the distance normalization tool was used to equally distribute the remaining data between each horizontal marker (GSSI, 2005). A finite impulse response (FIR) filter was then applied to samples lower in each radargram (approximately samples 300 to 450) to remove horizontal banding produced as an artifact by the antenna. Deconvolution facilitated removal of ringing or multiple reflections caused by "the radar signal bounc[ing] back and forth between" the antenna and something in the subsurface (e.g., a clay layer) (GSSI, 2005, p.63). A 2D spatial filter (frequency-wave number or F-K filter) removed excess noise from each radargram. Migration compressed hyperbola in the data and allowed approximation of radar velocity. To make up for the amplitude reduction caused by use of the aforementioned filters, automatic gain control (AGC) was used to amplify the signal for the final radargram. Finally, a second FIR filter was applied to smooth background noise created by application of the aforementioned filters and amplified by the AGC.

RADAN® radargrams were then converted to bitmap format and imported into Adobe Photoshop, where vertical and horizontal markers were added to the final images. This step was necessary because RADAN® attaches no vertical markers to files exported from the program; also, although RADAN® includes tiny horizontal markers when exporting a file, these horizontal markers are not readily visible. Vertical markers were then labeled with depth (m) and time (ns).

In contrast, processing of raw GPR data in GPR-SLICE© facilitated the production of radargrams labeled with both depth and time on the y-axis. Using GPR-SLICE©'s auto-detect tool, the dielectric constant, wave velocity, and total penetration depth were determined. This

tool assumed a constant wave velocity, which does not accurately represent the changing wave velocities associated with the different dielectric constants of subsurface materials (e.g., for sand versus clay). Thus, some error in depth calculations is introduced by use of the auto-detect tool; however, this method produced the most reliable assessments of wave velocity and depth available in this study.

## **Geochronology**

### ***Optically Stimulated Luminescence (OSL) Dating***

Using the Giddings hydraulic soil coring system, two additional sediment cores were collected for use in optically stimulated luminescence (OSL) dating. One core was collected from each side of the island: one core beside the GCF 50m core location and one core beside the UGA P core location (Fig. 2.2). By sampling these two locations, dates could be obtained for each side of the island. To allow use of the OSL dating method, these cores had to be shielded from light during collection. At approximate depths of 1-1.5 m and 2-2.5 m in each core, samples were collected in absolute darkness and stored in cardboard mailing tubes wrapped in duct tape until the sediments could be processed and dated. OSL dating of the four samples was performed by the University of Georgia Department of Geography's Luminescence Dating Laboratory.

### ***Accelerator Mass Spectrometry (AMS) Radiocarbon Dating***

Several wood fragments were recovered from depths below 300 cm in core UGA P (Fig. 2.4), the sediment core that was collected nearest the western side of Skidaway Island. Two pieces of wood were subsampled to undergo accelerator mass spectrometry (AMS) radiocarbon dating. Samples were pretreated and AMS radiocarbon dating was performed at the University of

Georgia's Center for Applied Isotope Studies (CAIS). Dates were obtained using a National Electrostatics Corporation Model 1.5SDH-1 Pelletron Accelerator Mass Spectrometer.



**Fig. 2.4** Wood recovered from ~ 315 cm depth in core UGA P.

## CHAPTER 3 RESULTS

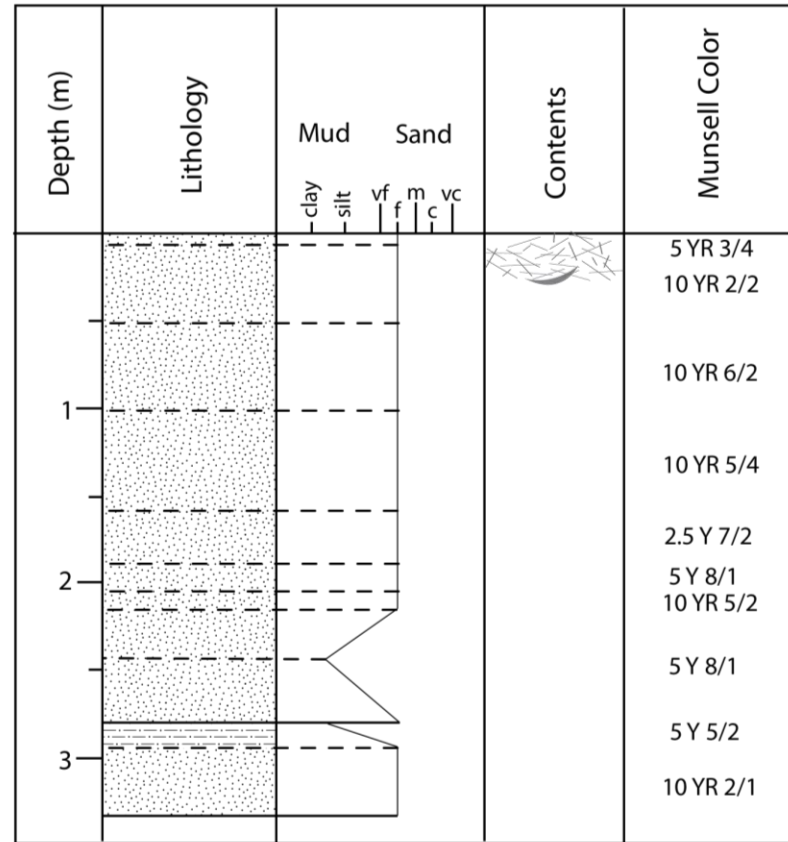
The first portion of this section provides a location-by-location overview of core collection results, the general mineralogic content of the cores as determined by XRD, the results of grain size analyses for each core, and an overview of the grain size statistics. Diffractograms are included in Appendix A, while all grain size composition by weight percent data and all Folk and Ward geometric statistical data are available in Appendix B. Next, in this section, the GPR results are presented for each transect. Finally, the dates obtained using OSL and AMS-RC analyses are reported.

### **Cores collected on UGA's Marine Extension Campus (UGA Cores)**

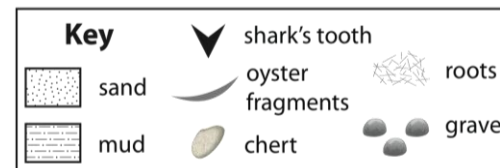
For the three UGA cores, total core depth varied from 307 cm to 423 cm (Table 3.1). The number of sub-cores collected (i.e., the number of times the Giddings probe had to be sent down the hole) to make up each core varied from four to eight (Table 3.1). Core photographs taken in the field and diagrams representing core attributes are shown in Figs. 3.1, 3.2, and 3.3.

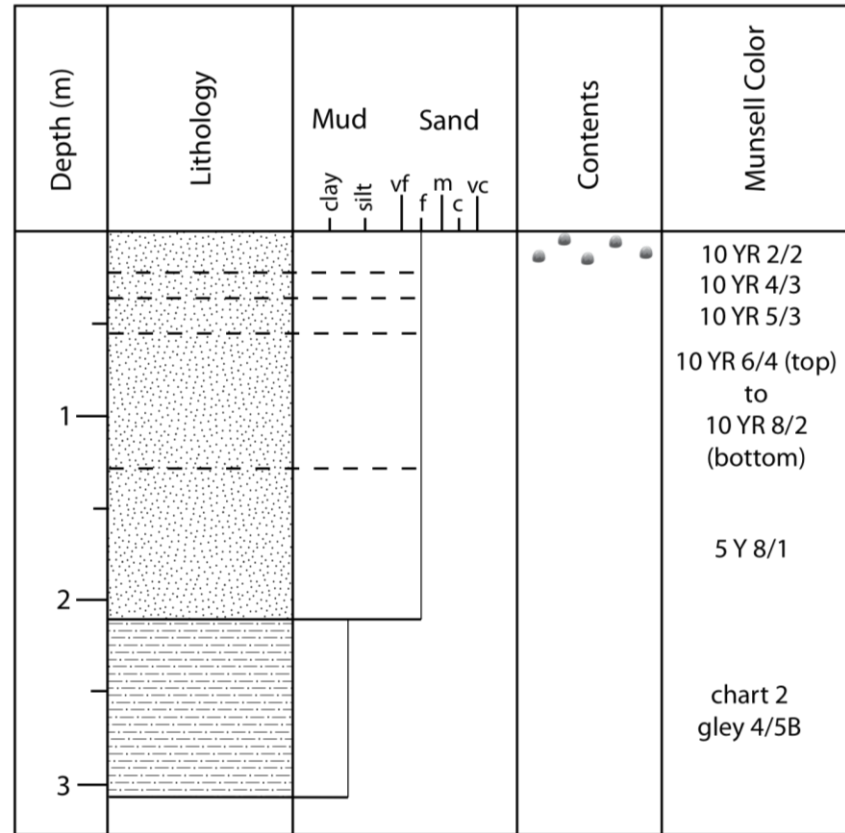
**Table 3.1** Overview of UGA Cores

<b>Core Name</b>	<b>Number of sub-cores</b>	<b>Total core depth</b>
<b>UGA P</b>	7	334 cm
<b>UGA 0m</b>	4	307 cm
<b>UGA 50m</b>	8	423 cm

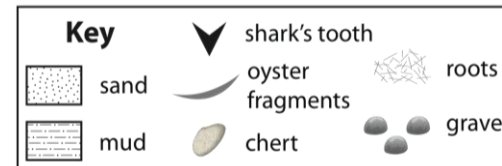


**Fig. 3.1** All UGA P cores stored in boxes after collection. Note the wood in the last core located roughly midway down the column. Scale: Each column is 62 cm long. Core lithology, contents, and Munsell colors are represented in the diagram.





**Fig. 3.2** All UGA 0m cores stored in boxes after collection. Scale: Each column is 62 cm long. Core lithology, contents, and Munsell colors are represented in the diagram. The gravel located at the top of the core is a result of human action rather than natural depositional processes.



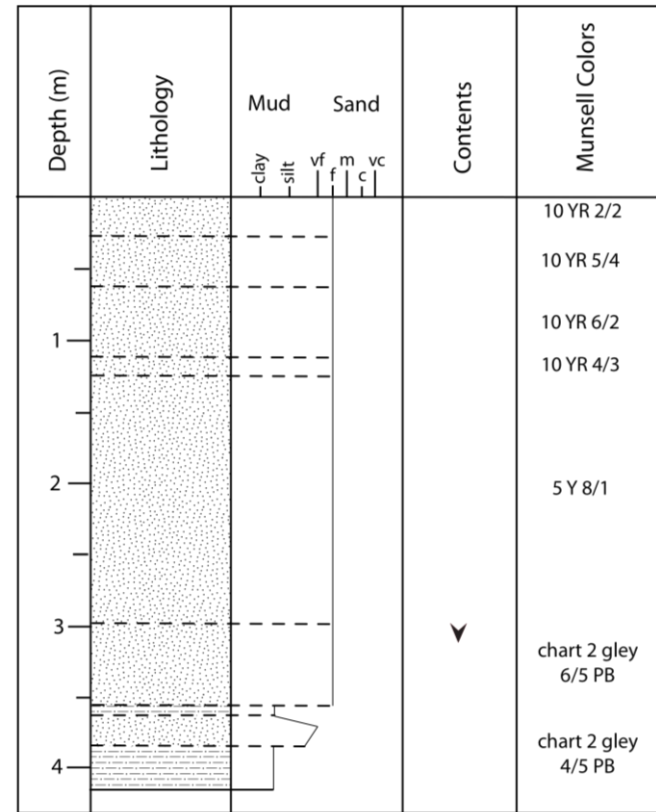
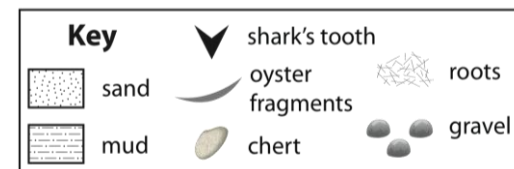


**Fig. 3.3** All UGA 50m cores stored in boxes after collection. Scale: Each column is 62 cm long. Core lithology, contents, and Munsell colors are represented in the diagram.



### ***UGA Cores: X-ray Diffraction***

In all bulk XRD samples, quartz and feldspar are the primary components (Table 3.2). Quartz and microcline are present in all samples, while albite is present in all samples from cores UGA P and UGA 50m. Samples UGA P 2 cm and UGA P 182 cm are the only samples from this location in which Fe-rich amphibole is detected. The bulk clay samples from 302 cm in UGA 0m and 423 cm in UGA 50m contain detectable amounts of muscovite, kaolinite, pyrite, and interlayered illite-smectite. Across all samples from all cores, these samples are the only specimens in which pyrite is detected.

XRD analysis of clay fraction slides reveals quartz, muscovite, kaolinite, and interlayered illite-smectite in all samples (Table 3.3). The only other minerals detected in the clay fraction are microcline and gibbsite, which are detected in samples UGA P 285 cm and UGA 50m 402 cm. Gibbsite is also detected in sample UGA P 254 cm. The apparent absence of some minerals in the clay fraction of sample UGA 50m 380 cm (Table 3.3) is likely due to a lack of infinite thickness for that sample (Fig. A.5). Samples lacking infinite thickness reduce the ability of the diffractometer to detect high angle peaks produced by some minerals present in the sample (Moore and Reynolds, 1997); thus the apparent absence of some minerals may actually be due to a lack of infinite thickness, rather than actual absence of those minerals.

**Table 3.2: Bulk XRD Results for All UGA Cores**

		<b>Minerals</b>									
		Quartz	Microcline	Albite	Anorthite	Muscovite	Kaolinite	Gypsum	Pyrite	Fe-rich Amphibole	Interlayered Illite/Smectite
<b>Core &amp; depth below surface (cm)</b>	<b>UGA P</b>	2 cm	x	x	x					x	
		86 cm	x	x	x						
		182 cm	x	x	x					x	
		286 cm	x	x	x						
		316 cm	x	x	x						
		334 cm	x	x	x		x		x		
	<b>UGA 0m</b>	13 cm	x	x							
		34 cm	x	x							
		66 cm	x	x							
		121 cm	x	x							
		147 cm	x	x							
		302 cm	x	x	x		x		x		x
	<b>UGA 50m</b>	95 cm	x	x	x						
		220 cm	x	x	x						
		359 cm	x	x	x		x				
		423 cm	x	x	x		x		x		x

**Table 3.3:** Clay Fraction XRD Results for All UGA cores

Core & depth below surface (cm)		Quartz	Microcline	Muscovite	Kaolinite	Gibbsite	Interlayered Illite/Smectite
UGA P	254 cm	x		x	x	x	x
	285 cm	x	x	x	x	x	x
UGA 0m	212 cm	x		x	x		x
	305 cm	x		x	x		x
UGA 50m	380 cm				x		x
	402 cm	x	x	x	x	x	x

### ***Core UGA P: Grain Size Analysis***

Core UGA P contains a fairly consistent grain size to a depth of 200 cm (Fig. 3.4). Fine sand is the dominant grain size and makes up 60-78% of all samples collected from the upper 200 cm. In these samples, medium sand comprises 10-33% of the grains and is the second most abundant fraction. Very fine sand, making up 3-11% of the grains, is the third most abundant fraction.

Below 207 cm depth, the amount of silt and clay generally increases, although this increase fluctuates. In samples from 234-244 cm, silt and clay compose 26-49% of the grains. However, in samples from 254-275 cm, the silt and clay fraction is reduced to only 5-10% of the grains before increasing again to make up 40-49% of the samples from 285-295 cm. Below 300 cm depth, the silt and clay fraction is reduced to  $\leq 16\%$  of the grains.

Despite the fluctuation in silt and clay content below 207 cm, fine sand is consistently the most abundant to second most abundant grain size, comprising 36-76% of all samples. The amounts of medium sand (3.5-13%) and very fine sand (4-20%) vary from second to fourth most abundant fractions in samples below 207 cm.

### ***Core UGA 0m: Grain Size Analysis***

Like the samples from core UGA P, the samples from core UGA 0m contain a consistent grain size to a depth of 200 cm (Fig. 3.5). Again, fine sand is the dominant grain size, making up 59-81% of each sample. Likewise, medium sand comprises 10-32% of the grains and is the second most abundant fraction. Very fine sand, making up 2-12% of the grains, is the third most abundant fraction.

Below 200 cm, there is a sharp increase in silt and clay content to compose  $\geq 94\%$  of all samples. Fine sand is reduced to 2-5% of all grains and is the second most abundant fraction in all of these samples except one (241 cm). At 241 cm, very fine sand is the second most abundant fraction and, at 0-5%, is the third most abundant fraction in all other samples below 200 cm.

### ***Core UGA 50m: Grain Size Analysis***

As with the other UGA cores, the upper portion of core UGA 50m contains predominantly fine sand, which constitutes the most abundant fraction to a depth of 359 cm in this core (Fig. 3.6). Fine sand makes up 70-86.5% of the grains in all samples above 338 cm, and also dominates the 359 cm sample at 51% of the grains. In most of these samples (to a depth of 338 cm), medium sand (2-13%) and very fine sand (5-18%) fluctuate as the second and third most abundant fractions.

Below 350 cm depth, the silt and clay content generally increases, although, as with core UGA P, this increase fluctuates. At 366 cm depth, silt and clay dominate the sample at 59% of the grains; in this sample, very fine sand (20%) is the second most abundant fraction, while fine sand and medium sand (both 10%) tie as the third most abundant fraction. However, at 380 cm depth, silt and clay have decreased to form only 10% of the sample, while very fine sand has drastically increased to comprise 75% of the grains. By 389 cm depth (37% silt and clay), silt and clay have begun to increase steadily and compose  $\geq 96\%$  of all samples at or below 393 cm.

### ***UGA Cores: Grain Size Statistics***

Most grain size statistics display general trends related to whether the sample composition is dominated by sand or more fine-grained sediments (Figs. 3.7, 3.8, 3.9). Mean

grain size, of course, is directly affected by the most prevalent grain size in a sample. Likewise, both sorting and skewness values and classifications closely follow whether the sample is sand-dominated or fine sediment-dominated. For example, sand-dominated samples tend to have sorting values that classify the sediment as moderately sorted to well sorted. Samples containing a greater proportion of silt and clay tend to have sorting values that classify the sediment as poorly to extremely poorly sorted.

Similar trends exist for skewness values. Sand-dominated samples tend to have skewness values that classify the sediment distribution as symmetrical to coarse skewed (i.e., negatively skewed). Fine sediment-dominated samples tend to have skewness values that classify the sediment distribution as symmetrical to very fine skewed (i.e., positively skewed).

In contrast, kurtosis values and classifications prove more variable. Generally, sand-dominated samples tend to display leptokurtic distributions, although this generalization is not true in all cases. Kurtosis values and classifications for fine sediment-dominated samples are similarly variable, but in general these samples display platykurtic distributions.

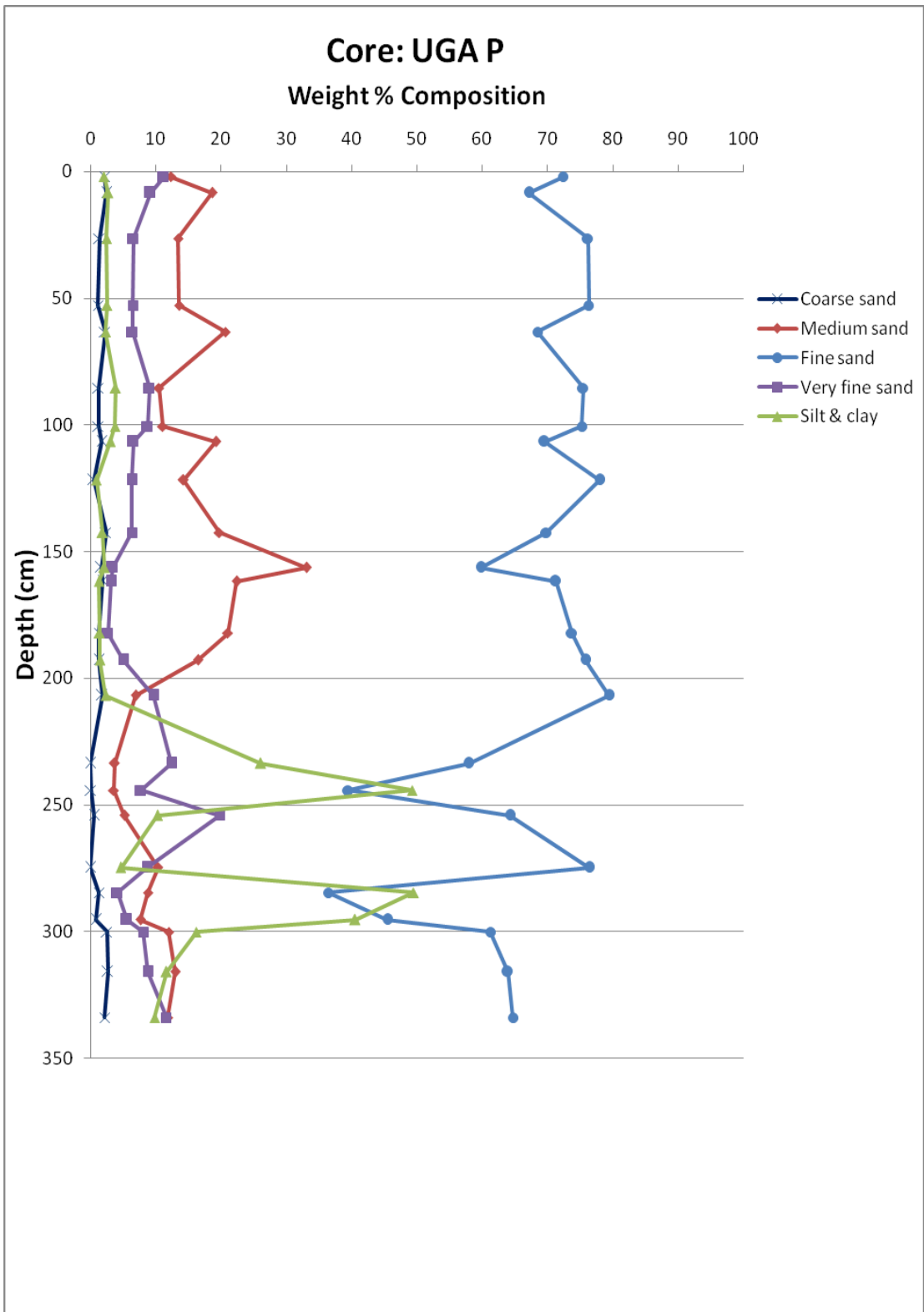


**Fig. 3.4** All grain size analysis results for core UGA P

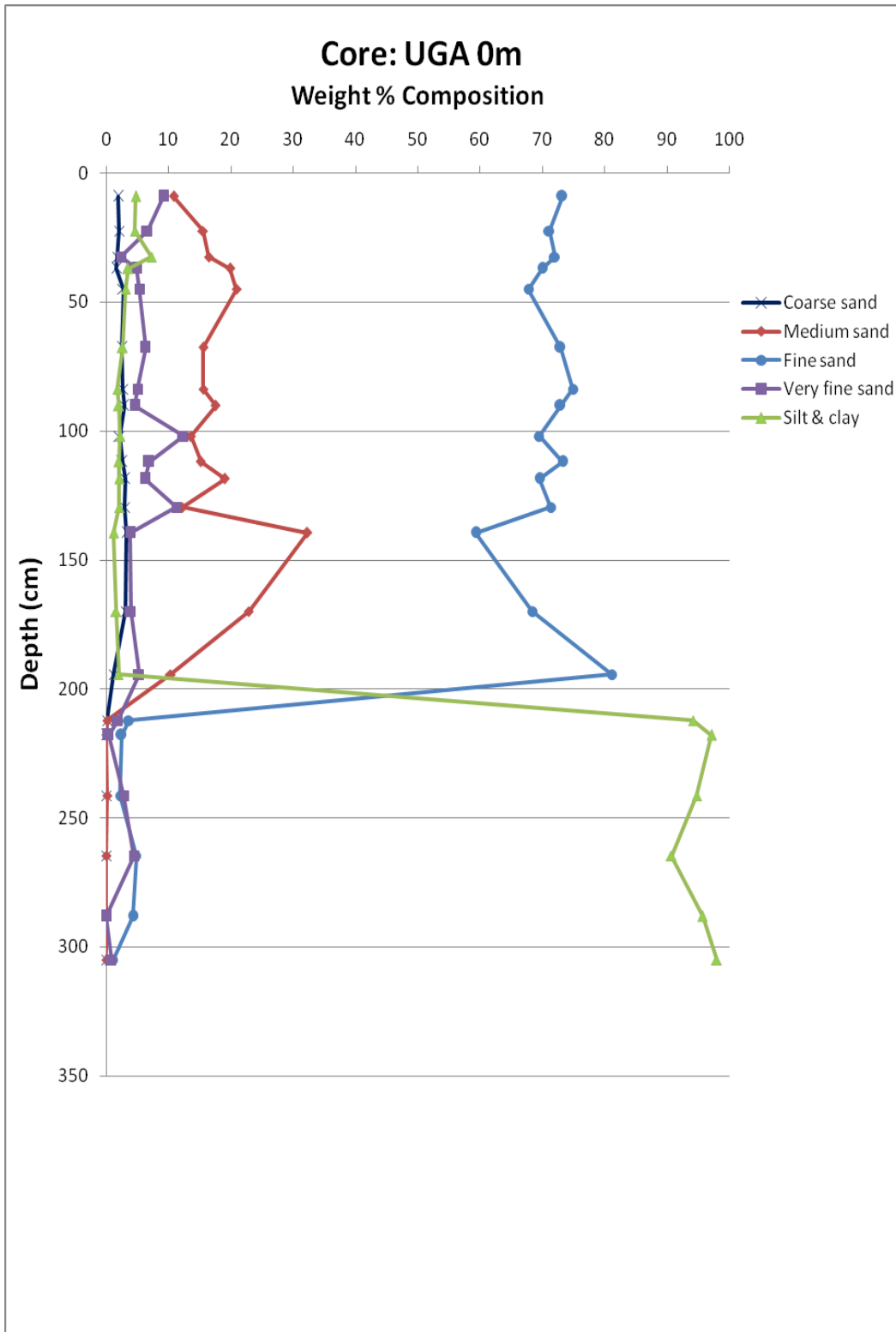


**Fig. 3.5** All grain size analysis results for core UGA 0m

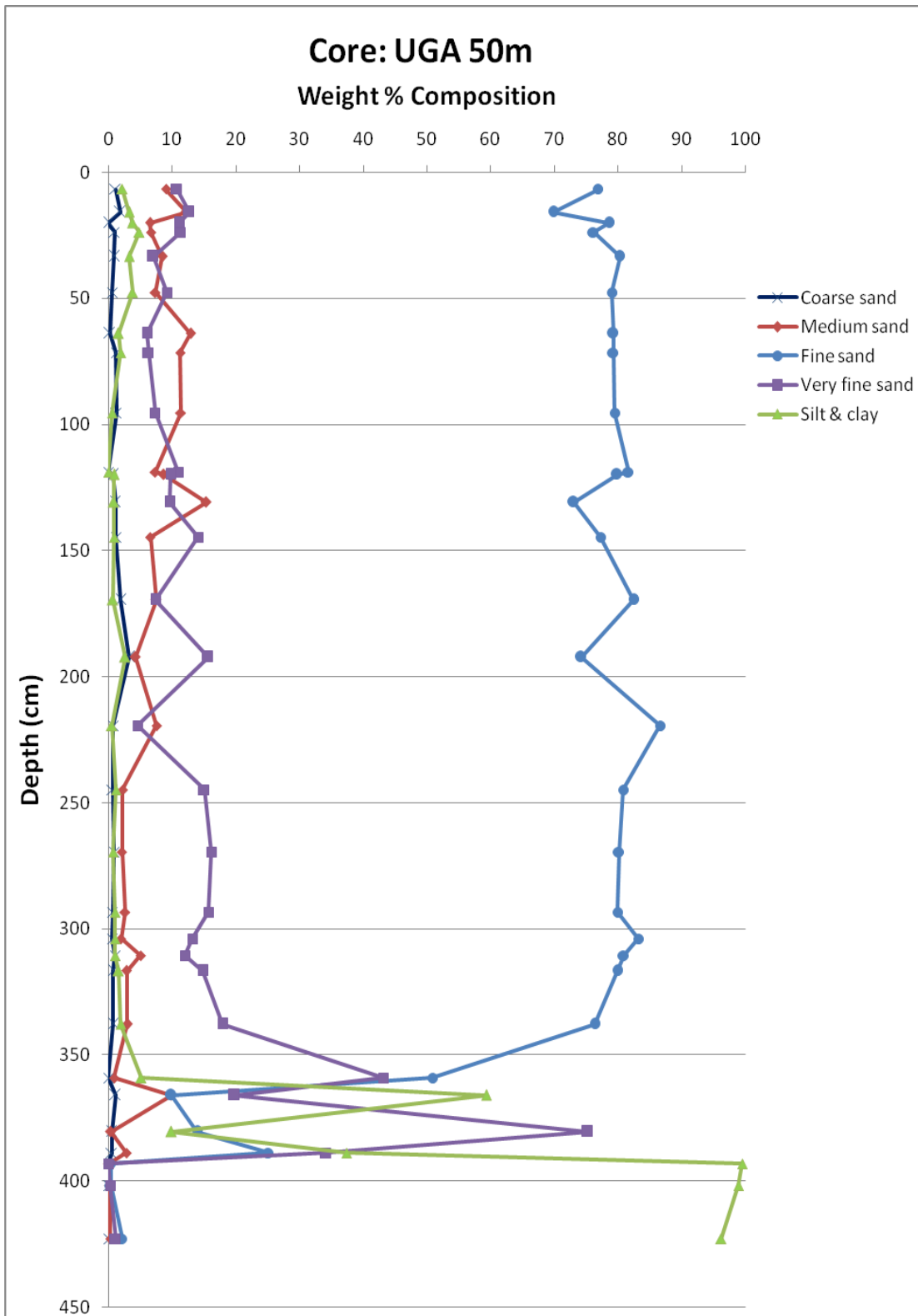


**Fig. 3.6** All grain size analysis results for core UGA 50m

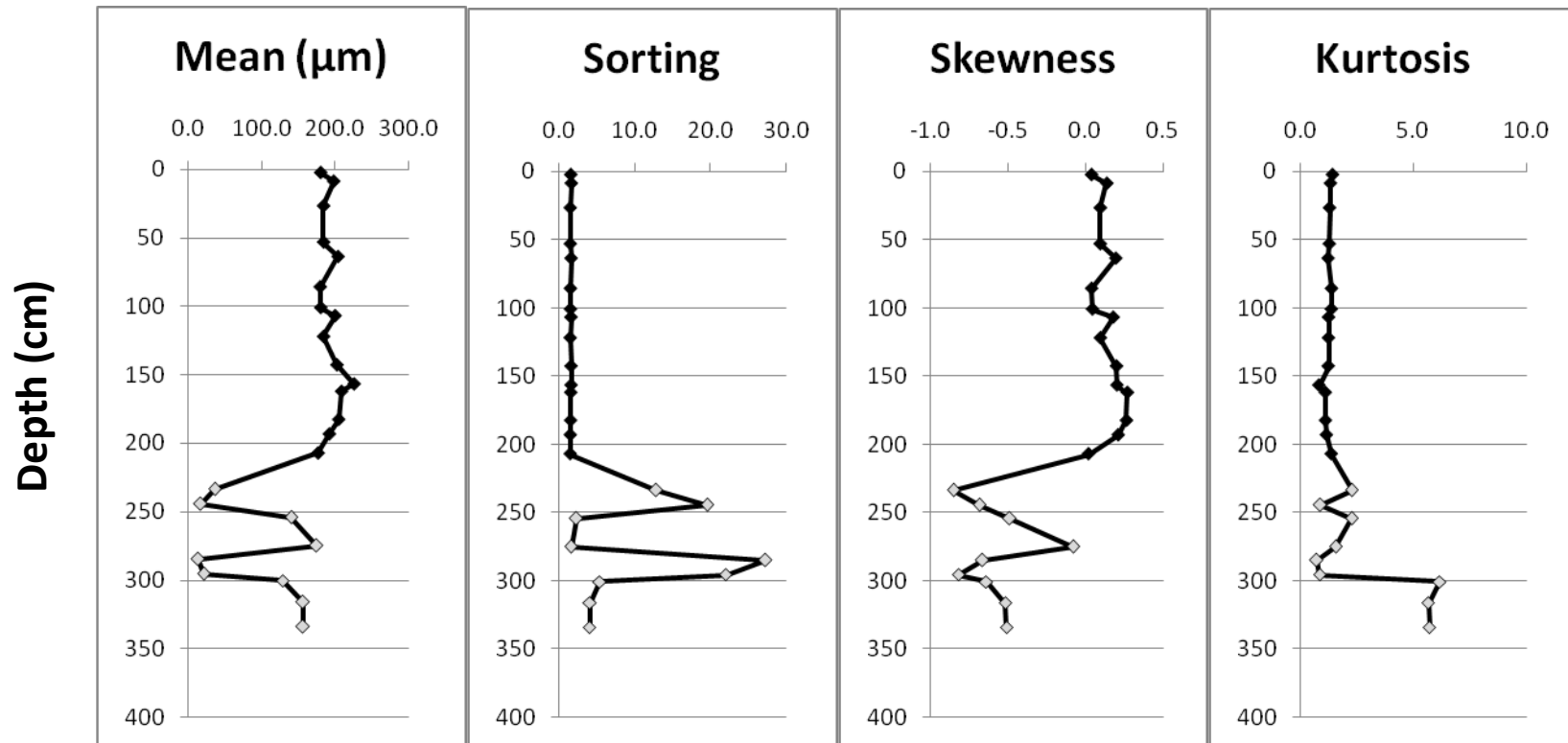


**Fig. 3.7** Grain size statistics for core UGA P. Points shaded grey represent grain size data obtained using wet sediment grain size analyses, which means that silt and clay content are included in those samples. Silt and clay are omitted from all dry sediment grain size statistic calculations. Points marked with a horizontal line represent grain size data obtained using dry sediment grain size analysis that contained > 5% silt and clay; these data likely contain a larger amount of error due to the omission of the silt and clay content. Key below from Blott and Pye, 2001.

Sorting		Skewness		Kurtosis	
Very well sorted	< 1.27	Very fine skewed	$^{-}0.3$ to $^{-}1.0$	Very platykurtic	< 0.67
Well sorted	1.27 to 1.41	Fine skewed	$^{-}0.1$ to $^{-}0.3$	Platykurtic	0.67 to 0.90
Moderately well sorted	1.41 to 1.62	Symmetrical	$^{-}0.1$ to $^{+}1.0$	Mesokurtic	0.90 to 1.11
Moderately sorted	1.62 to 2.00	Coarse skewed	$^{+}0.1$ to $^{+}0.3$	Leptokurtic	1.11 to 1.50
Poorly sorted	2.00 to 4.00	Very coarse skewed	$^{+}0.3$ to $^{+}1.0$	Very leptokurtic	1.50 to 3.00
Very poorly sorted	4.00 to 16.00			Extremely leptokurtic	> 3.00
Extremely poorly sorted	> 16.00				

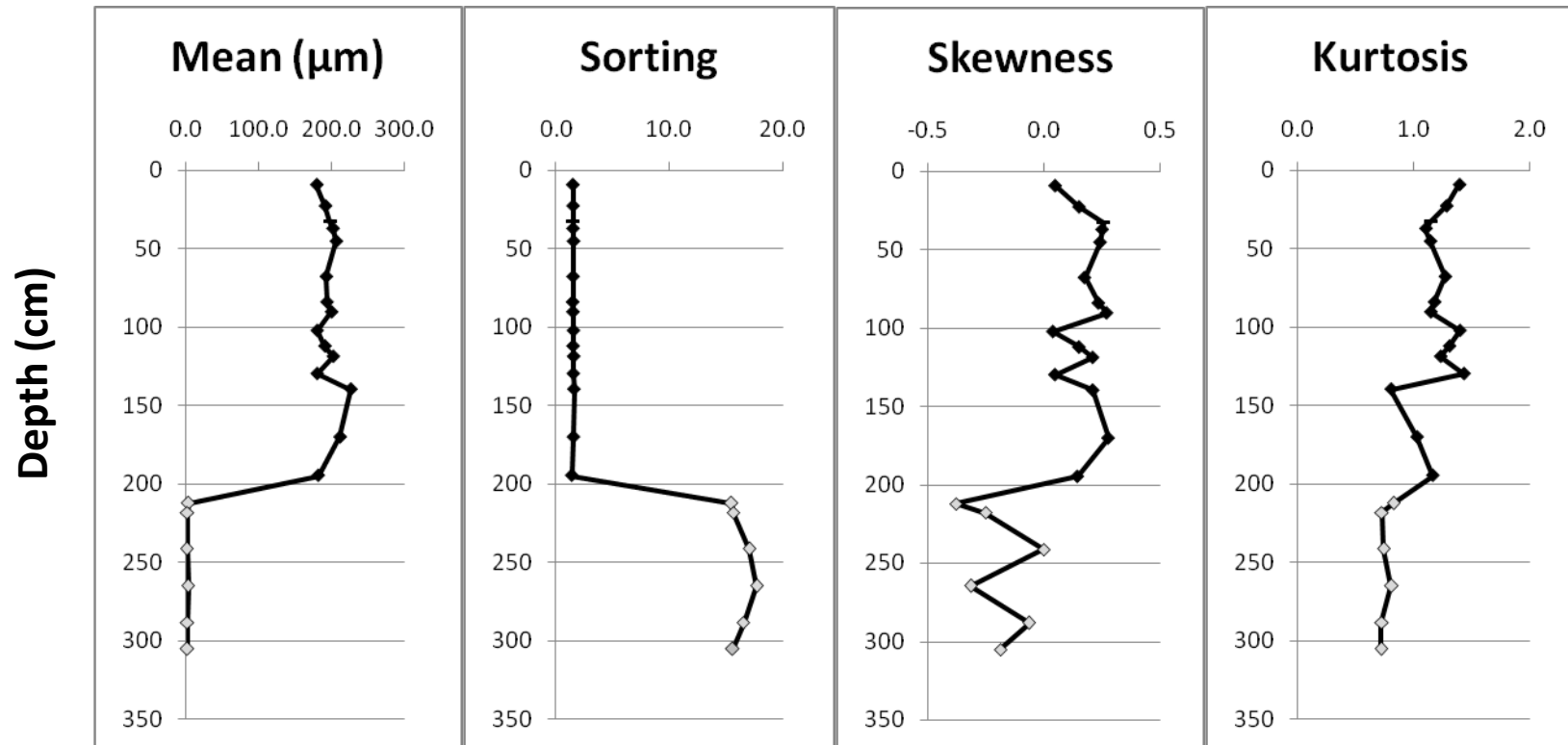


**Fig. 3.8** Grain size statistics for core UGA 0m. Points shaded grey represent grain size data obtained using wet sediment grain size analyses, which means that silt and clay content are included in those samples. Silt and clay are omitted from all dry sediment grain size statistic calculations. Points marked with a horizontal line represent grain size data obtained using dry sediment grain size analysis that contained > 5% silt and clay; these data likely contain a larger amount of error due to the omission of the silt and clay content. Key below from Blott and Pye, 2001.

Sorting		Skewness		Kurtosis	
Very well sorted	< 1.27	Very fine skewed	$^{-}0.3$ to $^{-}1.0$	Very platykurtic	< 0.67
Well sorted	1.27 to 1.41	Fine skewed	$^{-}0.1$ to $^{-}0.3$	Platykurtic	0.67 to 0.90
Moderately well sorted	1.41 to 1.62	Symmetrical	$^{-}0.1$ to $^{+}1.0$	Mesokurtic	0.90 to 1.11
Moderately sorted	1.62 to 2.00	Coarse skewed	$^{+}0.1$ to $^{+}0.3$	Leptokurtic	1.11 to 1.50
Poorly sorted	2.00 to 4.00	Very coarse skewed	$^{+}0.3$ to $^{+}1.0$	Very leptokurtic	1.50 to 3.00
Very poorly sorted	4.00 to 16.00			Extremely leptokurtic	> 3.00
Extremely poorly sorted	> 16.00				

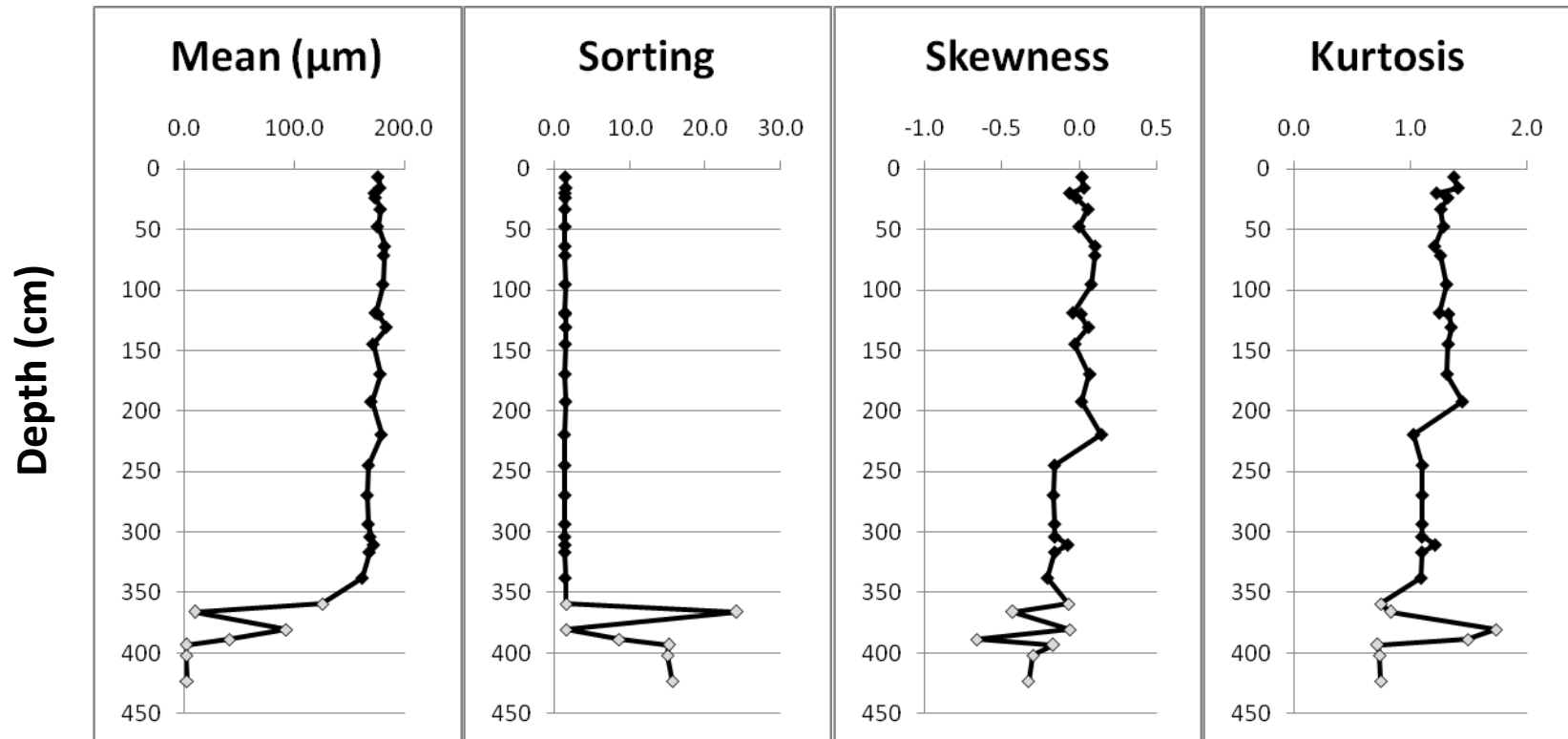


**Fig. 3.9** Grain size statistics for core UGA 50m. Points shaded grey represent grain size data obtained using wet sediment grain size analyses, which means that silt and clay content are included in those samples. Silt and clay are omitted from all dry sediment grain size statistic calculations. Points marked with a horizontal line represent grain size data obtained using dry sediment grain size analysis that contained > 5% silt and clay; these data likely contain a larger amount of error due to the omission of the silt and clay content. Key below from Blott and Pye, 2001.

<b>Sorting</b>		<b>Skewness</b>		<b>Kurtosis</b>	
Very well sorted	< 1.27	Very fine skewed	$^{-}0.3$ to $^{-}1.0$	Very platykurtic	< 0.67
Well sorted	1.27 to 1.41	Fine skewed	$^{-}0.1$ to $^{-}0.3$	Platykurtic	0.67 to 0.90
Moderately well sorted	1.41 to 1.62	Symmetrical	$^{-}0.1$ to $^{+}1.0$	Mesokurtic	0.90 to 1.11
Moderately sorted	1.62 to 2.00	Coarse skewed	$^{+}0.1$ to $^{+}0.3$	Leptokurtic	1.11 to 1.50
Poorly sorted	2.00 to 4.00	Very coarse skewed	$^{+}0.3$ to $^{+}1.0$	Very leptokurtic	1.50 to 3.00
Very poorly sorted	4.00 to 16.00			Extremely leptokurtic	> 3.00
Extremely poorly sorted	> 16.00				

### **Cores collected near the Bluff (B cores)**

For the two B cores, total core depth varied from 186 cm to 397 cm (Table 3.4). The number of sub-cores collected (i.e., the number of times the Giddings probe had to be sent down the hole) to make up each core varied from three to five (Table 3.4). Core photographs taken in the field and diagrams representing core attributes are shown in Figs. 3.10 and 3.11.

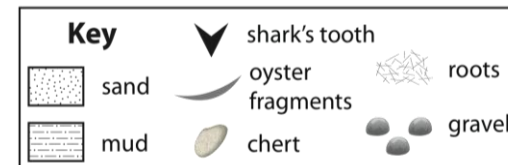
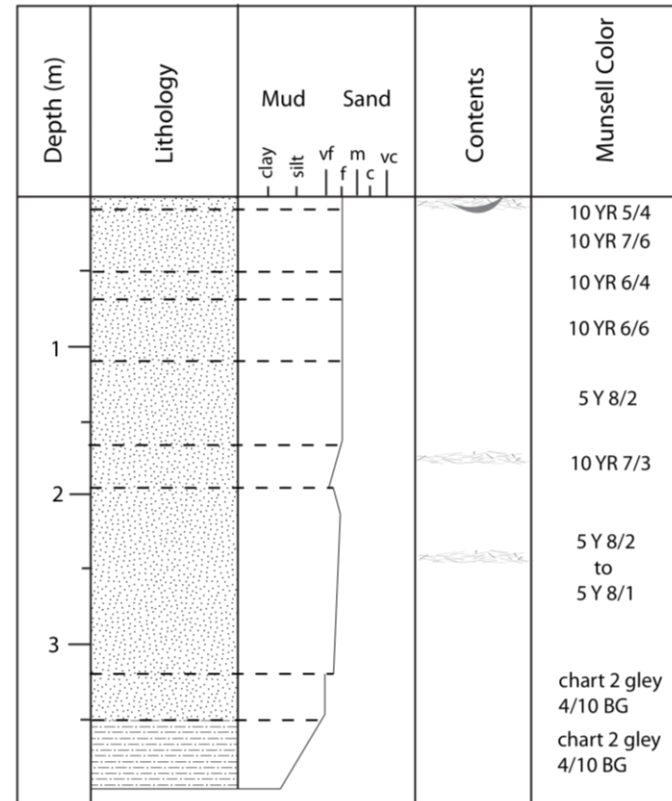
Obvious core contamination was only a problem in core B 100m, where sediment from nearer the surface contaminated the top of the third sub-core. This contamination is readily visible as an 8 cm-long zone of orangish sediment in the lower portion of the third column in Fig. 3.11. Areas of obvious contamination were subtracted from the total core depth of core B 100m, and subsamples that landed in contaminated areas (by default of sampling every 25 cm) were removed from further analyses.

**Table 3.4** Overview of B Cores

<b>Core Name</b>	<b>Number of sub-cores</b>	<b>Total core depth</b>
<b>B 0m</b>	5	397 cm
<b>B 100m</b>	3	186 cm



**Fig. 3.10** All B 0m cores stored in boxes after collection. Note the absence of a well developed A horizon. Scale: Each column is 62 cm long. Core lithology, contents, and Munsell colors are represented in the diagram.





Depth (m)	Lithology	Mud		Sand			Contents	Munsell Color
		clay	silt	vf	f	m		
1	[Dotted pattern]						[Shark's tooth]	10 YR 2/2
							[Oyster fragments]	10 YR 5/6
							[Roots]	2.5 Y 7/4
								5 Y 8/1
								5 Y 8/1

Key	
[Dotted pattern]	sand
[Solid grey]	mud
[Inverted triangle]	shark's tooth
[Crescent shape]	oyster fragments
[Irregular shape]	chert
[Fibrous shape]	roots
[Small circles]	gravel

**Fig. 3.11** All B 100m cores stored in a box after collection. Note the well developed A horizon and oyster fragments visible towards the bottom of the A horizon. The color change towards the bottom of the third column is the result of upcore contamination; this 8 cm of contamination was subtracted from the total core length, and is not included in the diagram. Scale: Each column is 62 cm long. Core lithology, contents, and Munsell colors are represented in the diagram.

### ***Bluff Cores: X-ray Diffraction***

As with the UGA cores, quartz and microcline are detected in all bulk XRD samples from the Bluff cores. Albite is detected in all B 0m XRD samples, but not in all B 100m XRD samples (Table 3.5). Fe-rich amphibole is detected in two samples from each core. The two deepest XRD samples (346 cm and 386 cm) from B 0m include muscovite and gypsum. The presence of gypsum is weakly detected at 346 cm, but is confirmed in the 386 cm sample. Also, the deepest sample (B 0m 386 cm) also includes kaolinite and interlayered illite-smectite.

XRD analysis of clay fraction slides reveals quartz, muscovite, and kaolinite in all B 0m and B 100m samples (Table 3.6). Interlayered illite-smectite is detected in all samples except B 0m 318 cm. However, as mentioned for UGA 50m 380 cm, this apparent absence of interlayered illite-smectite in B 0m 318 cm may be due to lack of infinite thickness (Fig. A.8) rather than actual absence of that mineral.

**Table 3.5: Bulk XRD Results for All B cores**

Core & depth below surface (cm)		Minerals									
		Quartz	Microcline	Albite	Anorthite	Muscovite	Kaolinite	Gypsum	Pyrite	Fe-rich Amphibole	Interlayered Illite/Smectite
<b>B 0m</b>	2 cm	x	x	x							
	13 cm	x	x	x							
	95 cm	x	x	x							
	147 cm	x	x	x						x	
	346 cm	x	x	x		x		x			
	386 cm	x	x	x		x		x		x	x
<b>B 100m</b>	4 cm	x	x								
	65 cm	x	x	x							
	108 cm	x	x	x						x	
	148 cm	x	x	x						x	
	183 cm	x	x								

**Table 3.6:** Clay Fraction XRD Results for All B cores

Core & depth below surface (cm)		Minerals					
		Quartz	Microcline	Muscovite	Kaolinite	Gibbsite	Interlayered Illite/Smectite
B 0m	318 cm	x		x	x		
	397 cm	x		x	x		x
B 100m	166 cm	x		x	x		x
	183 cm	x		x	x		x

### ***Core B 0m: Grain Size Analysis***

In core B 0m, samples above 25 cm contain 9-12% silt and clay (Fig. 3.12). However, the silt and clay content drops notably by 35 cm depth and remains low until depths below 315 cm are reached. Above 375 cm depth, the most abundant grain size fluctuates between fine sand and very fine sand. Fine sand is the dominant fraction to a depth of 187 cm, making up 48-64% of the grains. However, in samples from 197-212.5 cm depth, very fine sand (47-50%) is the most abundant grain size. From 223-236 cm depth, fine sand (45-49%) again becomes the dominant grain size; interestingly, the 236 cm depth sample also shows a marked increase in both coarse sand (14.5%) and medium sand (16.5%). In samples from 263-353 cm depth, very fine sand once again dominates the sample, comprising 45-66% of the grains. Without exception until 350 cm depth, when fine sand is the most abundant fraction, very fine sand is the second most abundant fraction, and vice versa.

After 350 cm depth, silt and clay steadily increase to become the most abundant grain size (81-86%) from 375 cm to the base of the core. In samples at and below 375 cm, very fine sand is the second most abundant fraction, composing 10-13% of the grains.

### ***Core B 100m: Grain Size Analysis***

Making up 54-74% of the grains, fine sand is the dominant fraction in all B 100m samples (Fig. 3.13). Above 150 cm depth, the second most abundant grain size fluctuates between medium sand (6-20%) and very fine sand (8-24.5%) throughout the core. Below 150 cm depth, the silt and clay content continues to steadily increase to a peak of 33% in the 183 cm sample. It should be noted that this core is significantly shorter than the others, with a maximum depth of only 186 cm.

### ***B Cores: Grain Size Statistics***

Grain size statistics for the cores collected at the Bluff display the same general trends (Figs. 3.14, 3.15) described on p. 33-34 for the UGA cores' grain size statistics. Mean grain size typically reflects the prevalent grain size in the sample. Sand-dominated samples tend to display sorting values that classify them as moderately sorted to well sorted, and to have skewness values that classify the sediment distribution as symmetrical to coarse skewed (i.e., negatively skewed). Fine sediment-dominated samples tend to display sorting values that classify the sediment as poorly to extremely poorly sorted, and to have skewness values that classify the sediment distribution as symmetrical to very fine skewed (i.e., positively skewed). Kurtosis values prove highly variable.

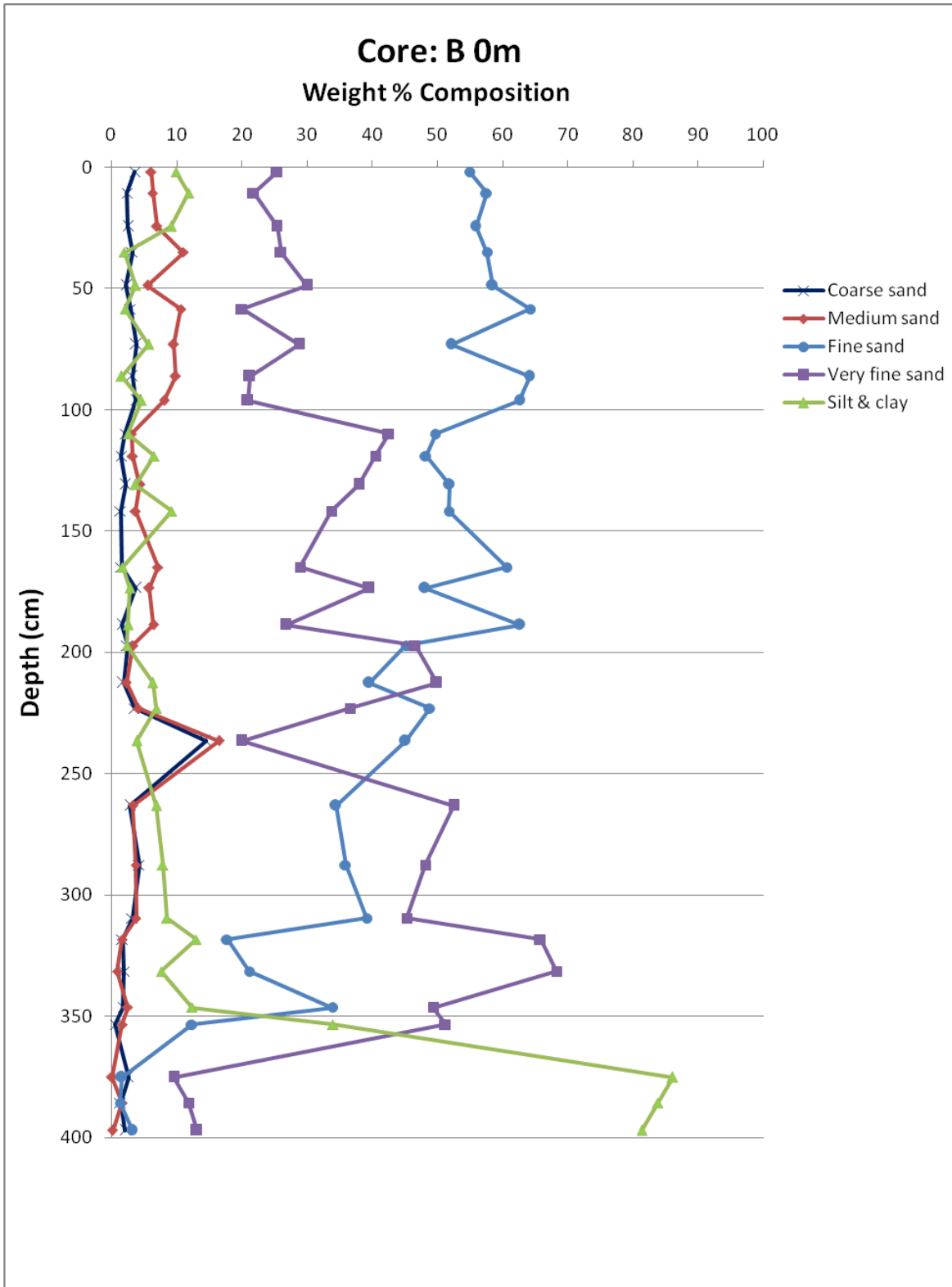


**Fig. 3.12** All grain size analysis results for core B 0m

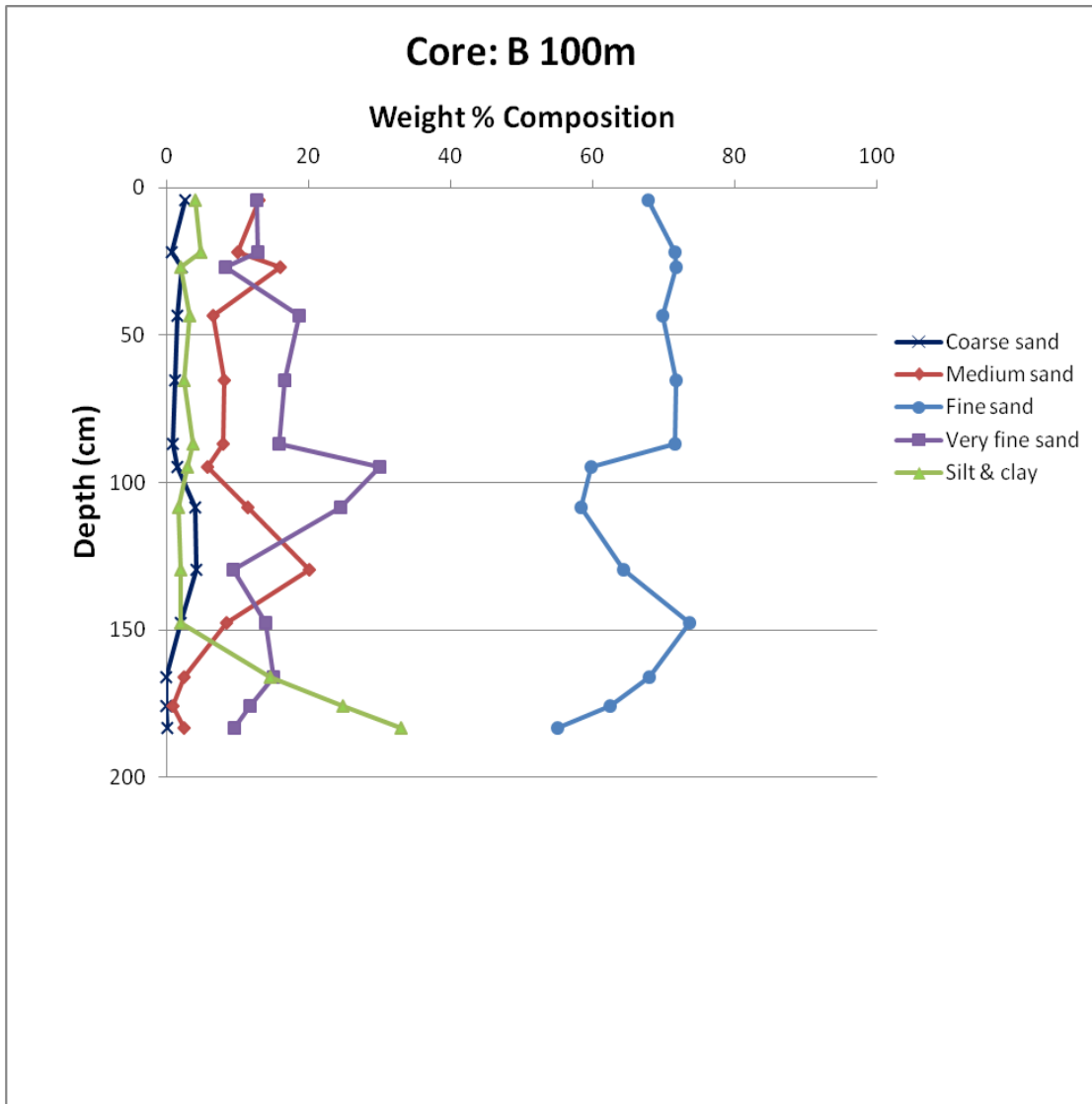


**Fig. 3.13** All grain size analysis results for core B 100m

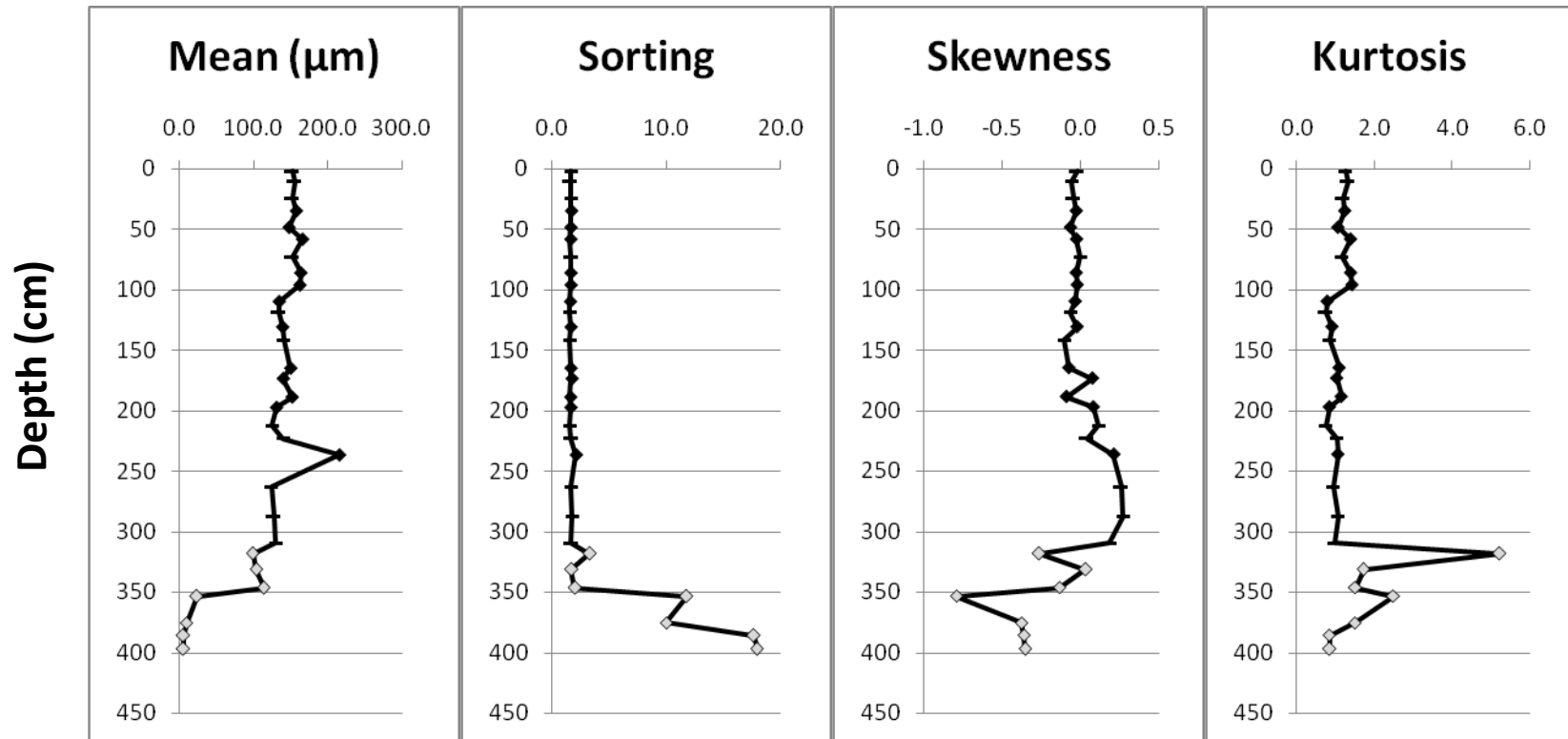


**Fig. 3.14** Grain size statistics for core B 0m. Points shaded grey represent grain size data obtained using wet sediment grain size analyses, which means that silt and clay content are included in those samples. Silt and clay are omitted from all dry sediment grain size statistic calculations. Points marked with a horizontal line represent grain size data obtained using dry sediment grain size analysis that contained > 5% silt and clay; these data likely contain a larger amount of error due to the omission of the silt and clay content. Key below from Blott and Pye, 2001.

Sorting		Skewness		Kurtosis	
Very well sorted	< 1.27	Very fine skewed	$-0.3$ to $-1.0$	Very platykurtic	< 0.67
Well sorted	1.27 to 1.41	Fine skewed	$-0.1$ to $-0.3$	Platykurtic	0.67 to 0.90
Moderately well sorted	1.41 to 1.62	Symmetrical	$-0.1$ to $+1.0$	Mesokurtic	0.90 to 1.11
Moderately sorted	1.62 to 2.00	Coarse skewed	$+0.1$ to $+0.3$	Leptokurtic	1.11 to 1.50
Poorly sorted	2.00 to 4.00	Very coarse skewed	$+0.3$ to $+1.0$	Very leptokurtic	1.50 to 3.00
Very poorly sorted	4.00 to 16.00			Extremely leptokurtic	> 3.00
Extremely poorly sorted	> 16.00				

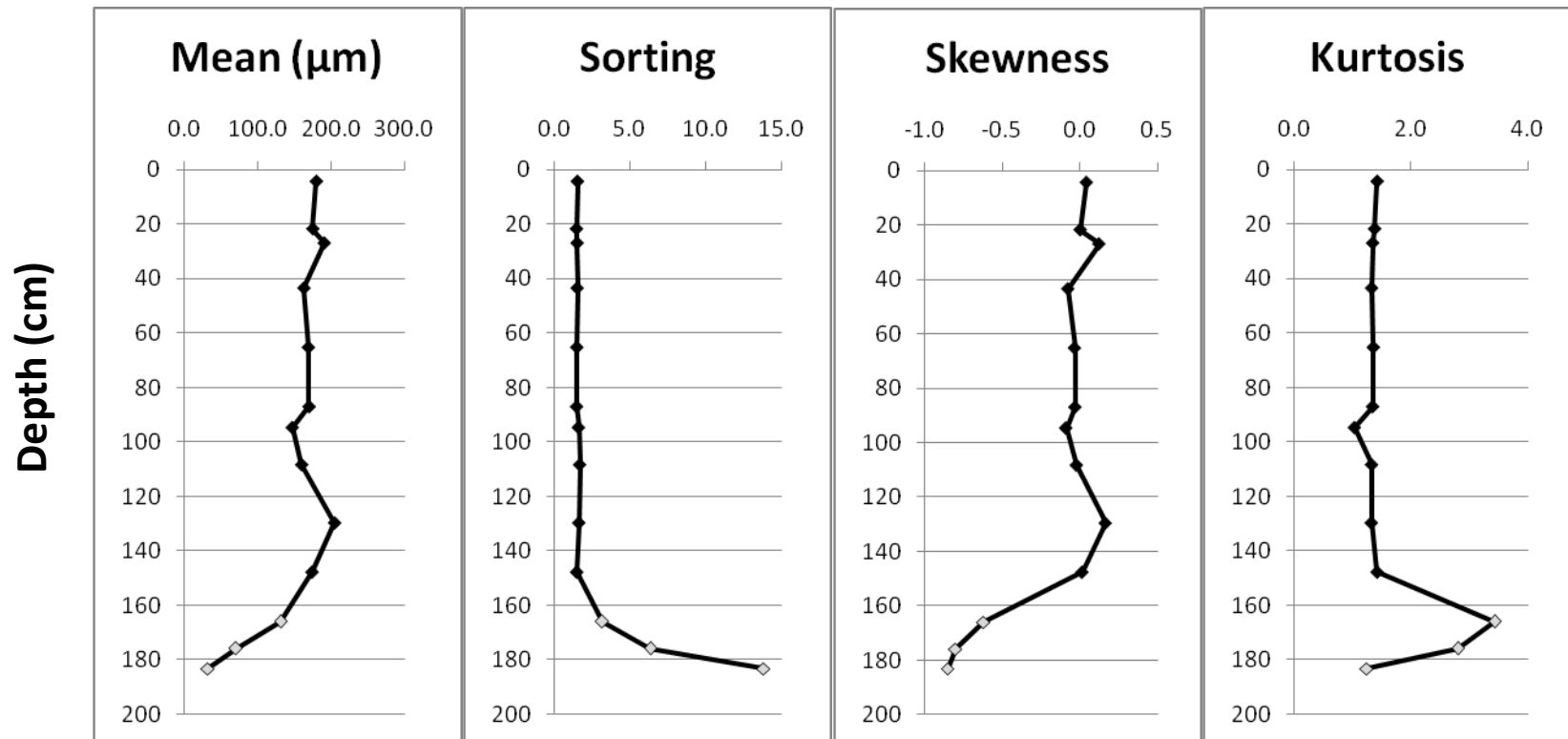


**Fig. 3.15** Grain size statistics for core B 100m. Points shaded grey represent grain size data obtained using wet sediment grain size analyses, which means that silt and clay content are included in those samples. Silt and clay are omitted from all dry sediment grain size statistic calculations. Points marked with a horizontal line represent grain size data obtained using dry sediment grain size analysis that contained > 5% silt and clay; these data likely contain a larger amount of error due to the omission of the silt and clay content. Key below from Blott and Pye, 2001.

Sorting		Skewness		Kurtosis	
Very well sorted	< 1.27	Very fine skewed	$-0.3$ to $-1.0$	Very platykurtic	< 0.67
Well sorted	1.27 to 1.41	Fine skewed	$-0.1$ to $-0.3$	Platykurtic	0.67 to 0.90
Moderately well sorted	1.41 to 1.62	Symmetrical	$-0.1$ to $+1.0$	Mesokurtic	0.90 to 1.11
Moderately sorted	1.62 to 2.00	Coarse skewed	$+0.1$ to $+0.3$	Leptokurtic	1.11 to 1.50
Poorly sorted	2.00 to 4.00	Very coarse skewed	$+0.3$ to $+1.0$	Very leptokurtic	1.50 to 3.00
Very poorly sorted	4.00 to 16.00			Extremely leptokurtic	> 3.00
Extremely poorly sorted	> 16.00				

### **Cores collected near the Grove's Creek Site (GCF cores)**

For the three GCF cores, total core depth varied from 269.5 cm to 379 cm (Table 3.7). The number of sub-cores collected (i.e., the number of times the Giddings probe had to be sent down the hole) to make up each core varied from four to eleven (Table 3.7). Core photographs taken in the field and diagrams representing core attributes are shown in Figs. 3.16, 3.17, 3.18.

Coring at the location of core GCF 100m proved especially difficult; two cores were attempted at that location, and the deeper of the two cores is presented here. High resistance- almost to refusal- at that coring location contributed to several cases of contamination in core GCF 100m, including a case of mid-core contamination (which will be explained later). This mid-core contamination is readily visible as an 8 cm long zone of anomalous dark brown, leaf- and pine straw-bearing sediment in the upper portion of the second to last column in Fig. 3.18. Areas of obvious contamination were subtracted from the total core depth of core GCF 100m, and subsamples that landed in contaminated areas (by default of sampling every 25 cm) were removed from further analyses.

**Table 3.7** Overview of GCF Cores

<b>Core Name</b>	<b>Number of sub-cores</b>	<b>Total core depth</b>
<b>GCF 0m</b>	11	375.5 cm
<b>GCF 50m</b>	5	379 cm
<b>GCF 100m</b>	4	269.5 cm



Depth (m)	Lithology	Mud		Sand			Contents	Munsell Color
		clay	silt	vf	f	m		
0							shark's tooth	10 YR 2/1
1								10 YR 3/2
2							oyster fragments	5 Y 8/2 to 5 Y 8/1
3								10 YR 6/2
								5 Y 8/1
								5 Y 5/1

**Fig 3.16** All GCF 0m cores stored in boxes after collection. Scale: Each column is 62 cm long. Core lithology, contents, and Munsell colors are represented in the diagram.

**Key**

-  sand
-  mud
-  shark's tooth
-  oyster fragments
-  chert
-  roots
-  gravel



**Fig. 3.17** All GCF 50m cores stored in boxes after collection. Scale: Each column is 62 cm long. Core lithology, contents, and Munsell colors are represented in the diagram. Note the increase in silt and clay just above 200 cm; this sedimentologic change represents accumulation of finer grained particles around fine roots.

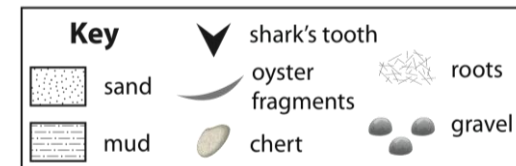
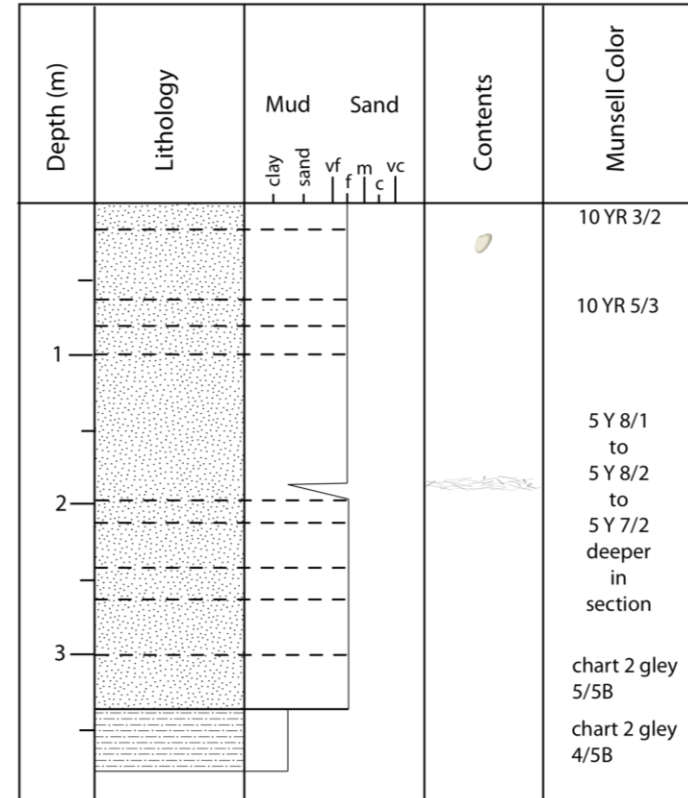
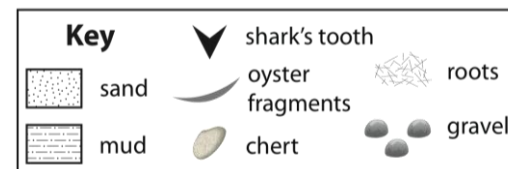
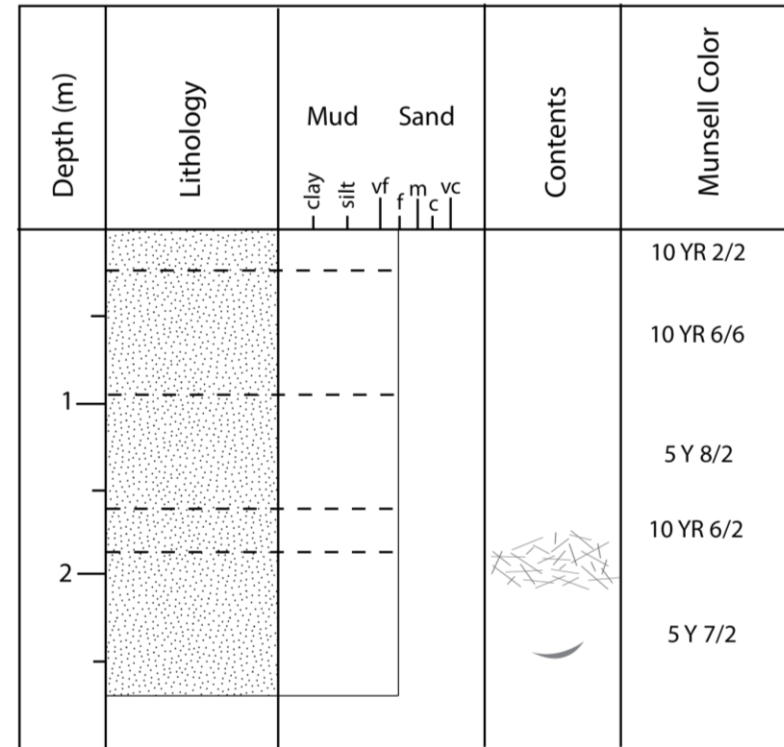




**Fig. 3.18** All GCF 100m cores stored in boxes after collection. Note the contaminated areas towards the bottom of the fourth column and top of the sixth column where pine straw and leaf litter from the surface are evident; these areas of contamination, a total of 20 cm, were subtracted from the total core length, and are not included in the diagram to the right. Scale: Each column is 62 cm long. Core lithology, contents, and Munsell colors are represented in the diagram.



### ***GCF Cores: X-ray Diffraction***

In XRD samples from the GCF cores, quartz is present in all samples and microcline is detectable in all samples except one (GCF 50m 26 cm). Albite is more commonly found in these samples, although anorthite is detected in one sample (GCF 50 m 368 cm) (Table 3.8). Muscovite occurs in numerous samples. Fe-rich amphibole is detected in at least one sample in each core. The detection of kaolinite and gypsum at this location is unique to the deepest samples of core GCF 50 m (317 cm and 368 cm).

XRD analyses of clay fraction slides reveal quartz, muscovite, and kaolinite in all samples (Table 3.9). Interlayered illite-smectite is detected in all samples except one (GCF 0m 349 cm). Again, exactly as with B 0m 318 cm, this apparent absence of interlayered illite-smectite in GCF 0m 349 cm may be caused by lack of infinite thickness for that sample (Fig. A.12) rather than actual mineral absence. Microcline is present in samples collected from above 300 cm. In the GCF clay fraction samples, gibbsite is detected in both samples from core GCF 50m.

**Table 3.8:** Bulk XRD Results for All GCF cores

		Minerals									
		Quartz	Microcline	Albite	Anorthite	Muscovite	Kaolinite	Gypsum	Pyrite	Fe-rich Amphibole	Interlayered Illite/Smectite
Core & depth below surface (cm)	GCF 0m	24 cm	x	x							
		71 cm	x	x	x						
		136 cm	x	x	x		x			x	
		207 cm	x	x	x		x			x	
		271 cm	x	x	x		x				
		330 cm	x	x	x		x				
	GCF 50m	5 cm	x	x							
		26 cm	x								
		86 cm	x	x							
		156 cm	x	x	x		x				
		233 cm	x	x			x				
		282 cm	x	x							
		317 cm	x	x	x		x	x	x		
		368 cm	x	x		x	x	x	x		x
	GCF 100m	61 cm	x	x	x						
		116 cm	x	x	x						
		164 cm	x	x	x					x	
		246 cm	x	x	x						
		266 cm	x	x	x		x				x

**Table 3.9:** Clay Fraction XRD Results for All GCF cores

		Minerals					
		Quartz	Microcline	Muscovite	Kaolinite	Gibbsite	Interlayered Illite/Smectite
Core & depth below surface (cm)	GCF 0m						
	349 cm	x		x	x		
	366 cm	x		x	x		x
	GCF 50m						
	188 cm	x	x	x	x	x	x
	351 cm	x		x	x	x	x
	GCF 100m						
	199 cm	x	x	x	x		x
	251 cm	x	x	x	x		x

### ***Core GCF 0m: Grain Size Analysis***

All samples to a depth of 217 cm in core GCF 0m contain dominantly fine sand, which makes up 44-78% of each sample (Fig. 3.19). In these samples, very fine sand is the second most abundant grain size, and comprises 12-48% of the grains. At 217 cm depth, very fine sand (48%) is slightly more abundant than fine sand (44%). From 228-249 cm depth, fine sand (41-50.5%) once again becomes the dominant grain size. However, after 217 cm depth, medium sand steadily increases to peak as the dominant fraction with 38% of the grains at 271 cm depth; likewise, coarse sand peaks at 16% in this sample. Medium sand (13-22%) thereafter decreases to third most abundant fraction until 330 cm depth; in all samples from 282-319 cm, fine sand (44-56%) dominates the grain size fraction and very fine sand (25-33%) is the second most abundant fraction. By 330 cm depth and below, very fine sand (51-62%) becomes the most abundant fraction, followed by fine sand (20-36%). Strikingly, in core GCF 0m, silt and clay content never exceeds 7.5%.

### ***Core GCF 50m: Grain Size Analysis***

In almost all GCF 50m samples above 335 cm depth, fine sand is the dominant grain size, constituting 44-72% of all samples except one (Fig. 3.20). This exception consists of a special case at 188 cm depth, where a clay lump formed around a root causes the silt and clay content to dominate with 60% of the grains; fine sand (25%) is second most abundant grain size here. In most other samples above 335 cm depth, very fine sand (7-33%) is the second most abundant fraction. However, in several samples, other grain sizes comprise the second most abundant fraction; these grain sizes are medium sand (21% at 99 cm depth; 18% at 179 cm depth) and silt and clay (29% at 245 cm depth; 30-36% from 299-334 cm depth). After 335 cm depth, silt and

clay (55-82%) dominate as the most abundant grain size, followed variably by very fine sand (10-15%) or fine sand (1-26%).

### ***Core GCF 100m: Grain Size Analysis***

For all samples in core GCF 100m, fine sand is the dominant fraction, making up 44-71% of the grains (Fig. 3.21). Above 125 cm depth, very fine sand (16-21%) comprises the second most abundant grain size and is followed by medium sand (7-13.5%) as the third most abundant fraction. However, in all samples from 132-190 cm depth, medium sand is the second most abundant fraction, constituting 13.5-23% of the grains in all samples. Very fine sand (7-10%) makes up the third most abundant fraction in all samples from 132-190 cm depth.

Below 190 cm depth, the second most abundant grain size fluctuates. From 199-227 cm, silt and clay content (14-27 %) increases to become the second most abundant fraction. Very fine sand (10-16%) is third most abundant, followed by medium sand (2-9%). However, at 246 cm, very fine sand (17%) becomes the second most abundant grain size, followed by silt and clay (15%). At 251 cm depth, silt and clay peak at 42% to once again become the second most abundant fraction. Although the silt and clay content decreases to 21.5% by 266 cm depth, silt and clay still remain more abundant than very fine sand (third most abundant at 9-12% below 269 cm depth) for the remainder of the core.

### ***GCF Cores: Grain Size Statistics***

Once again, grain size statistics for cores collected near the Grove's Creek site display the general trends described on p. 33-34 for the UGA cores' grain size statistics (Figs. 3.22, 3.23, 3.24). Mean grain size typically reflects the prevalent grain size in the sample. Sand-dominated

samples tend to display sorting values classified as moderately sorted to well sorted, while fine sediment-dominated samples tend to display sorting values that classify the sediment as poorly to extremely poorly sorted. Skewness values for sand-dominated samples tend to classify the sediment distribution as symmetrical to coarse skewed (i.e., negatively skewed), while skewness values for fine sediment-dominated samples tend to classify the sediment distribution as symmetrical to very fine skewed (i.e., positively skewed). Kurtosis values prove highly variable.

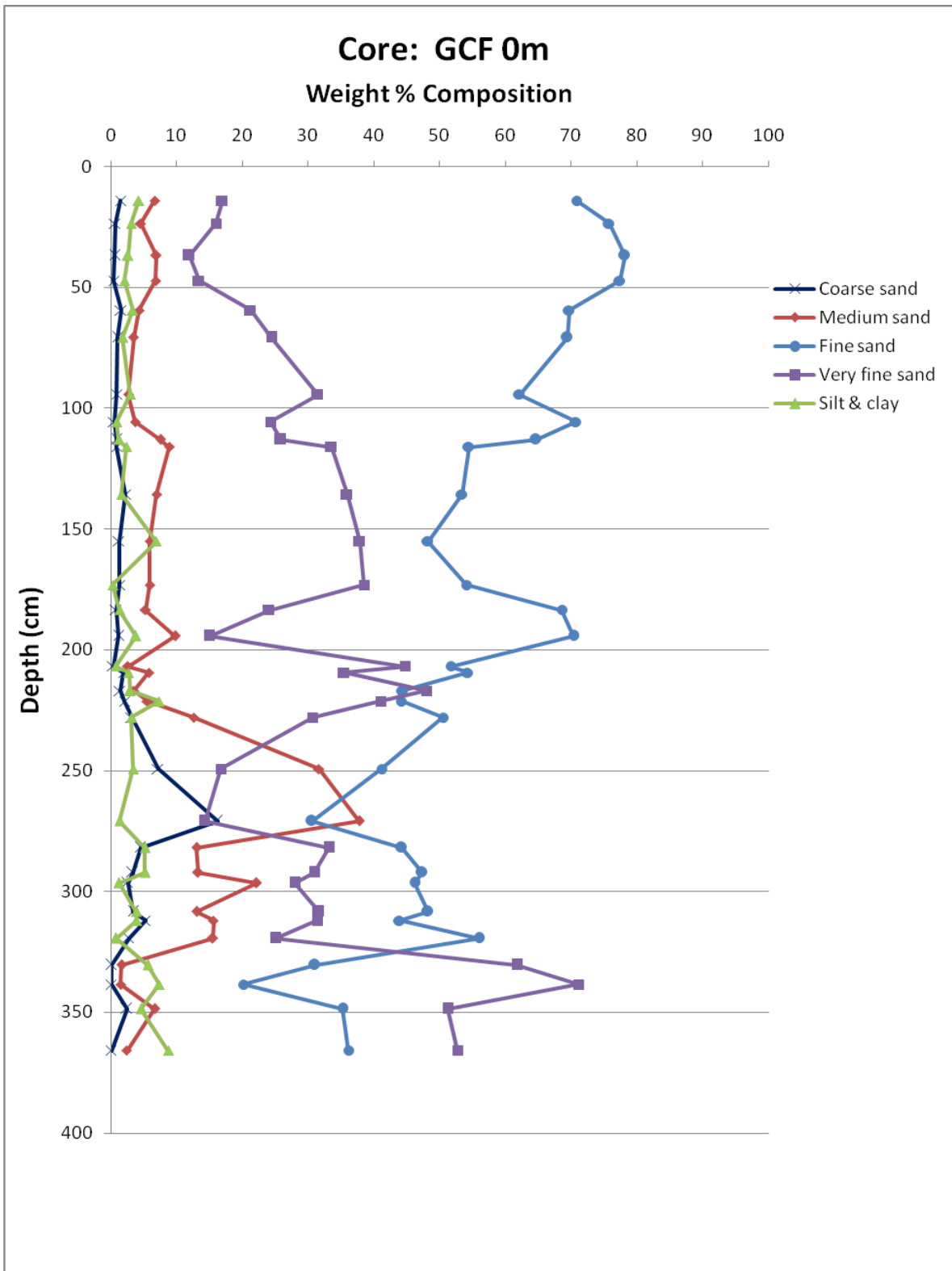


**Fig. 3.19** All grain size analysis results for core GCF 0m

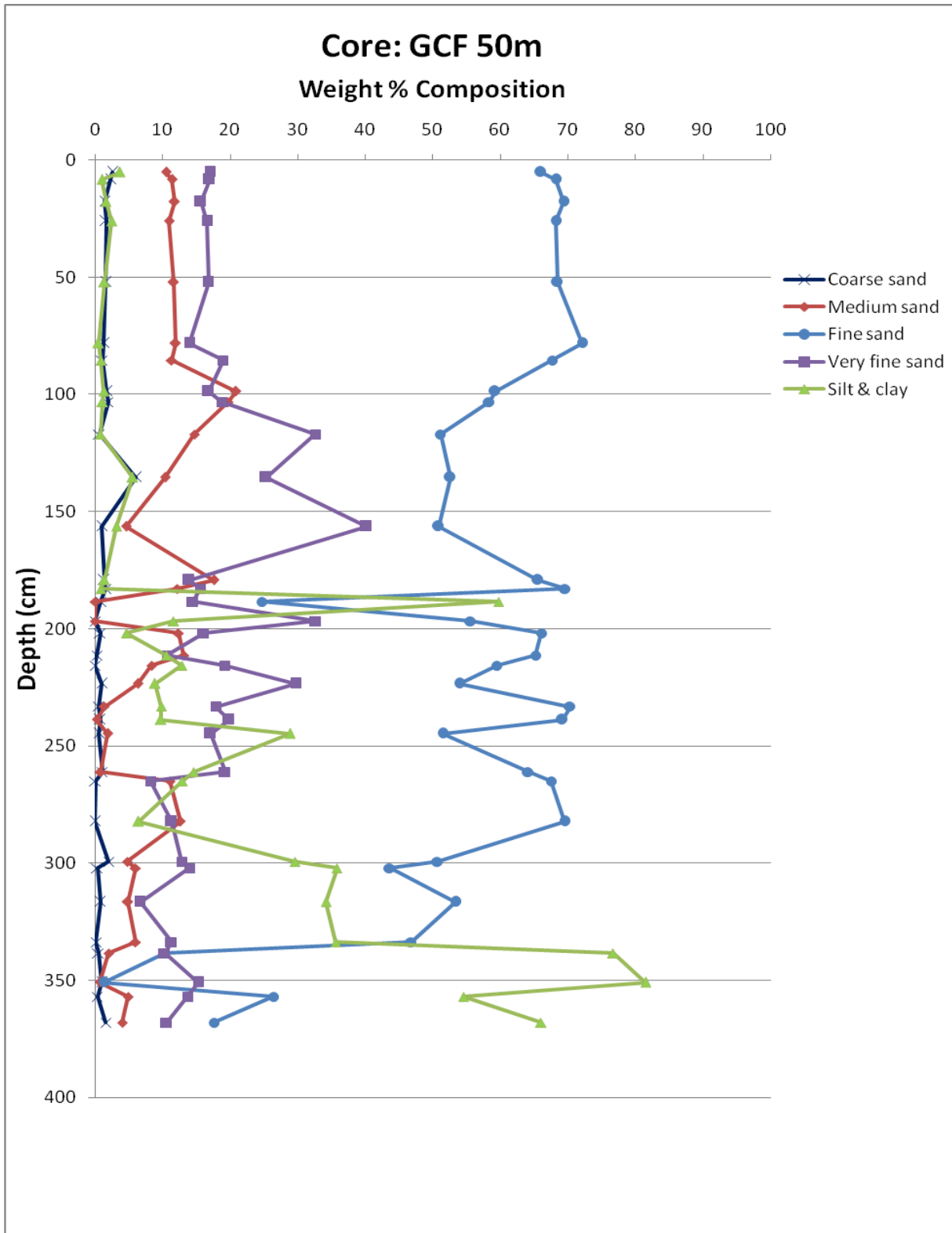


**Fig. 3.20** All grain size analysis results for core GCF 50m

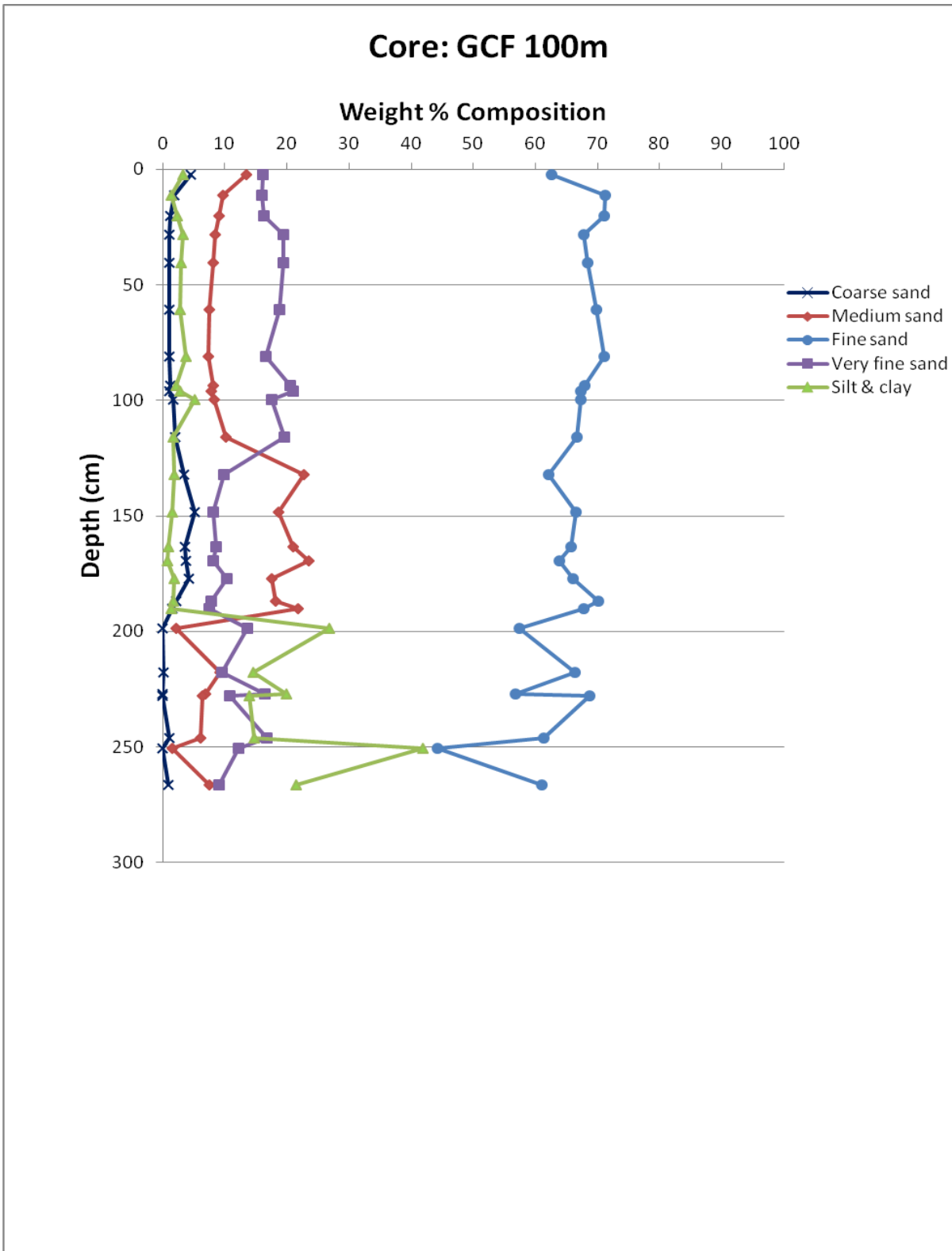
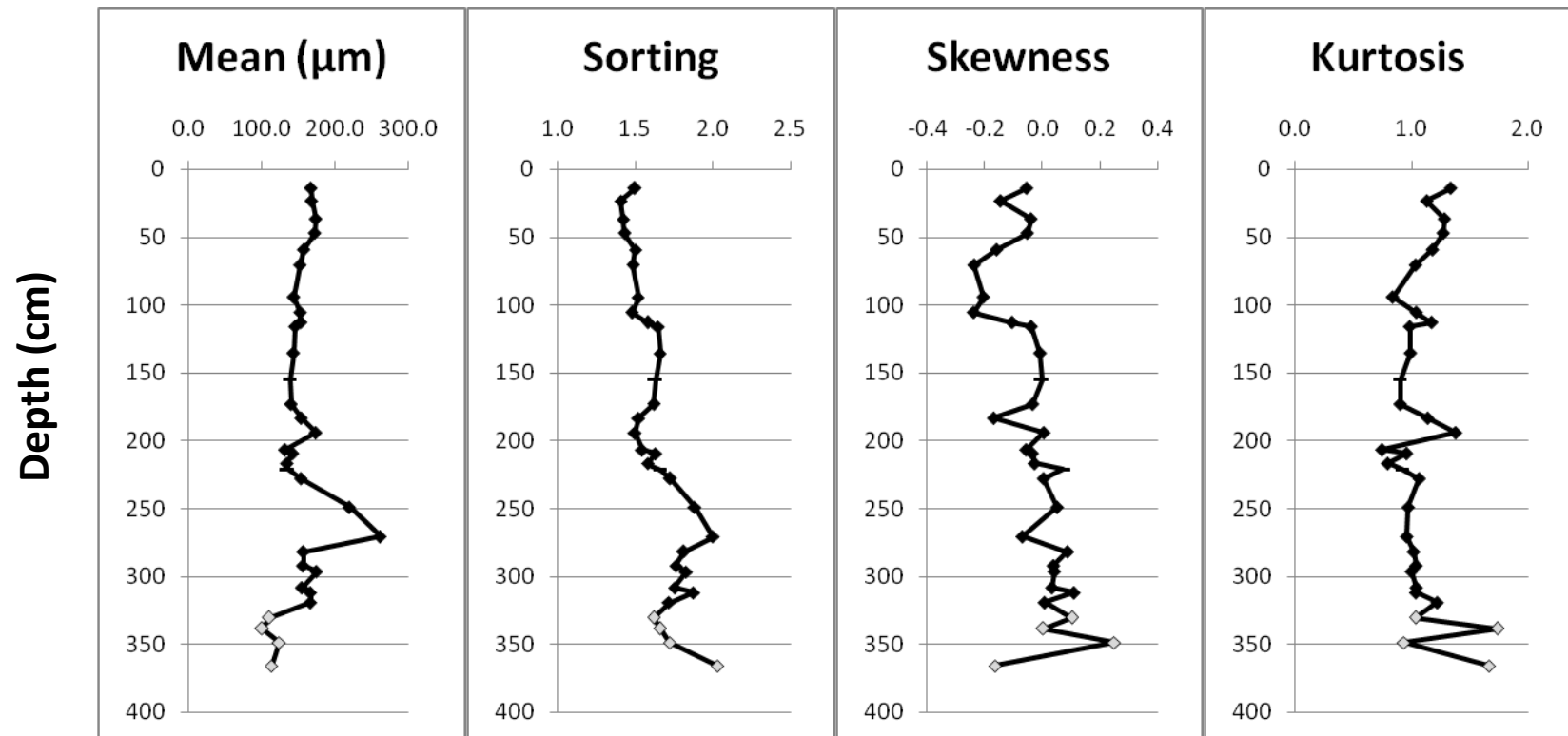
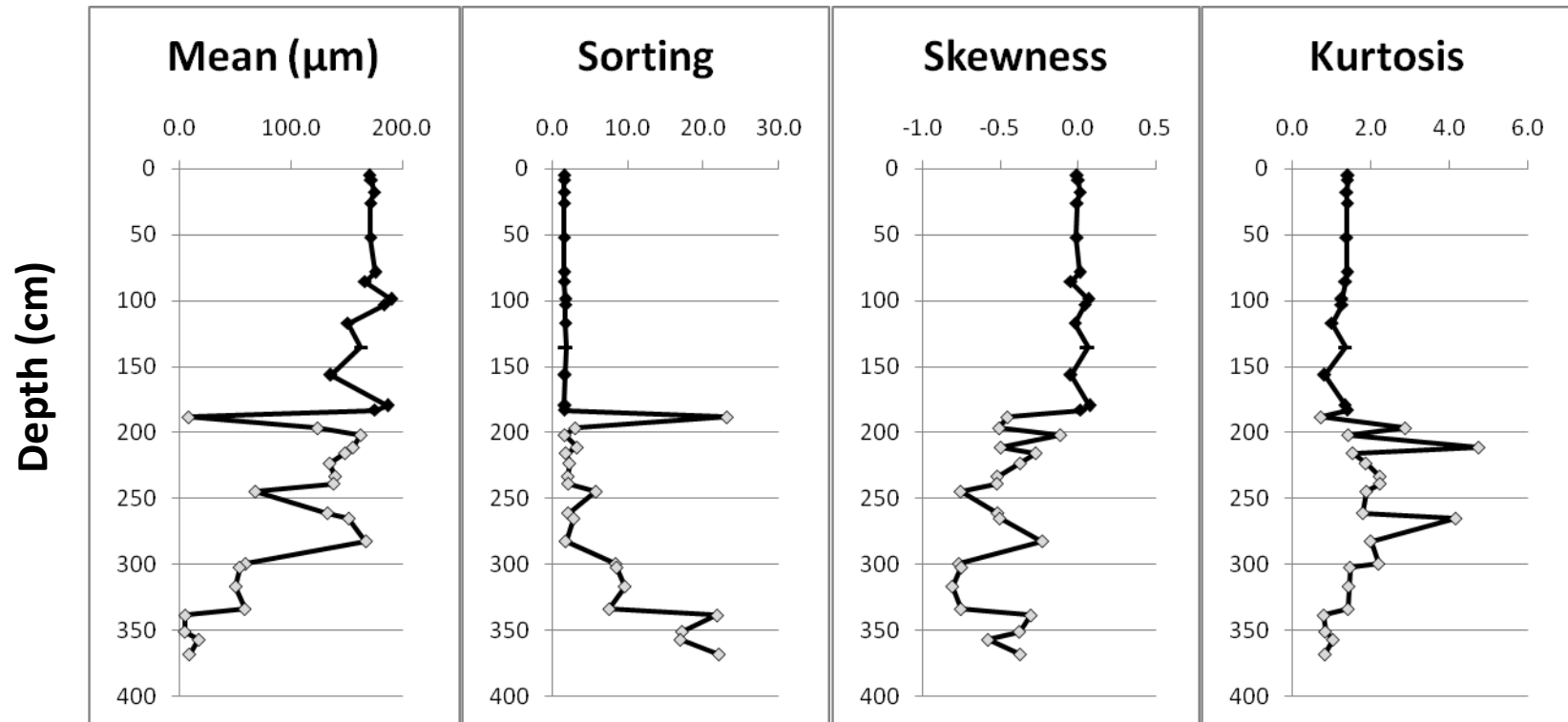


Fig. 3.21 All grain size analysis results for core GCF 100m



**Fig. 3.22** Grain size statistics for core GCF 0m. Points shaded grey represent grain size data obtained using wet sediment grain size analyses, which means that silt and clay content are included in those samples. Silt and clay are omitted from all dry sediment grain size statistic calculations. Points marked with a horizontal line represent grain size data obtained using dry sediment grain size analysis that contained > 5% silt and clay; these data likely contain a larger amount of error due to the omission of the silt and clay content. Key below from Blott and Pye, 2001.

Sorting		Skewness		Kurtosis	
Very well sorted	< 1.27	Very fine skewed	$-0.3$ to $-1.0$	Very platykurtic	< 0.67
Well sorted	1.27 to 1.41	Fine skewed	$-0.1$ to $-0.3$	Platykurtic	0.67 to 0.90
Moderately well sorted	1.41 to 1.62	Symmetrical	$-0.1$ to $+1.0$	Mesokurtic	0.90 to 1.11
Moderately sorted	1.62 to 2.00	Coarse skewed	$+0.1$ to $+0.3$	Leptokurtic	1.11 to 1.50
Poorly sorted	2.00 to 4.00	Very coarse skewed	$+0.3$ to $+1.0$	Very leptokurtic	1.50 to 3.00
Very poorly sorted	4.00 to 16.00			Extremely leptokurtic	> 3.00
Extremely poorly sorted	> 16.00				



**Fig. 3.23** Grain size statistics for core GCF 50m. Points shaded grey represent grain size data obtained using wet sediment grain size analyses, which means that silt and clay content are included in those samples. Silt and clay are omitted from all dry sediment grain size statistic calculations. Points marked with a horizontal line represent grain size data obtained using dry sediment grain size analysis that contained > 5% silt and clay; these data likely contain a larger amount of error due to the omission of the silt and clay content. Key below from Blott and Pye, 2001.

Sorting		Skewness		Kurtosis	
Very well sorted	< 1.27	Very fine skewed	$\bar{0}.3$ to $\bar{1}.0$	Very platykurtic	< 0.67
Well sorted	1.27 to 1.41	Fine skewed	$\bar{0}.1$ to $\bar{0}.3$	Platykurtic	0.67 to 0.90
Moderately well sorted	1.41 to 1.62	Symmetrical	$\bar{0}.1$ to $\bar{+}1.0$	Mesokurtic	0.90 to 1.11
Moderately sorted	1.62 to 2.00	Coarse skewed	$\bar{+}0.1$ to $\bar{+}0.3$	Leptokurtic	1.11 to 1.50
Poorly sorted	2.00 to 4.00	Very coarse skewed	$\bar{+}0.3$ to $\bar{+}1.0$	Very leptokurtic	1.50 to 3.00
Very poorly sorted	4.00 to 16.00			Extremely leptokurtic	> 3.00
Extremely poorly sorted	> 16.00				

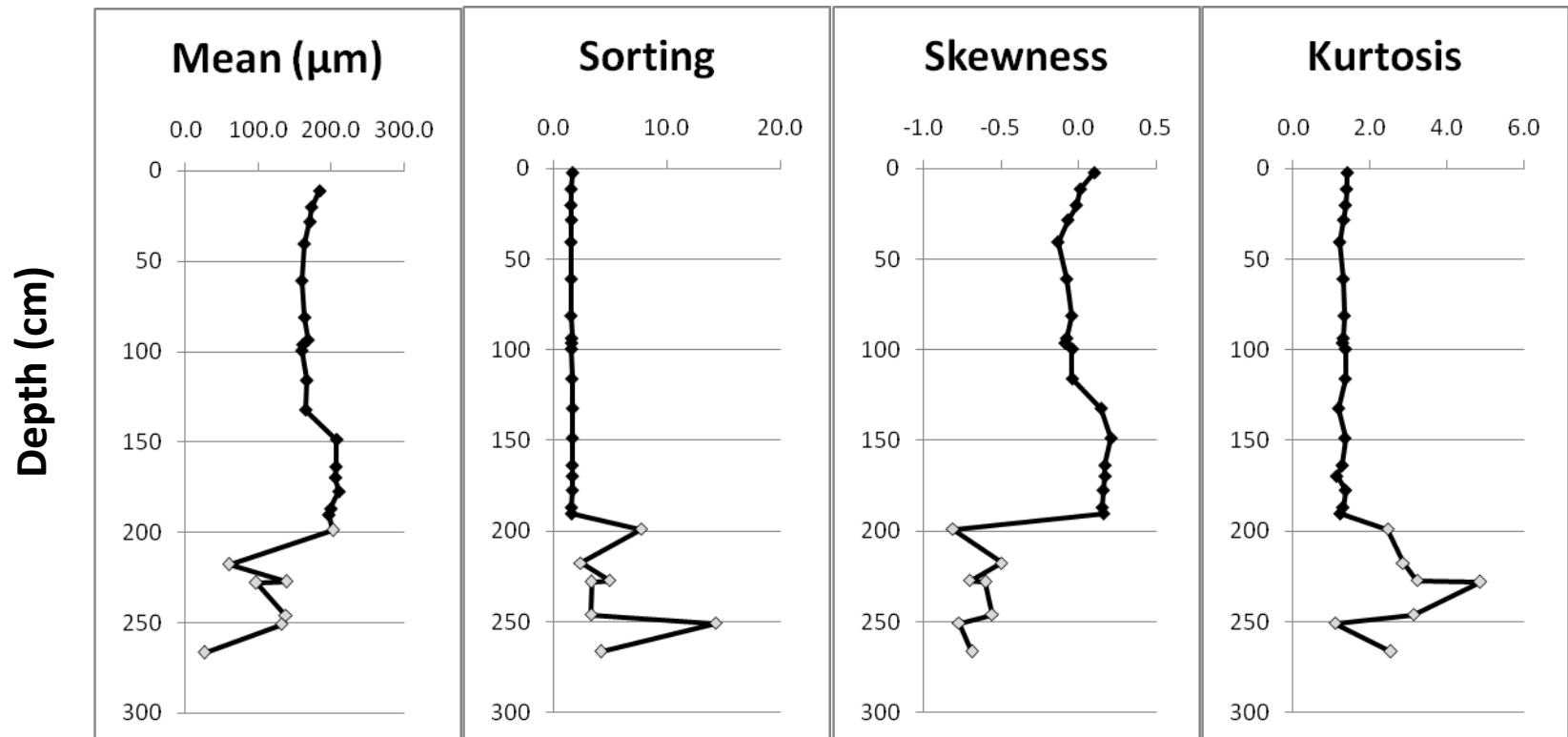


**Fig. 3.24** Grain size statistics for core GCF 100m. Points shaded grey represent grain size data obtained using wet sediment grain size analyses, which means that silt and clay content are included in those samples. Silt and clay are omitted from all dry sediment grain size statistic calculations. Points marked with a horizontal line represent grain size data obtained using dry sediment grain size analysis that contained > 5% silt and clay; these data likely contain a larger amount of error due to the omission of the silt and clay content. Key below from Blott and Pye, 2001.

Sorting		Skewness		Kurtosis	
Very well sorted	< 1.27	Very fine skewed	$-0.3$ to $-1.0$	Very platykurtic	< 0.67
Well sorted	1.27 to 1.41	Fine skewed	$-0.1$ to $-0.3$	Platykurtic	0.67 to 0.90
Moderately well sorted	1.41 to 1.62	Symmetrical	$-0.1$ to $+1.0$	Mesokurtic	0.90 to 1.11
Moderately sorted	1.62 to 2.00	Coarse skewed	$+0.1$ to $+0.3$	Leptokurtic	1.11 to 1.50
Poorly sorted	2.00 to 4.00	Very coarse skewed	$+0.3$ to $+1.0$	Very leptokurtic	1.50 to 3.00
Very poorly sorted	4.00 to 16.00			Extremely leptokurtic	> 3.00
Extremely poorly sorted	> 16.00				

## **GPR**

In September 2011, four GPR transects were collected directly along the 50 m to 100 m lines where cores had been collected in June 2011 (Fig. 2.2). As aforementioned, since the location of core UGA P did not directly align with the locations of cores UGA 0m and UGA 50m, a 50 m transect was collected starting at the location of core UGA P and running inland to the southeast 50 m. Thus, 50 m transects were collected starting at the location of core UGA P and between the locations of cores UGA 0m and UGA 50m. Between the locations of cores B 0m and B100m, a 100 m transect was collected. Another 100 m transect was collected running between the locations of cores GCF 0m and GCF 100m, intersecting the location of core GCF 50m along the way.

Post-processing of transects in RADAN® and addition of markers in Adobe Photoshop facilitated production of the radargrams included herein (Figs. 3.25, 3.26, 3.27, 3.28). Using GPR-SLICE®'s auto-detect tool, a dielectric constant of 18.37 and a wave velocity of 0.07 m/ns was estimated. This dielectric constant falls just below the typical range of dielectric constants for wet sand (20-30) and within the range of dielectric constants for clay (5-20) (Milsom and Erikson, 2011), and therefore should serve as a fairly accurate estimation of the true dielectric constants of the saturated sands and clays underlying the study locations. The dielectric constant and wave velocity determined by GPR-SLICE®'s auto-detect tool were used to calculate the time and depth scales for each radargram (Figs. 3.25, 3.26, 3.27, 3.28). However, due to the complexities of navigating GPR-SLICE® and the impracticality of editing the figures produced in GPR-SLICE®, the GPR-SLICE® figures are not included in this document.

In some locations, the 100 MHz antenna and RADAN® post-processing facilitated clear imaging of contacts between materials with different dielectric constants, whereas in other

locations, the contrast in subsurface material as represented in the radargrams was less pronounced. For example, in the 50 m transect that began at the location of core UGA P, no strong, continuous lateral reflectors are observed (Fig. 3.25). The most obvious reflectors in this radargram (Fig. 3.25) are the slightly inclined reflectors occurring in the top 3 m depth running horizontally from 0 m to ~9 m. Moderate subhorizontal reflectors are present at ~2 m depth from ~11 m to ~40 m horizontally, and are slightly shallower toward the island interior (i.e., towards 40 m horizontally).

Likewise, the 100 m transect collected along the locations of cores GCF 0m, GCF 50m, and GCF 100m displays no strong, continuous lateral reflectors. A weak lateral reflector is present at ~1 m depth across most of the radargram (Fig. 3.28). Near the location of core GCF 0 m, from ~85 m to 100 m horizontally in Fig 3.28, a strong isolated anomaly occurs at ~2 m depth. No additional strong isolated anomalies were observed elsewhere (or in any of the other radargrams).

In the remaining radargrams, Fig. 3.26 and Fig. 3.27, strong, continuous lateral reflectors are present. The 50 m transect collected between the locations of cores UGA 0m and UGA 50m contains a strong, inclined lateral reflector running from ~2 m depth at the location of core UGA 0m to ~3 m at the location of core UGA 50m. The 100 m transect collected between cores B 0m and B 100m contains a strong, slightly inclined lateral reflector running from ~3 m depth near the location of core B 0m to ~5 m depth at the location of core B 100m. Both of these radargrams (Figs. 3.26, 3.27) also contain moderately strong to strong continuous lateral reflectors at ~1 m depth.

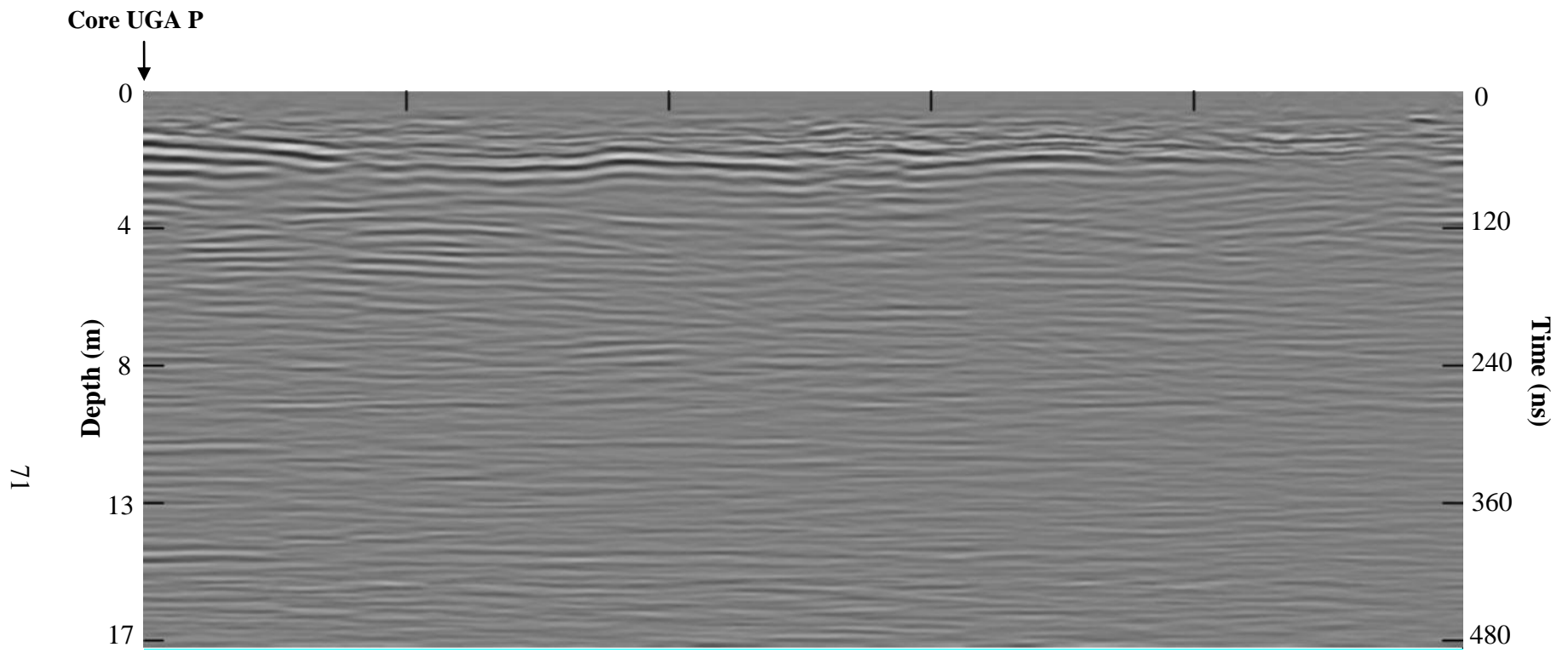


**Fig. 3.25** GPR radargram for a transect collected from the location of core UGA P running 50 m towards the island's interior. Horizontal distance is indicated by marks every 10 m across the top of the radargram.

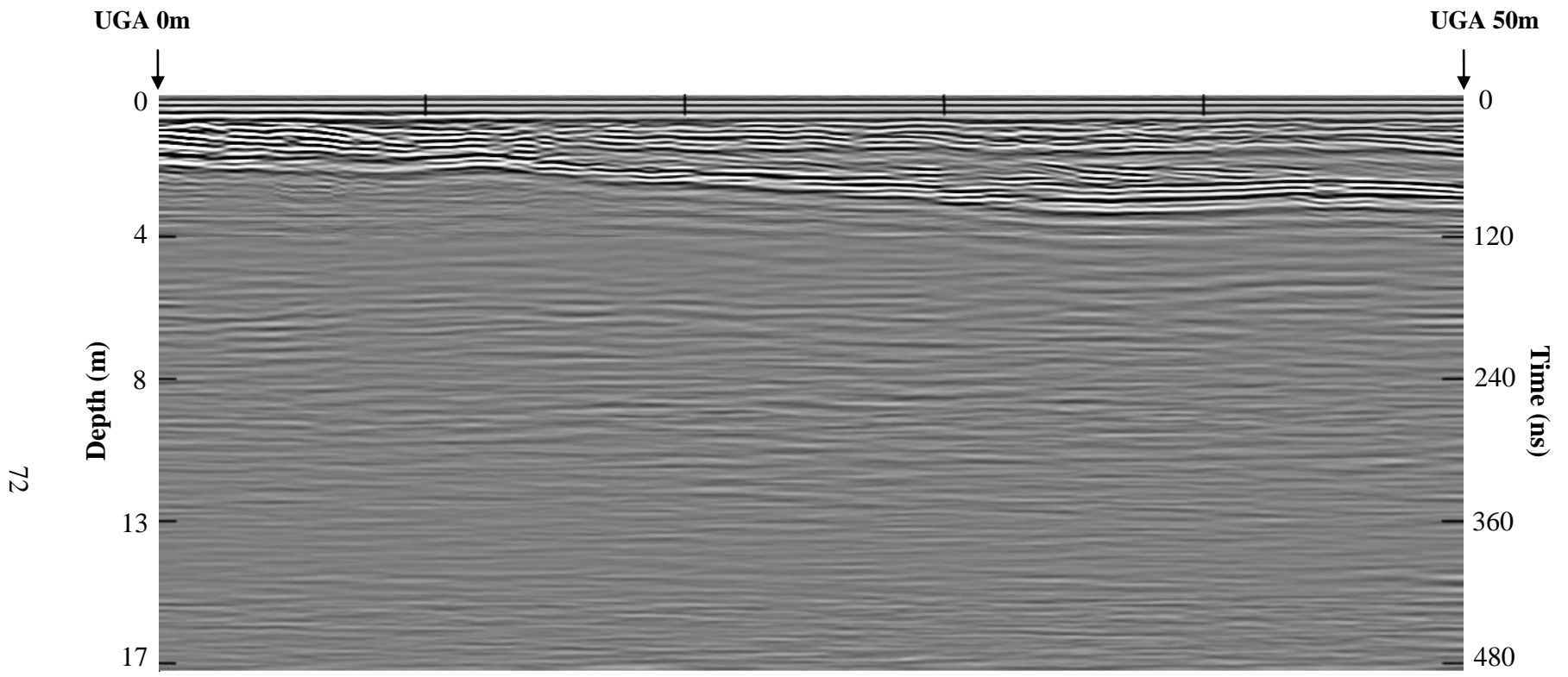


**Fig. 3.26** GPR radargram for a transect collected from the location of core UGA 0m running 50 m to the location of core UGA 50m. Horizontal distance is indicated by marks every 10 m across the top of the radargram.

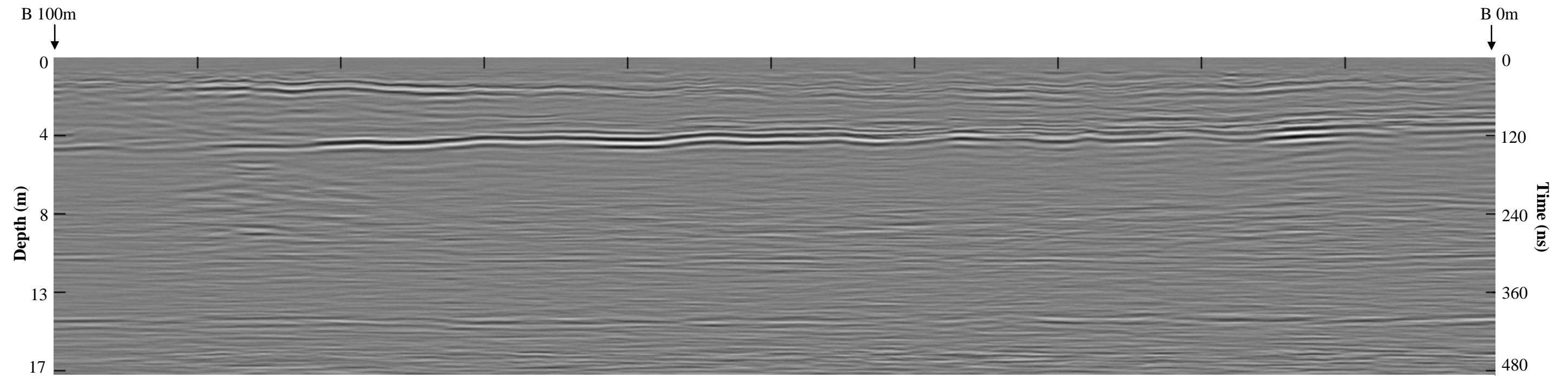


**Fig. 3.27** GPR radargram for a transect collected from the location of core B 100m running 100 m to the location of core B 0m. Horizontal distance is indicated by marks every 10 m across the top of the radargram.

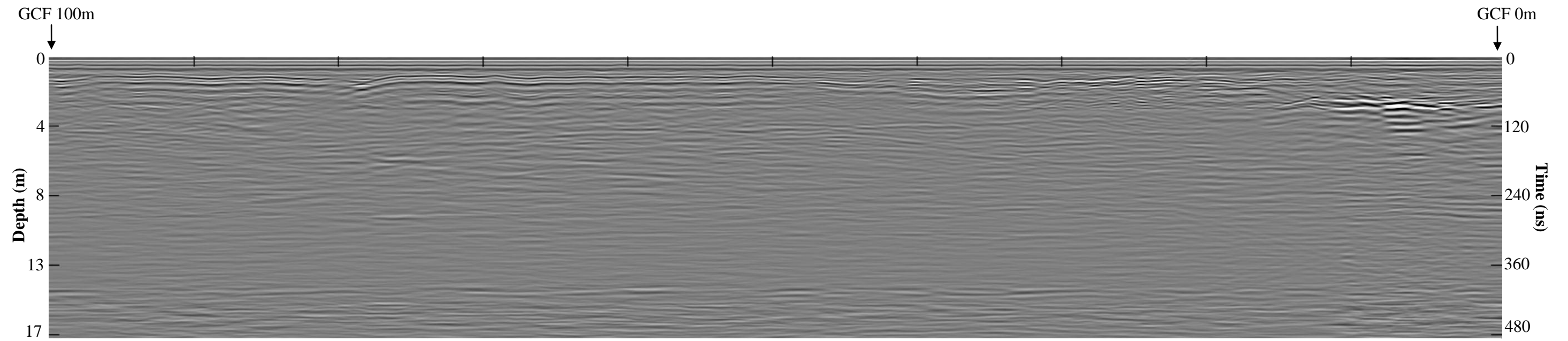


**Fig. 3.28** GPR radargram for a transect collected from the location of core GCF 100m running 100 m to the location of core GCF 0m. Horizontal distance is indicated by marks every 10 m across the top of the radargram.

## Geochronology

Four sediment samples were dated using OSL, and two wood samples were dated using AMS-RC dating (Table 3.10). The OSL dates from UGA P are acceptable in that the deeper sample returns an older date; however, the relatively deep AMS-RC samples from UGA P returned dates that were younger than the dates produced for the overlying sediment using OSL. Likewise, the OSL dates for the GCF 50m samples are problematic in that the deeper sample produced a younger date.

**Table 3.10:** Summary of absolute dating results

Core	Depth (cm)	Age (ka BP or <sup>14</sup> C BP)	Method
<b>GCF 50 m</b> (Sample UGA12OSL-857)	~137 cm	101.91 ± 10.91 ka BP	OSL
<b>GCF 50 m</b> (Sample UGA12OSL-858)	~257 cm	70.85 ± 9.87 ka BP	OSL
<b>UGA P</b> (Sample UGA11OSL-788)	~100 cm	54.01 ± 6.75 ka BP	OSL
<b>UGA P</b> (Sample UGA11OSL-787)	~200 cm	103.01 ± 10.4 ka BP	OSL
<b>UGA P</b> (Sample UGAMS#11308)	313.5 - 317 cm	46,380 ± 320 <sup>14</sup> C age in years BP	AMS
<b>UGA P</b> (Sample UGAMS#11309)	318.4 - 322 cm	> 57,560 <sup>14</sup> C age in years BP	AMS

Data provided along with the OSL dates by the UGA Luminescence Dating Laboratory is presented in Table 3.11. Note the high uranium content of the sample from ~ 257 cm in core GCF 50m relative to the uranium content measured in all other samples. To double-check this difference, scientists at the UGA Luminescence Dating Laboratory calculated the dose rate for sample GCF 50m ~257 cm twice and obtained similar results each time (George Brook, personal communication).

**Table 3.11:** OSL age data as reported by the UGA Luminescence Dating Laboratory

	<b>Core: GCF 50m</b>	<b>Core: GCF 50m</b>	<b>Core: UGA P</b>	<b>Core: UGA P</b>
	<b>Depth: ~137 cm</b>	<b>Depth: ~257 cm</b>	<b>Depth: ~100 cm</b>	<b>Depth: ~200 cm</b>
<b>Lab number</b>	UGA12OSL-857	UGA12OSL-858	UGA11OSL-788	UGA11OSL-787
<b>Aliquots</b>	22	24	19	23
<b>Dose (Gy)</b>	126.67 ± 3.34	165.05 ± 6.11	105.65 ± 3.01	120.44 ± 1.64
<b>U (ppm)</b>	1.69 ± 0.21	5.45 ± 0.8	2.94 ± 0.66	2.34 ± 0.29
<b>Th (ppm)</b>	2.84 ± 0.76	9.46 ± 2.76	11.19 ± 2.25	4.08 ± 1.0
<b>K (%)</b>	0.5	0.4	0.3	0.3
<b>Water content (%)</b>	5 ± 2.5	10 ± 5	5 ± 2.5	13 ± 5
<b>Cosmic dose rate (Gy/ka)*</b>	0.17	0.15	0.18	0.16
<b>Dose rate (Gy/ka)</b>	1.24 ± 0.13	2.33 ± 0.31	1.96 ± 0.24	1.17 ± 0.12
<b>Age (ka BP)</b>	101.91 ± 10.91	70.85 ± 9.87	54.01 ± 6.75	103.01 ± 10.4

\* Cosmic dose rate error bar is ±0.02 Gy/ka

## CHAPTER 4 DISCUSSION

### Geological Interpretations

#### *Geochronology*

By comparing the OSL and AMS-RC dates (Table 3.10) with the data displayed in Fig. 4.1, each date can be correlated with the appropriate Marine Isotope Stage (MIS) and each stage's corresponding sea level relative to modern sea level. Thus, the  $54.01 \pm 6.75$  ka BP age of the sediments from 100 cm in core UGA P corresponds to early MIS 3 and a sea level at roughly -85 m below the modern sea level. The  $101.91 \pm 10.91$  ka BP age of the sediments from ~137 cm in core GCF 50m and the  $103.01 \pm 10.4$  ka BP age of the sediments from ~200 cm in core UGA P correspond to MIS 5c and a sea level at roughly -30 m below the modern sea level.

The OSL dates from core UGA P correspond well by depth (i.e. the deeper sample returns an older age, as expected), while the OSL dates between two samples in each core (~137 cm in core GCF 50m and 200 cm in core UGA P) correspond well laterally. Likewise, the AMS sample from 318.4-322 cm in core UGA P, whose age falls outside the limits of radiocarbon dating, does not conflict with the aforementioned dates (Table 3.10). However, reconciliation of the OSL date from ~257cm in core GCF 50m and the AMS date from 313.5-317 cm in core UGA P proves less straightforward, since these samples returned dates that are younger than dates provided by the overlying strata. The problem with the deeper, but younger (according to OSL), sample from core GCF 50 m might be explained by the disproportionately high uranium content of that sample (Table 3.11). The presence of radioactive heavy minerals in sands may

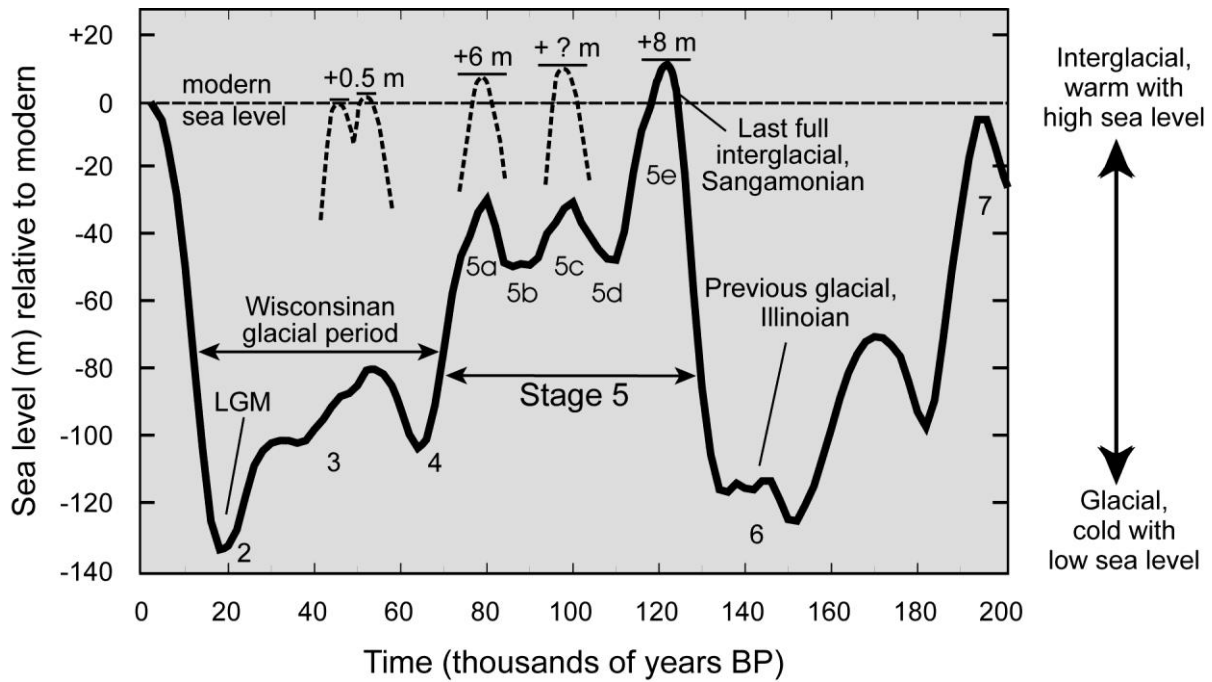


**Fig. 4.1** Marine Isotope Stages correlated with sea level fluctuation over time (Krantz, 2011; data from Martinson et al., 1987).

cause saturation of the signal over time; when dated using OSL, such signal saturation can cause the sample to appear younger than its true age. This problem is not uncommon in Pleistocene-aged sands (Clark Alexander, personal communication).

Furthermore, the discrepancy caused by the AMS date from 313.5-317 cm in core UGA P (Table 3.10) could be explained by the effects of bioturbation. The wood dated for this sample might have been part of a root that grew down into older strata, or have been relocated into older strata by a burrowing creature. Similar mechanisms should be considered for emplacement of the second AMS sample (from 318.4-322 cm in core UGA P). Although the potential age of this deeper AMS sample does not overtly conflict with the geochronology established by the overlying OSL samples, the proximity of this sample to the other AMS sample along with the

possibility that the sample's true age falls close to the  $> 57,560$   $^{14}\text{C}$  age in years BP date (and thereby does conflict with the overlying OSL geochronology) renders such considerations worthwhile.

Therefore, the OSL dates indicate that the core of northwestern Skidaway Island formed no more recently than the Late Pleistocene. These results confirm Hoyt and Hails' (1974) designation of western Skidaway Island as part of the Princess Anne terrace, which formed part of Georgia's coastline during MIS 5. The results likewise do not conflict with Markewich et al.'s (2013) tentative designation of the Princess Anne terrace as forming during MIS 5e..

### ***Implications for Skidaway Island's Architecture and Depositional History***

The blue-grey silt- and clay-rich sediments found at the bases of cores UGA 0m, UGA 50m, B 0m, and GCF 50m represent an ancient marsh upon which sandy sediments were later deposited. The kaolinite and interlayered smectite/illite commonly detected and the pyrite occasionally detected within these sediments are typical of the mineralogy of marsh deposits on the Georgia coast (Freile et al., 2004; Cowan et al., 2004). This marsh formed behind an ancient shoreline, and likely formed directly behind a paleobarrier island whose sediments were later pushed back on top of the marsh by transgressing sea level to form the core of modern Skidaway Island. Based on OSL dates obtained in this study ( $101.91 \pm 10.91$  ka at ~137 cmbs in core GCF 50m and  $103.01 \pm 10.4$  ka at 200 cmbs in core UGA P), this basal ancient marsh can be relatively dated to *at least* the Late Pleistocene. In all cores where it is present, the basal marsh lies well below the absolutely dated sediments from cores GCF 50m and UGA P (Table 4.1). Thus, although an exact date for the basal marsh cannot be determined without obtaining further absolute dates, the marsh likely dates to near the start of the Late Pleistocene, during MIS 5e.

**Table 4.1** Comparison of Depths to OSL-dated Sediments and Top of Basal Marsh Sediments

Core	UGA P	UGA 0m	UGA 50m	B 0m	GCF 50m
Depth to OSL sample (cm)	~200 cm	-	-	-	~137 cm
Depth to top of basal marsh (cm)	-	212 cm	393 cm	375 cm	339 cm

The discontinuity of the basal marsh sediments across all cores- in terms of both presence and depth- attests to the complexity of sediment deposition and preservation in coastal environments. Granted, some cores, like B 100m at 186 cm total depth and GCF 100m at 269.5 cm total depth, did not penetrate deep enough to assess the presence or absence of basal marsh sediments in those locations. Other cores, however, like UGA P at 334 cm and GCF 0m at 375.5 cm, penetrated as deep as or deeper than their nearest marsh clay-containing neighbor without reaching a continuous basal clay layer. Even in adjacent marsh clay-containing cores, the depth to the top of the basal clay proves highly variable (Table 4.1); cores UGA 0m and UGA 50m were collected only 50 m apart, yet the basal clay is encountered 181 cm deeper in core UGA 50m. Therefore, the basal clay layer does not appear to be laterally continuous across the island and, in places where the basal clay layer is laterally continuous, the depth to that layer is highly variable. This variability in depth may account for the apparent lack of a basal clay layer in relatively deep cores like UGA P and GCF 0m, under which an even deeper-lying basal clay layer may exist. However, based on both the cores and GPR data (discussed later) obtained in this study, no continuous layer of clay exists at the locations of cores UGA P and GCF 0m.

Additional data are needed to reliably interpret whether a basal clay layer was deposited and later eroded from these locations, or whether different depositional environments adjacent to or within

the ancient marsh resulted in deposition of different sediment types at the locations of cores UGA P and GCF 0m.

A unique horizon encountered at the base of core UGA P certainly indicates that, at some point in this location's depositional history, different depositional (and possibly erosional) or pedogenic processes were acting upon this location. From 295 cmbs to the base of core UGA P (334 cmbs), a black, organic-rich sediment layer is present (Fig. 3.1). This layer is dominated by fine sand (45-65%), although it is overlain by a silt- and clay-rich layer (49%), and the uppermost sample from this horizon contains 40% silt and clay. The wood samples dated using AMS-RC analysis (Table 3.10) came from this layer.

The presence of large organic materials (i.e., the wood samples) along with the apparent abundance of organic materials throughout this black sediment suggest that the organic-rich nature of this layer is due to the depositional environment in which it formed. If so, then the organic-rich layer likely represents a buried A horizon, or paleosol. However, the organic-rich nature of this layer could also be attributed to translocation and consolidation of fine organic materials into a spodic horizon that was later penetrated by roots (i.e., the wood samples) (Bill Miller, personal communication).

To evaluate these competing hypotheses, the Fe and Al content of the organic-rich sediments could be chemically extracted and measured (Soil Survey Staff, 1992). A buried A horizon would exhibit low Fe and Al content, whereas a spodic horizon by definition contains relatively higher amounts of Fe and Al (Bill Miller, personal communication; McKeague et al., 1983). The Fe and Al test could not be conducted within the timeframe of this study.

Moving up all cores from the basal marsh and laterally neighboring environs, fine sand is the dominant grain size in nearly every sample. In some cases, very fine sand is the dominant grain size, and there are also occasional cases of silt and clay dominating the grain size fraction. A single sample in core GCF 0m, at 271 cmbs, contains medium sand as the dominant grain size; there are notable occurrences of medium sand and even occasional coarse sand increase in other cores, but this sample represents the only case where relatively coarse-grained sand dominates. These exceptions to the general dominance of fine sand above the basal clay layer indicate that different depositional and/or erosional processes were acting upon the island during the time periods represented by these sediments.

A unique area of coarse sediment increase in the two cores nearest the eastern border of Skidaway Island likely represents distinct depositional and erosional processes. At 236 cmbs in core B 0m and 271 cmbs in core GCF 0m, both medium and coarse sand content increase appreciably. These samples represent the only samples from any core containing > 10% coarse sand, and the GCF 0m 271 cm sample represents the only sample where medium sand is the dominant grain size. Relative dating places these sediments' ages well before the MIS 5c OSL dates obtained from ~137cmbs in core GCF 50m and ~200 cmbs in core UGA P. Thus, I propose that the observed increases in coarse and medium sand observed only in the eastern-most cores represent a period early in the Princess Anne portion of the island's depositional history, perhaps when these eastern-most locations were relatively close to the active coast, where medium to coarse grained sands are prevalent (Gorsline, 1963). Identifying these locations as nearest the active coastline during the periods represented by an increase in coarse grained sediments would explain why only the eastern-most cores display this trend. The proposed relative ages for the sediments in question would fit this explanation, since this area would have been an active

coastline just before or after the highstand of MIS 5e (Fig. 4.1). However, additional absolute age controls are needed to confirm or disprove this idea.

Below ~200 cm in cores GCF 50m and GCF 100m, fine sand dominated samples contain relatively high amounts of silt and clay, and appreciable amounts of very fine sand and medium sand as well. The relatively diverse sediments are sufficient to cause samples from below 200 cm in these cores to be statistically classified as poorly to extremely poorly sorted (with the exception of three moderately sorted samples below 200 cm in core GCF 50m). These mixed sediments could represent reworking of underlying fine-grained marsh sediments into new deposits as sea level fluctuated and coarser-grained sediments were deposited atop the ancient marsh facies. Indeed, at the relatively older Wicomico terrace, Markewich et al. (2013) describe a "zone of mixing" located between eolian sands and underlying finer-grained deposits that displays grain size characteristics very similar to the characteristics described here (p. 60). In core GCF 50m, silt- and clay-rich marsh sediments directly underlie the mixed sediments; core GCF 100m did not penetrate deep enough to determine whether an underlying clay facies is present at that location.

However, it should also be noted that sediments from 188 cm in core GCF 50m and 199 cm in core GCF 100m show notable increases in silt and clay content (Figs. 3.20, 3.21) and were sampled from areas containing relatively abundant fine to very fine roots (Figs. 3.17, 3.18). The increase in fine-grained sediments and root matter in these samples may indicate that a shallow water body once existed in this location. Relative dating places these deposits' ages near the MIS 5c OSL dates obtained from ~137 cmbs in core GCF 50m and ~200 cmbs in core UGA P. The -30 m sea level (relative to modern sea level) during MIS 5c (Fig. 4.1) would have left Skidaway Island subaerially exposed during that time; thus, interpretation of the relatively fine-grained,

rooty deposits from ~200 cm in cores GCF 50m and GCF 100m as evidence of an inland shallow water body in that location is plausible.

Above 200 cm in all cores, fine sand is the dominant grain size; a single exception occurs at the previously discussed silt- and clay-dominated sample from 188 cm in core GCF 50m. All fine sand dominated samples that do not contain an appreciable amount of silt and clay are statistically classified as moderately to moderately well sorted. These subangular sands likely represent former dune or beach sediments that have been well sorted by eolian winnowing (Alexander et al., 2008). The leptokurtic distributions of most of these relatively well sorted, fine sand dominated samples further supports interpretation of these sands as former dune sands (Leigh, 1998). Sedimentary structures (e.g., dipping bedding or layers of heavy mineral accumulation) are typically used to confirm past dune and beach environments (Frey and Howard, 1988; Darrell et al., 1993; Wells, 2001; Alexander et al., 2011), but those indicators (if present in the subsurface of Skidaway Island) were not well preserved in my predominantly unconsolidated sediment cores.

In at least one sample in every core, there is a noticeable increase in medium sand (although this grain size dominates only the sample from 271 cmbs in core GCF 0m). Medium sand is the second most abundant grain size for all samples above 200 cm in cores UGA 0m and UGA P. These cores were collected closest to the western side of the island, which lies adjacent to the Skidaway River (Fig. 2.2). Thus, the sustained increase in medium sand above 200 cm in these cores may represent the influence of deposition of relatively coarse-grained sediments from the Skidaway River (and any paleorivers that occupied similar channels) along the western border of the island. This explanation is bolstered by the fact that no other cores show sustained increases in medium sand content.

However, as aforementioned, all cores including samples deeper in cores UGA 0m and UGA P do show occasional marked increases in medium sand. These areas of relatively coarse sediment increase may represent periods of regression and erosion, as rivers deposited coarser grained sediments further out along the continental shelf and exposed fine sediments were eroded away. In a study of a Pleistocene-aged outcrop associated with the Pamlico terrace, Howard and Scott (1983) attributed an increase in coarse sands at the base of a transgressive sequence as the contact with previous (presumably eroded) deposits. Likewise, in modern riverine dunes, eolian processes acting on exposed sands leave behind a layer of coarse sediments (Ivester and Leigh, 2003).

Comparison of marked medium sand increases to ~32% in samples from ~150 cmbs in cores UGA 0m and UGA P with the OSL dates obtained from core UGA P supports the idea that the increase in coarse sediments represents an erosional contact produced by a period of prolonged subaerial exposure. The increase in medium sand in these cores lies between sediments dated to the relatively warm MIS 3 and MIS 5 periods; thus, the increase in coarser grained sediments may represent increased erosion as sea level regressed even farther during relatively cold MIS 4. However, this idea cannot be confirmed without additional absolute age controls for the sediments in question. Areas of medium sand increase in other cores may likewise correspond to periods of regression and subaerial erosion, but, again, additional dates are needed to further test this idea.

Finally, sediment mineralogy may yield a clue regarding the island's depositional history. In a study relating mineralogy to provenance for sediments located on the continental shelf off of Georgia, Carver (1971) concluded that hornblende-rich sediments represented periods of sea level stillstand when longshore currents transported hornblende-rich sediment southward from

northern sediment sources. At least one bulk XRD sample from every core except cores UGA 0m and UGA 50m contained detectable amounts of an Fe-rich amphibole. The amphibole-bearing sample from UGA P 2 cm represents sediments deposited during the most recent stillstand. Likewise, the amphibole-bearing sediments in other cores may represent past periods of stillstand and longshore transport, since the typical source of sediment for Georgia's northern barrier islands- the Savannah River- contains relatively amphibole-poor sediments (Carver, 1971). As with the previously discussed interpretations, more robust age controls are needed to further evaluate the validity of this idea.

#### ***Comparison of GPR Results with Cores***

As anticipated, the 100 MHz antenna facilitated clear imaging of the contact between sand and clay facies in the subsurface due to the contrast between the dielectric constants of these two materials. For example, the strong lateral signal observed in the radargram from the Bluff corresponds well with the start of the clay horizon at 352 cmbs in core B 0m (Figs. 3.10, 3.27). The weakening of that reflector towards the inland side of the field, where core B 100m was collected, may indicate that a continuous clay layer would not have been reached even if core B 100m had extended further into the subsurface. However, without deeper core penetration, it is impossible to determine whether or not a clay horizon exists below ~5 mbs at the location of core B 100 m, as the radargram (Fig. 3.27) seems to suggest.

Similar to the comparison for the location of core B 0m, comparison of cores UGA 0m and UGA 50m with the GPR results proves very straightforward. The slightly dipping strong lateral signal observed in the radargram from the UGA field corresponds well with the start of the clay horizons observed in cores UGA 0m and UGA 50m (Figs. 3.2, 3.3, 3.26). Towards the

island edge, the clay horizon is encountered at 211 cmbs (in core UGA 0m) and dips down as one moves towards the island interior, as reflected by the radargram and relatively deeper location of the clay horizon at 392 cmbs in core UGA 50 m.

In contrast, no vertically continuous clay horizon is observed in nearby core UGA P, which is located closest to the western edge of the island. Accordingly, no strong lateral reflector exists in the radargram collected starting at the location of core UGA P and moving inland. Thus, it seems that no vertically or laterally continuous clay horizon exists in that area.

The correlation of continuous clay horizons or lack thereof between the aforementioned cores and the GPR transects collected directly above those core locations proves relatively simple. However, the analysis of a potential clay horizon when interpreting both the GPR results and cores from the field adjacent to the Grove's Creek site proves difficult. In the GCF cores, a vertically continuous clay horizon is only encountered below 339 cm in core GCF 50m. No vertically continuous clay horizon is encountered in either core GCF 0m or core GCF 100m, although the relative grain size of both cores is fining downwards in the last horizon collected for each core. Accordingly, the radargram from this location is equally ambiguous. A weak signal detected at ~4 m depth running horizontally from 0 m to ~64 m across the transect may indicate the presence of a continuous clay horizon at this location (Fig. 3.28). However, deeper cores are needed to confirm or disprove this interpretation.

Near the location of core GCF 0m, a strong isolated anomaly was observed in the radargram (Fig. 3.28) from the field adjacent to the Grove's Creek archaeological site (9CH71). This anomaly and its implications will be further discussed in the following section. No additional strong isolated anomalies were observed in radargrams from the other locations.

## **Archaeological Interpretations**

### *Near Grove's Creek site (archaeological site 9CH71)*

#### *Geophysical Evidence*

One potential and one definite indicator of past human presence were found in the data collected from the field adjacent to the Grove's Creek archaeological site. The potential indicator consists of a strong anomaly detected in the GPR radargram near the location of core GCF 0m, which is the core located closest to the Grove's Creek site (Fig. 4.2). The anomaly measures approximately 15 m horizontally and extends from ~2 m below the surface to ~5 m depth (Fig. 3.28). Apparently the bulk of the anomaly is located just adjacent to the location of the GCF 0m core, since no clues as to the anomaly's identity (i.e., a change in grain size or saturation, or any archaeological indicators) were recovered from core GCF 0m.

The proximity of this anomaly to the Grove's Creek site raises the question of whether or not this anomaly indicates the location of a previously unknown archeological deposit. Typical archaeological deposits that can cause geophysical anomalies include house floors and middens (Conyers and Goodman, 1997). However, this anomaly is likely too big, too deep, and too peripheral to the known extent of the Grove's Creek site (as indicated by the excavation units shown in Fig. 4.2) to be a structure or a midden. Also, the depth of the anomaly proves problematic in associating the anomaly, which lies  $\geq 2$  m below the surface, with the Grove's Creek archaeological materials; no artifacts or features have been found below 1.5 m depth at the Grove's Creek site (Garrison, 2007). If the anomaly is archaeological in origin, then one final potential explanation exists; the anomaly could represent a borrow pit for the slight mound upon which the Grove's Creek structures appear to be built (Mark Williams, personal communication)

(Fig. 4.3). However, it is also possible that the anomaly is purely geologic in origin, in which case the anomaly may represent a buried extension of the drainage apparent in Fig. 4.2.

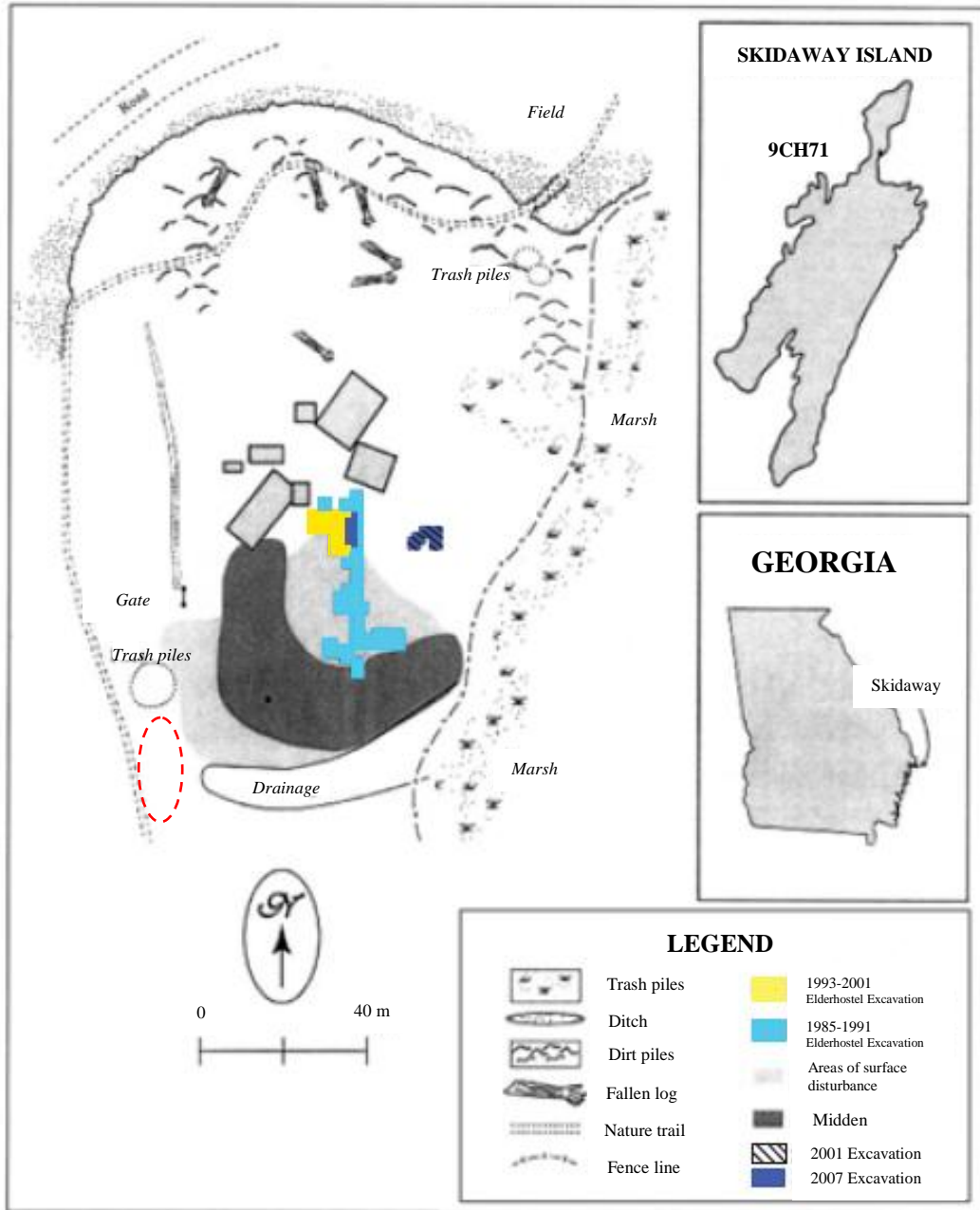


**Fig. 4.2** Map of the Grove's Creek site (9CH71) with the approximate location of core GCF 0m indicated by the dashed red circle (modified from Garrison, 2007).

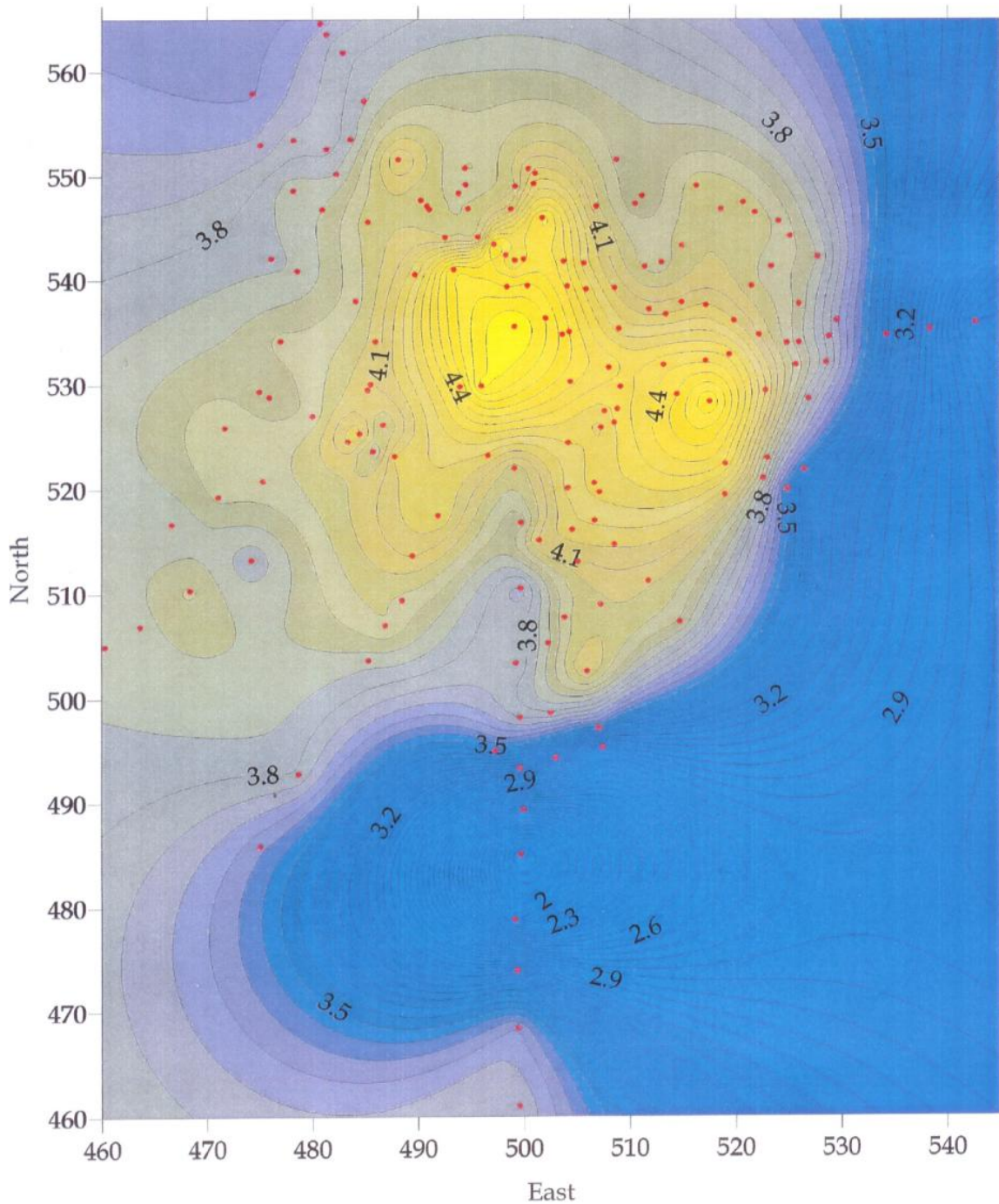


**Fig. 4.3** Topographic map of the Grove's Creek site (9CH71). Lighter colors represent topographically higher elevations. Note the roughly circular topographic high displayed in the map's upper half; this circular high may represent a low mound that the inhabitants of the site constructed upon which to built their homes. The structures excavated at the site are located in this topographically high area (Garrison, 2007, courtesy of Mark Williams).

### *Physical Evidence*

The only tangible proof of past human presence found in the GCF cores was a small fragment of Coastal Plain chert recovered from 26 cmbs in core GCF 50m (Fig. 4.4). This tertiary flake fragment exhibits no bulb of percussion and no platform, and has not been heat treated. The fragment shows evidence of human modification but displays no signs of wear, and retains a sharp edge. Due to the fragment's small size (approximately 19 mm x 6 mm x 4 mm), it is impossible to determine whether this fragment was part of a larger tool or merely a byproduct of tool manufacture. Likewise, the fragment displays no diagnostic shape or features and is therefore impossible to date. At 26 cm depth, the fragment was recovered from within the acceptable depth limits of archaeological remains from the nearby Grove's Creek site, where artifacts and features were excavated that reached as deep as 1.5 m below the present ground surface (Garrison, 2007). However, the fragment's location relatively near the surface could either be *in situ* placement or a byproduct of plowing and/or disturbance from timber harvesting.

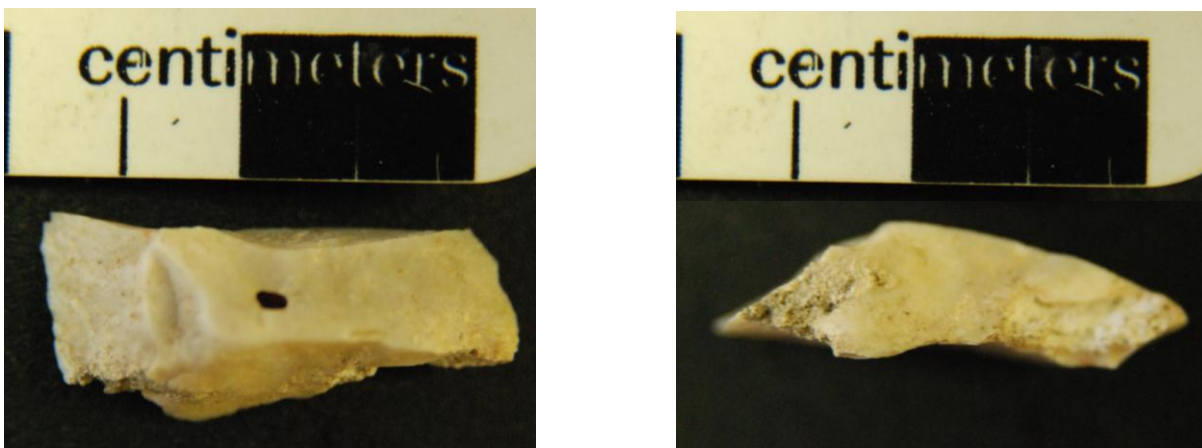


**Fig. 4.4** Piece of chert recovered from 26 cm depth in core GCF 50m.

### *At the Bluff (archaeological site 9CH127)*

Notably, core B 0m is the only core that contains a relatively high silt and clay content of 9-12% in the top horizon (Fig. 3.12); above 25 cm in all other cores, silt and clay content does not exceed 5%. This distinction is one of several indicators that something unusual affected soil formation or preservation in core B 0m's uppermost horizons. In addition to a relatively high silt and clay content, core B 0m's uppermost horizon lacks the dark brown color that characterizes the first horizon of all other cores (Fig. 3.10). Thus, it appears that core B 0m has only a very weak A horizon, which suggests that either something affected A horizon development at this location or that core B 0m's A horizon has "gone missing."

Several lines of evidence support the latter theory. First, all other cores display a well developed A horizon; since depositional environments and pedogenic processes are similar for all sample locations, why should core B 0m's uppermost horizon be so different? Second, the ground surface where core B 0m was collected displays a noticeable shallow depression relative to the surrounding topography. Third, both B 0m and B 100m were collected from a field containing sheet oyster middens and artifacts (DePratter, 1974; Pluckhahn, 1995a,b,c); both B cores contain oyster fragments in subsamples from their uppermost depths (Figs. 3.10, 3.11).

Assuming that a strong A horizon once existed at the site of core B 0m, where did it go? Multiple potential explanations could explain the absence of B 0m's A horizon and the increased clay content in that core. First, the core was collected near an erosional bluff, where recent human recreational traffic (e.g., fishing, canoeing, etc.) in addition to natural in-cutting of Grove's Creek has increased erosion of the nearby landscape (Fig. 4.5). Alternatively (or additionally), easily accessible fields on the island have historically been used as borrow sites for fill dirt during construction of roads and structures (DePratter, 1974). When designating the field

of interest as archaeological site 9CH127, DePratter (1974) noted that the site was undisturbed at that time. During further archaeological survey and testing, Pluckhahn (1995a,b) did not report any significant disturbance of the field. Thus, these descriptions, along with the unlikelihood of collecting fill dirt so close to the bluff edge when dirt could easily be collected from the field's inland borders, exclude fill dirt borrowing as the cause of the lost A horizon.



**Fig. 4.5** Proximity of B 0m core site (where truck and Giddings probe are located) relative to erosional bluff and Grove's Creek. Note abundant oyster fragments visible in the sand near the bluff edge.

Before discussing the final, favored explanation for the differences observed in core B 0m, alternative explanations for the clay increase observed in samples above 25 cm depth in core B 0m will be addressed. The aforementioned recent human recreational traffic (e.g., fishing, canoeing, etc.) may track some silt and clay from the adjacent marshy shoreline onto the edge of the bluff; however, since this recreational traffic is infrequent, it seems an implausible culprit for the sustained silt and clay increase observed in the upper core. Alternatively, as a low-lying area

adjacent to Grove's Creek, flooding events could potentially deposit fine-grained overbank sediments in this location. A  $> 2$  m vertical rise by the tidal Grove's Creek would be required to overtop the bluff (Fig. 4.6). The lack of visible evidence of any such overtopping events (e.g., marsh detritus deposited atop the mainland), and the fact that- due to extensive erosion- the location of core B 0m has been situated directly adjacent to the bluff for a relatively short time (Fig. 4.7) discredits the attribution of the silt and clay increase near the top of core B 0m to overbank events. Thus, additional potential explanations must be examined.



**Fig. 4.6** View of bluff adjacent to Grove's Creek looking north during low tide, as seen in June 2011. Note the fine-grained marsh sediments deposited atop the sandy bluff sediments.

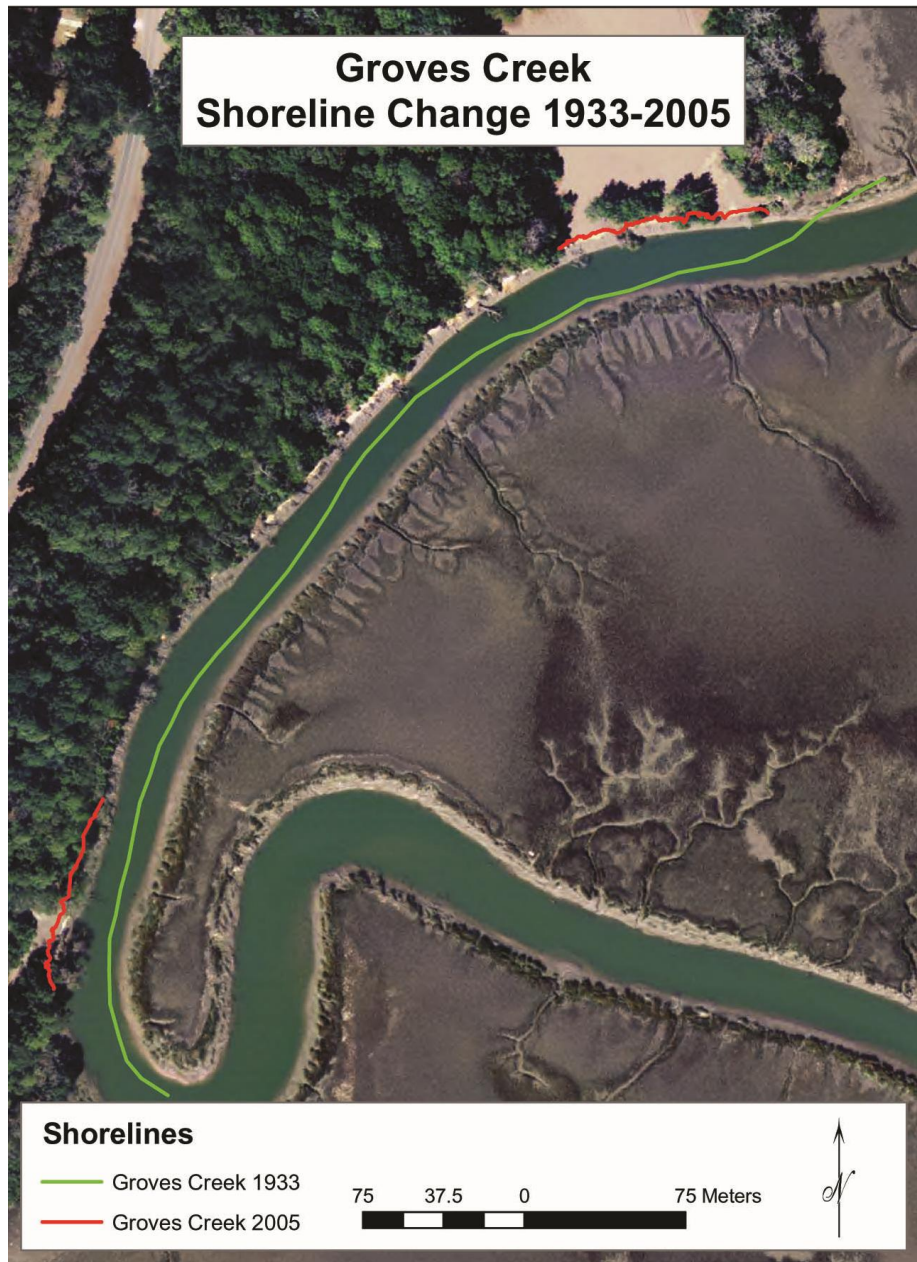


**Fig. 4.7** Shoreline change adjacent to Grove's Creek between 1933 and 2005 (Courtesy of Clark Alexander).

A unified geoarchaeological explanation exists that could explain both the depletion of the A horizon and the clay increase observed in core B 0m. This explanation revisits C. B. Moore's explorations in 1896, when Moore and his crew excavated three mounds on Skidaway Island. One of these mounds (known as archaeological site 9CH23 or 9CH274), whose location is currently unknown, was "completely dug down" by Moore and his crew (Moore, 1897, p. 223). The mound, approximately 0.61 m high by 14 m in diameter, was located "in a field formerly under cultivation, about 1.25 miles in a S.S.W. direction from the northern end of the island" (Moore, 1897, p. 223). Moore's cursory published notes regarding the mound's contents describe "several skeletons[, ...] the lower part of a vessel of the ordinary type[, ...] one fragment of calcined bone [nearby, and] no artifacts of interest" (Moore, 1897, p. 223).

Thankfully, Larson (1998) gleaned additional details from Moore's unpublished notes. The unpublished notes reveal that sherds recovered from the mound "were either plain or cord marked" and that the vessel found "bore a complicated stamped decoration" (Larson, 1998, p. 50). Furthermore, in close proximity to the vessel, "two good-sized fragments of a [complicated stamped] red ware vessel" were recovered, which were interpreted as "remnants of a bowl used as a cover for the first vessel" (Larson, 1998, p. 50). Although Larson (1998) and Pluckhahn (1995c) assign no temporal designation to these materials, DePrattter (1974) interprets the vessel as an "Irene burial urn" (p. 12).

How are Moore's lost mound and associated artifacts related to the current study? I propose that the lack of a strong A horizon and the clay increase observed in core B 0m are evidence that C. B. Moore's lost mound was possibly once located at and excavated from the location where core B 0m was collected. Core B 0m was acquired from the edge of an open field located ~1.30 miles south of the northern end of Skidaway Island, which is very close to Moore's

estimated 1.25 miles south of the island's north end. The field is adjacent to Grove's Creek (Fig. 4.8), which is significant given that Moore's selection of excavation sites was largely influenced by "the proximity of the site to a landing that was accessible to [his primary means of transportation- his steamship-] the *Gopher*" (Larson, 1998, p. 3) (Fig. 4.9).



**Fig. 4.8** View north of Grove's Creek as seen in June 2011 from the bluff adjacent to core B 0m.



**Fig. 4.9** The steamship *Gopher*, C. B. Moore's primary means of transportation when conducting excavations (Modified from Knight, 1996).

Additionally, the field is already recognized as an archaeological site (9CH127). Surveys and test excavations at the site by Pluckhahn (1995a,b) recovered ceramic sherds dating from the Early Woodland to Late Mississippian periods, including several Irene complicated stamped sherds and several undated complicated stamped sherds. During test excavations, Middle and Late Mississippian sherds comprised 23.7% of total ceramics recovered, and Pluckhahn (1995b) found the "lack of more substantial quantities of Irene sherds [to be] somewhat surprising, given the density of occupation in the area during this period" (p. 52). Pluckhahn (1995b) proposed that

a denser Irene phase occupation may have been located in the immediate area to the east of his test area (Figs. 4.10, 4.11). Additionally, Pluckhahn (1995b) noted "that the topsoil was darker, thicker, and contained more artifacts and shell in shovel tests nearer to the edge of the bluff" (p. 33) (Figs. 4.10, 4.11).

Thus, I propose that an Irene phase occupation could have extended south of Pluckhahn's (1995a,b) test areas, on the bluff adjacent to Grove's Creek. Although potential archaeological resources have been lost to the marsh as large amounts of land have been eroded over time by Grove's Creek (Fig. 4.7), Moore's (1897) publication and the differences observed in core B 0m may hint at what once existed near the bluff edge. The absence of an A horizon in core B 0m could be explained by the actions of Moore and his crew when they "completely dug down" the mound, scooping away any A horizon that once existed there along with the mound (Moore, 1897, p. 223). Similarly, Moore's excavation would explain the shallow depression surrounding the location of core B 0m; indeed, at the Irene phase South Mound I located on St. Catherines Island, which was also excavated by Moore, 20th century researchers noted a "large depression" left behind nearly 100 years after Moore's excavation (Larsen, 2002, p. 9). The relatively high clay content observed in the upper 25 cm of core B 0m might be the result of decomposition of mound fill and/or ceramic sherds over time and illuviation of silt and clay-sized particles into the underlying strata, prior to mound excavation. For example, in an Irene phase cemetery excavated at the Irene Mound site (9CH1), archaeologists found nineteen "burial pits sealed with clay plugs" (Caldwell and McCaan, 1941, p. 27). Thus, similar materials in Moore's lost mound at the location for core B 0m could have decomposed and weathered down profile over time to cause the increased clay and silt content observed in the upper 25 cm of this core. Recommendations for further testing of this interpretation are provided at the end of this report.

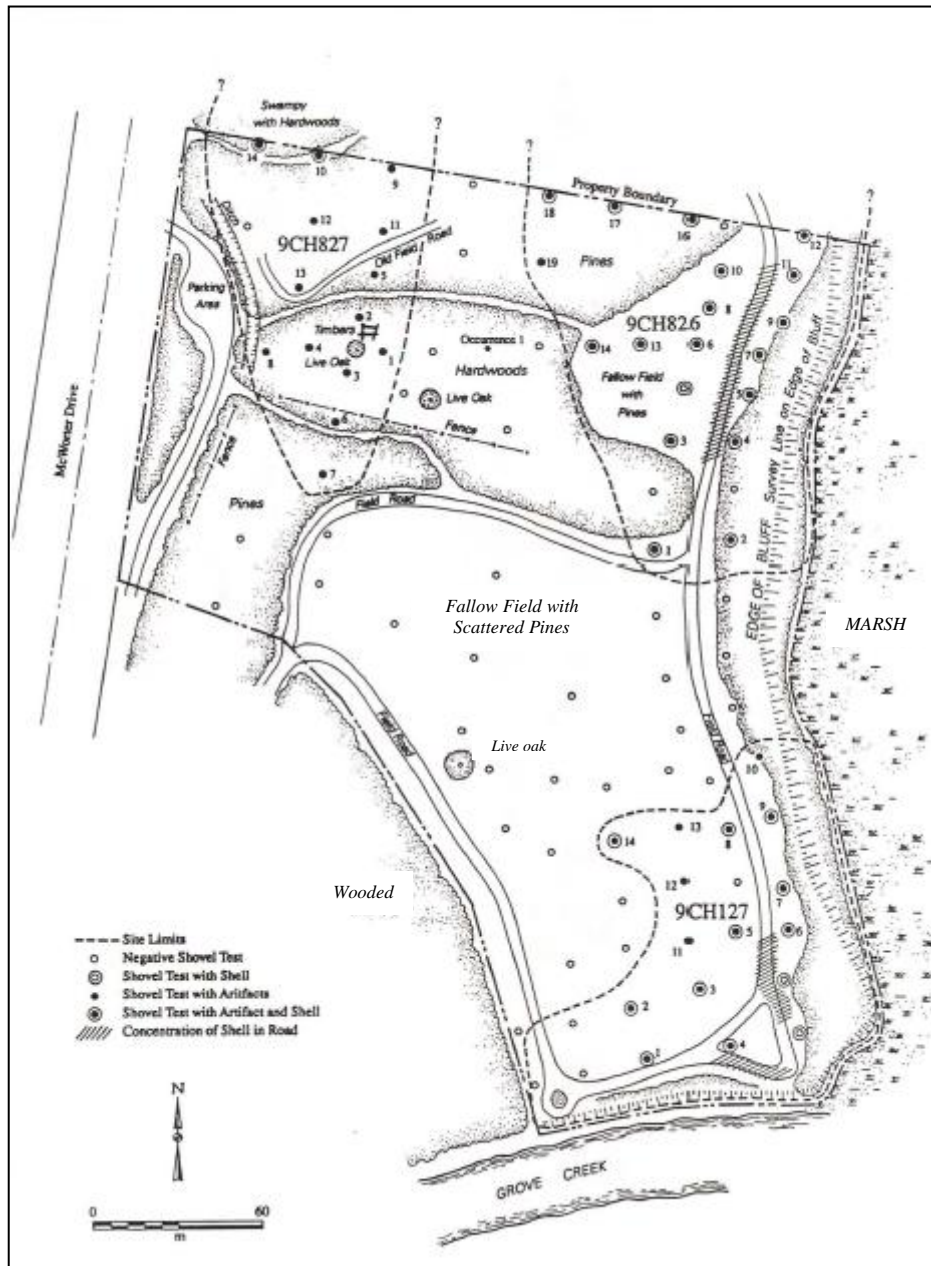


**Fig. 4.10** Locations and general results (sterile vs. nonsterile sediments) of Pluckhahn's shovel tests (Pluckhahn, 1995a). During the present study, core B 0m was collected south of the triangle where the field roads meet towards the bottom of this figure, directly adjacent to the bluff.

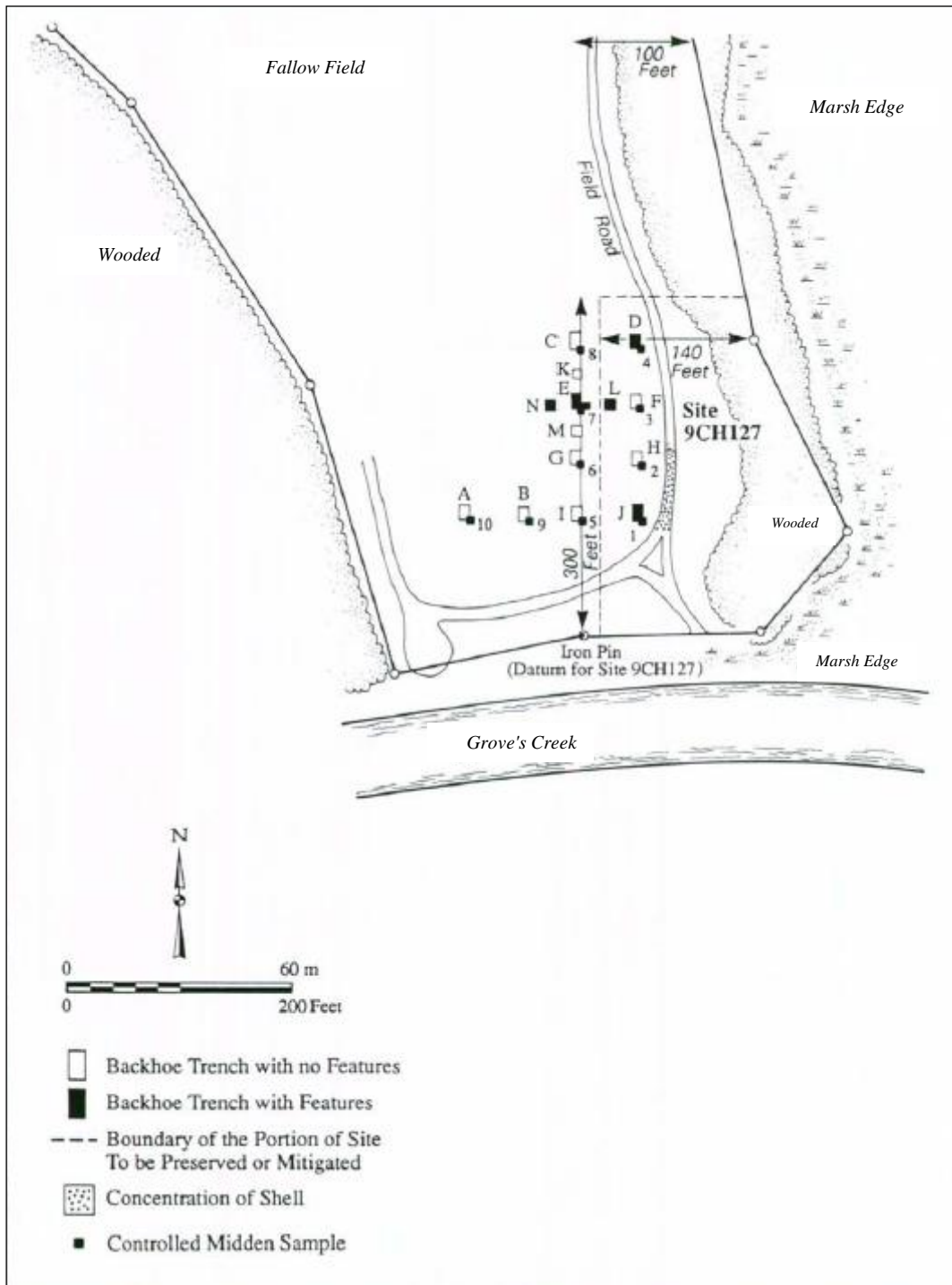


**Fig. 4.11** Locations and general results (sterile vs. nonsterile sediments) of Pluckhahn's backhoe trench and midden excavations (Pluckhahn, 1995b). During the present study, core B 0m was collected south of the triangle where the field roads meet in this figure, directly adjacent to the bluff.

When considering this interpretation, one should also realize that the Grove's Creek site (9CH71) also represents a potential candidate for the location of Moore's lost mound. As discussed previously, the Grove's Creek archaeological site appears to be constructed on a low mound (Fig. 4.3). In fact, the Georgia Archaeological Site Form from 1990 for the Grove's Creek site acknowledges that this site may be the location of "one of C. B. Moore's sites" (included in Pluckhahn, 1995c, Appendix A). Although the Grove's Creek site is located farther south than the 1.25 miles south of the north end of the island indicated by Moore, Moore may have been mistaken or downright dishonest about the location of his excavation; thus, the Grove's Creek site cannot be discounted as an alternative potential location for C. B. Moore's lost mound.

## **Methodological Implications**

### ***Sampling using a truck-mounted Giddings probe***

Several factors should be evaluated when considering using a truck-mounted Giddings probe to collect sediment cores. The first of these factors is accessibility of the study area. For example, choice of sample locations was limited in one case during this study because the truck-mounted Giddings probe could not navigate a large ditch and forested area blocking a desired sample location.

After sample location has been selected and successfully navigated, additional factors may impact the quality of data obtained when using a Giddings probe. One such factor that should be carefully measured during coring is compaction of sediment as the probe forces its way through the subsurface. The amount of compaction can be measured to some degree by carefully observing the depth that the probe extends into the subsurface, rather than the thickness of sediments retrieved in the core tube. However, in soft sediments like saturated silt and clay,

the probe can push some distance past a full tube-worth of sediment before meeting resistance, which will affect the accuracy of depth measurements (Fig. 4.12). Also, in sediments of mixed grain size or areas of thinly interbedded sand and finer grained sediments, compaction pressure from the coring process sometimes forces fine-grained material to the edges of the core tube, thereby creating an artificial clay ring around sediments and obliterating any interbedding that may have originally existed in the sample (Fig. 4.13).



**Fig. 4.12** Clay atop the mandril (where top of core tube attaches to truck-mounted Giddings corer) in core UGA 0m



**Fig 4.13** Gleyed clay pushed out by compaction pressure to form artificial ring around sandy sediments in core UGA 50m

Likewise, when sampling in unconsolidated sediment and/or in a saturated environment using a method that requires successive cores to be collected from an open core hole, the chances of contamination between cores increases. As the probe tube is raised, emptied, and re-lowered down the open core hole, sediment from up-core can easily be dislodged and thereby contaminate the tops of successive cores. In saturated environments, sediment may seep or slump

laterally into the open core hole, thereby contaminating successive cores (Fig. 4.14).

Additionally, if a core tube with an open viewing slit on one side is used (which can be useful for evaluating sediments and contacts prior to core extrusion), mid-core contamination can become a problem (Fig. 4.14). Up-core contaminants can gain access to the core via the viewing slit mid-core if particularly resistant sediments require raising, lowering, and spinning of the core tube to obtain successive cores.



**Fig. 4.14** Saturated sediment oozing from the open slit and base of the core tube in core GCF 50m

If contaminants differ greatly from the sediment currently being sampled (i.e., contain modern organic debris or bear an obvious resemblance to previously sampled, distinct sediments), then contaminants can be manually removed from the core. Even so, infilling by contaminants will affect the quality of depth calculation and compaction monitoring. Moreover,

if contaminants are similar to the sediment currently being sampled, then their presence may pass completely undetected, introducing more error into data. As the number of sub-cores required to sufficiently sample a single location (core hole) increases, so too does the likelihood and amount of error introduced into the dataset by up-core contamination when using a Giddings probe.

In this study, up to 10 cm of contamination per contaminated area, whether it be at the top of a successive core or (less often) mid-core, was observed. A strong attempt was made to monitor and remove contamination as often as possible. However, lingering contamination and/or removal of some non-contaminants along with contaminants likely is a large source of error in true depth below ground versus apparent depth of horizons as observed in cores. Comparing clay horizon depths observed in cores with strong lateral anomalies observed in GPR transects may help to resolve true depth issues. Nonetheless, use of the velocity auto-detect tool in GPR-SLICE to calculate depth for the GPR transects may introduce error into true depth calculations as well. Some idea of the potential amount of contamination (and thereby depth miscalculation) per core may be gleaned by considering the number of sub-cores required to obtain each full core (Tables 3.1, 3.4, 3.7): the greater the number of sub-cores, the greater the potential for contamination.

A final concern with regard to using a Giddings corer to sample sediments in a barrier island environment is the loss of structural features that may be of interest. Each core must be immediately extruded from the sampling tube so that successive cores can be collected. As cores are extruded, unconsolidated sediments tend to lose any semblance of cohesion and mix together with nearby sediments in the core boxes. This issue proves particularly problematic with regard to unconsolidated sandy sediment, the primary constituent of barrier islands.

## ***GPR***

Overall, use of GPR to identify major subsurface sediment changes in a barrier island environment proved successful in this study. The contrast between the dielectric constants of sand versus finer grained sediments facilitated reliable detection of the top of laterally and vertically continuous clay horizons (or the lack thereof) at three out of four sample locations. Also, a strong isolated anomaly that may represent a buried archaeological feature was detected near the Grove's Creek site (9CH71).

However, further steps should be taken to maximize accuracy of velocity and depth calculations for GPR transects collected in this environment. In this study, the absence of strong hyperbola in the GPR data, along with the varying grain size and levels of saturation in the subsurface, undoubtedly introduced error into the automatic calculation of velocity and depth for this dataset using GPR-SLICE. Recommendations for obtaining more reliable velocity and depth calculations are made at the end of this report.

## CHAPTER 5 CONCLUSIONS

### Summary of Findings

The integrated geoarchaeological approach used in this study facilitated development of a more complete understanding of northern Skidaway Island's depositional history, island architecture, and archaeological deposits. Analyses of cores and GPR data identified fine-grained marsh sediments underlying sandy sediments in most study locations. OSL dates obtained during this study relatively date the basal marsh sediments to at least the Late Pleistocene, and confirm Hoyt and Hails' (1974) designation of the western portion of Skidaway Island as part of the Princess Anne terrace. The generally well sorted sands that dominate at least the upper 2 m of each core are predominantly fine sand, and likely represent former dune or beach sediments. Sediments containing relatively high amounts of medium (and sometimes coarse) sand may represent the influence of fluvial deposition on the northwestern side of the island or the influence of active coastal deposition on the northeastern side of the island. Alternatively, some sediments containing relatively high amounts of medium sand may represent periods of subaerial exposure and erosion during sea level regressions. However, additional absolute dating controls need to be established to more accurately determine the exact timing of different depositional and erosional events on Skidaway Island, and to test the validity of these interpretations.

Comparison with previous studies (e.g., Moore, 1897; DePratter, 1974; Pluckhahn, 1995a,b,c; Larsen, 1998; Keene and Garrison, 2013; Garrison, 2007; Keene, 2004; Keene, 2002) from known archaeological sites positioned near the current study locations aided immensely in

interpretation of archaeological finds from this investigation. These previous studies shed light on the most likely time periods and cultures associated with the present archaeological finds. Evidence of past human activities at the current study locations includes a chert fragment and a geophysical anomaly in the field adjacent to the Grove's Creek Site (9CH71), and indirect evidence for the presence and subsequent excavation of a burial mound located at archaeological site 9CH127.

Cores collected in the field adjacent to the Grove's Creek Site (9CH71) returned only one tangible piece of evidence that may be associated with the nearby site. The chert fragment recovered from 26 cm in core GCF 50m shows evidence of human manufacture, but provides no diagnostic features to allow it to be definitely linked to an archaeological time period. However, the GPR transect collected in the field adjacent to Grove's Creek site located an isolated anomaly from ~2 m to ~5 m below the surface that may or may not be associated with the Grove's Creek site (Fig. 3.28). The location of the anomaly near the known archaeological site, and the fact that this anomaly was unique among all GPR data collected during this study, suggests that something unusual has affected the subsurface at that location. Further study is required to evaluate the exact nature of that anomaly.

The location of core B 0m is a strong candidate for the location of C. B. Moore's lost mound on northern Skidaway Island. The distance from the tip of the island to this location as described by Moore is almost exact, and the site is located adjacent to Grove's Creek, which could have been navigated by Moore's steamship. Furthermore, the known archaeological site (9CH127) contains pottery sherds that are contemporary with the sherds excavated by Moore in 1896. Also, the topographic depression from which core B 0m was collected and the apparent absence of a strong A horizon in core B 0m may be products of Moore's complete excavation of

the mound, and the relatively high silt and clay content observed in the upper 25 cm of core B 0m may represent illuviation of fine particles from the overlying mound into the subsurface during the hundreds of years before Moore's excavation. By all accounts, the location of core B 0m matches Moore's descriptions of the lost mound site. Nonetheless, the Grove's Creek site (9CH127) should also be considered as a potential location for Moore's lost mound.

### **Recommendations for Future Research**

Procurement of additional OSL dates at more frequent intervals downcore, along with testing of sediments from a similar level in directly adjacent cores, would shed more light on the success of this dating method in the barrier island environment. Dates obtained using OSL could be compared to dates obtained using other direct sediment dating methods. For example, relatively young sediments could be directly dated by measuring  $^{14}\text{C}$  content in gibbsite, since  $\text{CO}_2$  is incorporated from soil gas into the structure of gibbsite during formation (Schroeder and Melear, 1999). Also, abundance of  $^{10}\text{Be}$  and  $^{26}\text{Al}$  in quartz could be used to determine the amount of time that sediments have been exposed to surficial weathering processes (Schroeder et al., 2001). Comparison of direct sediment dates obtained using different methods would facilitate development of a more robust understanding of Skidaway Island's depositional history . Obtainment of additional sediment dates is needed to further test the interpretations of Skidaway Island's architecture and depositional history proposed in this study.

Further coring directly through the anomaly detected near the location of core GCF 0m (located near the Grove's Creek site) is recommended to better assess the nature of this anomaly. If coring returns evidence of archaeological resources at that location, then the site could be considered for excavation.

Several avenues for future research exist with regard to evaluating whether the location of core B 0m is truly the location of C. B. Moore's lost mound. First, the upper 30 cm of the area surrounding where core B 0m was collected could be cored or shovel tested and grain size analyses could be performed to test for the lateral extent of the relatively high silt and clay content. In this way, the extent and shape of the anomalous area might be determined.

Direct comparison of core B 0m's characteristics with the characteristics of a core or data from a known mound site would prove even more useful. Comparison with sediment at South End Mound I located on St. Catherine's Island, GA would be optimal. South End Mound I is another mound that was excavated by C.B. Moore and then lost to history for some time, before being rediscovered in 1974 (Larsen, 2002). Thus the sediments underlying the excavated portion of South Mound I provide the best proxy for how the sediments underlying Skidaway Island's lost mound might appear.

Excavations at South End Mound I during the 20th century also shed light on another important consideration regarding Moore's lost mound on Skidaway Island; the potential presence of human remains. Moore kept very few of the skeletal remains encountered at South End Mound I, instead leaving the bulk of the remains behind in his backdirt (Larsen, 2002). Thus, any plans for further investigation at the location of core B 0m should include a plan for how to handle any human remains that may be encountered at that location.

Finally, with regard to the methodology used in studies similar to the one described herein, two recommendations are advised. First, use of a closed-coring system like vibracorer could help to mitigate some of the issues encountered in this study. For example, a vibracorer would allow more flexibility in determining sample site location, since a vibracorer can be manually transported in the field. Also, vibracores do not have to be immediately extruded in the

field to collect successive cores, and instead are kept in their casing and later cut in half in the lab, thus facilitating better preservation of subsurface contacts and structural features.

Second, to maximize accurate calculation of GPR velocity and depth, it is recommended that a field test of velocity be conducted. A field test and subsequent calculation of velocity facilitates the most accurate calculation of GPR velocity (Conyers and Goodman, 1997). Such a test could be easily conducted in the barrier island environment by pounding a metal rod into an exposed cut bank at a known depth, passing the GPR over this buried rod, and then using the wave travel time and known depth of the rod to calculate wave velocity.

## REFERENCES

- Alexander, C., Ivester, A., and Brook, G., 2008, Formation and chronology of Georgia back-barrier islands: Geological Society of America, Southeastern Section, Abstracts with Programs, v. 40, no. 4, p. 26.
- Alexander, C.A., Rink, W.J., Jackson, C.W., Brook, G.A., and Ivester, A., 2011, Late Holocene geologic development of the Georgia coast: Geological Society of America, Southeastern Section, Abstracts with Programs, v. 43, no. 2, p. 11-12.
- Blott, S.J., and Pye, K., 2001, GRADISTAT: A grain size distribution and statistics package for the analysis of unconsolidated sediments: Earth Surface Processes and Landforms, v. 26, p. 1237-1238.
- Booth, R.K., Rich, F.J., and Bishop, G.A., 1999, Palynology and depositional history of Late Pleistocene and Holocene coastal sediments from St. Catherines, Georgia, USA: Palynology, v. 23, p. 67-86.
- Booth, R.K., Rich, F.J., and Jackson, S.T., 2003, Paleoecology of Mid-Wisconsinan peat clasts from Skidaway Island, Georgia: PALAIOS, v. 18, no.1, p. 63-68.
- Bristow, H.M., and Jol, C.S., 2003, An introduction to ground penetrating radar in sediments, *in* Bristow, H.M., and Jol, C.S., eds., Ground Penetrating Radar in Sediments: Geological Society, London, Special Publication, no. 211, p. 1-7.
- Caldwell, J., and McCaan, C., 1941, Irene Mound Site: Chatham County, Georgia: Athens, Georgia, The University of Georgia Press, 84 p.
- Caldwell, J.R., and Waring, Jr., A.J., 1939, Some Chatham County pottery types and their sequence: Southeastern Archaeological Conference Newsletter 1(5):4-12 and 1(6): 1-9, *reprinted in* Williams, S., ed., 1968, The Waring Papers: The collected works of Antonio J. Waring, Jr.: Cambridge, The Peabody Museum, p. 110-134.
- Carver, R.E., 1971, Holocene and Late Pleistocene sediment sources, continental shelf off Brunswick, Georgia: Journal of Sedimentary Petrology, v. 41, no. 2, p. 517-525.
- Conyers, L.B., and Goodman, D., 1997, Ground penetrating radar: An introduction for archaeologists: Walnut Creek, California, Altamira Press, 232 p.

- Cowan, B., Julian, M.E., Kane, J.R., Oliver, J.W., Shaffer, M.D., Christensen, B.A., Freile, D., Malchow, R., 2004, A sedimentological, geochemical, and micropaleontological analysis of a Skidaway Island (Georgia) marsh: Geological Society of America, Southeastern Section, Abstracts with Programs, v. 36, no. 2, p. 47
- Darrell, J.H., Brannen, N.A., and Bishop, G.A., 1993, Contribution 4: The Beach *in* Farrell, K.M., Hoffman, C.W., and Henry, Jr., V.J., eds., Geomorphology and facies relationships of Quaternary barrier island complexes near St. Marys, Georgia: 28th annual field trip Georgia Geological Society: Georgia Geological Society Guidebooks, vol. 13, no.1, p. 16-18.
- DePratter, C. B., 1974, A preliminary archaeological survey of University of Georgia property on Skidaway Island: Georgia Archeological Site File Report No. 0021.
- DePratter, C. B., 1975, An archaeological survey of P. H. Lewis property, Skidaway Island, Chatham County, Georgia: Georgia Archeological Site File Report No. 5604.
- DePratter, C. B., 1977, Environmental changes on the Georgia coast during the Prehistoric Period: Early Georgia, v. 5, no.1, p. 1-14.
- DePratter, C. B., 1978, Prehistoric settlement and subsistence systems, Skidaway Island, Georgia: Early Georgia, v. 6, no. 2, p. 65-80.
- DePratter, C.B., and Howard, J. D., 1977, History of shoreline changes determined archaeological dating: Georgia coast, U.S. Gulf Coast Association of Geological Societies XXVII, Transactions p. 252-258.
- Elliott, D.T., and Holland, J.L., 2006, Archaeological survey of Priests Landing, Skidaway Island, Georgia: LAMAR Institute Publication Series Report Number 86: [http://shapiro.anthro.uga.edu/Lamar/images/PDFs/publication\\_86.pdf](http://shapiro.anthro.uga.edu/Lamar/images/PDFs/publication_86.pdf) (March 2010)
- Folk, R.L., 1954, The distinction between grain size and mineral composition in sedimentary-rock nomenclature: Journal of Geology, v. 62, p.344–359.
- Folk, R.L., 1974, Petrology of Sedimentary Rocks: Austin, Texas, Hemphill Publishing Company, p. 33-40.
- Folk, R.L., and Ward, W.C., 1957, Brazos River bar: a study in the significance of grain size parameters: Journal of Sedimentary Petrology, v. 27, no. 1, p. 3–26.
- Freile, D., Christensen, B.A., Alexander, C.R., Donnelly, V., Layfield, T., Venherm, C., Elliott, W.C., and Elser, A., 2004, Out of the blue; evidence of a blue clay zone on Skidaway Island; promising indication of a Quaternary marker on the Georgia coast?: Geological Society of America, Southeastern Section, Abstracts with Programs, v. 36, no. 2, p. 47.

- Frey, R.W., and Howard, J.D., 1988, Beaches and beach-related facies, Holocene barrier islands of Georgia: *Geological Magazine*, v. 6, no. 6, p. 621-640.
- Garrison, E.G., 2007, Excavation and development of educational materials for Grove's Creek Site: Final technical report prepared for Cycle IX Coastal Incentive Grant.
- Garrison, E.G., McFall, G., and Noakes, S. E., 2008, Shallow marine margin sediments, modern marine erosion and the fate of sequence boundaries – Georgia Bight (USA): *Southeastern Geology*, v. 45, no. 3, p.127-142.
- Georgia Department of Natural Resources, 1976, Wetlands and geologic resources: Atlanta, Department of Natural Resources, Office of Planning and Research.
- Google Earth 6, 2013, Skidaway Island: Google, Inc.
- Gorsline, D.S., 1963, Bottom sediments of the Atlantic shelf and slope off the Southern United States: *The Journal of Geology*, v. 71, no. 4, p. 422-440.
- Geophysical Survey Systems, Inc. (GSSI), 2005, RADAN 6.5 User's Manual: North Salem, Geophysical Survey Systems, Inc., 63 p.
- Historic Services, Inc., 1971, The history of Northern Skidaway Island: Savannah, manuscript [as cited in Weinland, 1981; Manuscript could not be located during the course of this research].
- Howard, J. D., and DePratter, C.B., 1980, Field trip guide to the archaeology-geology of the Georgia Coast, *in* Howard, J. D., DePratter, C.B., and Frey, R.W., *Excursions in southeastern geology: The archaeology-geology of the Georgia Coast (Guidebook 20)*: Geological Society of America, p. 234–253.
- Hoyt, J.H., 1967, Barrier island formation: *Geological Society of America Bulletin*, v. 78, no. 9, p. 1125-1136
- Hoyt, J.H., 1968, Geology of the Golden Isles and lower Georgia Coastal Plain *in* D. S. Maney, ed., *The future of the marshlands and sea islands of Georgia*: Georgia Natural Areas Council and Coastal Area Planning and Development Commission, p. 18-32.
- Hoyt, J.H., and Hails, J.R., 1974, Pleistocene stratigraphy of Southeastern Georgia, *in* Oaks, R.Q., and DuBar, J.R., eds., *Post-Miocene stratigraphy, Central and Southern Atlantic Coastal Plain*: Logan, Utah State University Press, p. 191- 205.
- Hoyt, J.H., and Henry Jr., V.J., 1967, Influence of island migration on barrier-island sedimentation: *Geological Society of America Bulletin*, v. 78, 86 p.
- Howard, J.D., and Scott, R. M., 1983, Comparison of Pleistocene and Holocene barrier island beach-to-offshore sequences, Georgia and northeast Florida coasts, USA: *Sedimentary Geology*, v. 34, p. 167-183.

- Huddleston, P.F., 1988, A revision of the lithostratigraphic units of the Coastal Plain of Georgia-Miocene through Holocene: Georgia Geological Survey Bulletin, v. 104, 162 p.
- Ivester, A.H., and Leigh, D.S., 2003, Riverine dunes on the Coastal Plain of Georgia, USA: *Geomorphology*, v. 51, p. 289-311.
- Johnson, R.E., 1990, Archaeological testing of the Exchange Tract Parcel, Skidaway Island, Chatham County, Georgia: Florida Archeological Services, Inc. prepared for the Branigar Organization, Georgia Archaeological Site File Report no.5680, 105 p.
- Keene, D.A., 2002, Archaeological and geophysical investigations at Grove's Creek Site (09CH71), Skidaway Island, Georgia [Ph.D. Dissertation]: Department of Geology, University of Georgia, Athens. 230 p.
- Keene, D.A., 2004, Reevaluating Late Prehistoric coastal subsistence and settlement strategies: New data from Grove Creek's Site, Skidaway Island, Georgia: *American Antiquity* v. 69, no. 4, p. 671-688.
- Keene, D.A., and Garrison, E.G., 2013, A survey of Irene phase architecture on the Georgia coast, *in* Thompson, V.D., and Thomas, D.H., eds., *Life among the tides: Recent archaeology on the Georgia Bight: Anthropological Papers of the American Museum of Natural History*, no. 98, in press.
- Kelly, V.E., 2003, A short history of Skidaway Island, Third edition, V. E. Kelly and the Branigar Organization, 162 p.
- Knight, Jr., V. J., 1996, Introduction, *in* Knight, Jr., V. J., ed., *The Moundville Expeditions of Clarence Bloomfield Moore: Tuscaloosa, The University of Alabama Press*, 224 p.
- Krantz, D., 2011, Geology of the Virginia Coast figures: [http://www.eescience.utoledo.edu/Faculty/Krantz/Va\\_Coast\\_figures/Virginia\\_Coast\\_figures.htm](http://www.eescience.utoledo.edu/Faculty/Krantz/Va_Coast_figures/Virginia_Coast_figures.htm) (December 2011).
- Larsen, C.S., 2002, Bioarchaeology of the Late Prehistoric Guale: South End Mound I, St. Catherines Island, Georgia: *Anthropological Papers of the American Museum of Natural History*, no. 84, 104 p.
- Larson, L.H., 1998, Introduction *in* Larson, L.H., ed., *The Georgia and South Carolina coastal expeditions of Clarence Bloomfield Moore: Tuscaloosa, The University of Alabama Press*, 296 p.
- Leckebusch, J., 2003, Ground-penetrating radar: a modern three-dimensional prospection method: *Archaeological Prospection*, v.10, p. 213-240.

- Leigh, D.S., 1998, Evaluating artifact burial by eolian versus bioturbation processes, South Carolina Sandhills, USA: *Geoarchaeology: An International Journal*, v. 13, no. 3, p. 309-330.
- Lewis, D.W., and McConchie, D., 1994, *Analytical Sedimentology*: New York, Chapman & Hall, 197 p.
- Markewich, H.W., Hack, C.M., and Huddleston, P.F., 1992, Emergent Pliocene and Pleistocene sediments of Southeastern Georgia: An anomalous, fossil-poor, clastic section *in* Fletcher, C.H. and Wehmiller, J.F., eds., *Quaternary coasts of the United States: Marine and lacustrine systems: Special publication- Society of economic paleontologists and mineralogists*, no. 48, p. 173-189.
- Markewich, H.W., Pavich, M.J., Schultz, A.P., Mahan, S.A., Aleman-Gonzalez, W.B., and Bierman, P.R., 2013, Geochronologic evidence for a possible MIS-11 emergent barrier/beach-ridge in southeastern Georgia, USA: *Quaternary Science Reviews*, v. 60, p. 49-75.
- Martinson, D.G., Pisias, N.G., Hays, J.D., Imbrie, J., Moore, T.C., Jr., and Shackleton, N.J., 1987, Age dating and the orbital theory of the ice ages; development of a high-resolution 0 to 300,000-year chronostratigraphy: *Quaternary Research*, v. 27, no. 1, p. 1-29.
- McGowan, J.F., 1983, An historical sketch of Skidaway Island: Skidaway Island, Marine Science Center. 16 p.
- McGowan, J. F., and DePratter, C. B., 1980, Skidaway Island: A frontier outpost, 1733-1740, *in* Howard, J. D., DePratter, C. B., and Frey, R. W., eds., *Excursions in southeastern geology: The archaeology-geology of the Georgia Coast*: Atlanta, Geological Society of America, Guidebook 20, p. 225-233.
- McKeague, J.A., Wang, C., Coen, G.M., DeKimpe, C.R., Laverdiere, M.R., Evans, L.J., Kloosterman, B., and Green, A.J., 1983, Testing chemical criteria for spodic horizons in podzolic soils in Canada: *Soil Science Society of America Journal*, v. 47, no. 5, p. 1052-1054.
- Milsom, J., and Erikson, A., 2011, *Field Geophysics, Fourth Edition*: Singapore, John Wiley & Sons, Ltd., 287 p.
- Moore, C. B., 1897, The Georgia and South Carolina Coastal Expeditions of Clarence Bloomfield Moore *in* Larson, L.H., ed., 1998, *The Georgia and South Carolina coastal expeditions of Clarence Bloomfield Moore*: Tuscaloosa, The University of Alabama Press, 296 p.
- Moore, D.M., and Reynolds, Jr., R. C., 1997, *X-ray diffraction and the identification and analysis of clay minerals*, 2nd edition: New York, Oxford University Press, 378 p.

- Munsell Color, 1994, Munsell Soil Color Charts, 1994 Revised Edition: New York GretagMacbeth.
- National Park Service (NPS), 2005, The Islands *in* An ecological survey of the coastal region of Georgia: NPS Science Monograph no. 3:  
[http://www.nps.gov/history/history/online\\_books/science/3/chap3.htm](http://www.nps.gov/history/history/online_books/science/3/chap3.htm) (April 2013).
- Oertel, G.F., 1975, Post Pleistocene island and inlet adjustment along the Georgia coast: *Journal of Sedimentary Petrology*, v. 45, no. 1, p.150-159.
- Oertel, G.F., 1979, Barrier island development during the Holocene recession, Southeastern United States, *in* Leatherman, S.P., ed., *Barrier islands: from the Gulf of St. Lawrence to the Gulf of Mexico*: New York, Academic Press, Inc., p. 273-290.
- Oertel, G.F., 1985, The barrier island system *in* Oertel, G.F., and Leatherman, S.P., eds., *Barrier islands: Marine Geology*, v. 63, p. 1-18.
- Pluckhahn, T.J., 1995a, An intensive cultural resources survey of the 15 acre Avian Tract on Skidaway Island, Chatham County, Georgia: Southern Archaeological Services Inc. prepared for Hussey, Gay, Bell and DeYoung, Inc., Georgia Archeological Site File Report no. 5651, 61 p.
- Pluckhahn, T.J., 1995b, Archaeological testing of two sites on northern Skidaway Island, Chatham County, Georgia: Southern Archaeological Services Inc. prepared for Hussey, Gay, Bell and DeYoung, Inc., Georgia Archeological Site File Report no. 1783, 91 p.
- Pluckhahn, T.J., 1995c, An intensive cultural resources survey of a 310 acre tract on northern Skidaway Island, Chatham County, Georgia: Southern Archaeological Services Inc. prepared for Hussey, Gay, Bell and DeYoung, Inc., Georgia Archeological Site File Report no. 5599, 235 p.
- Rich, F.J., and Pirkle, F.L., 1994, Paleoecological interpretation of the Trail Ridge sequence, and related deposits in Georgia and Florida, based on pollen sedimentation and clastic sedimentology, *in* Traverse, A., ed., *Sedimentation of Organic Particles*: Cambridge, England, Cambridge University Press, p. 287-310.
- Russo, M., 2002, Archaic shell rings of the Southeast U.S.: National Historic Landmarks Historic Context: Tallahassee, Florida, Southeast Archaeological Center, National Park Service, 171 p.
- Schoettle, T., 2001, A guide to a Georgia barrier island: Featuring Jekyll Island with St. Simons and Sapelo Islands and a field guide to Jekyll Island: Darien, Georgia, Darien Printing and Graphics, 159 p. (Original work published 1996.)

- Schroeder, P. A., and Melear, N.D., 1999, Stable carbon isotope signatures preserved in authigenic gibbsite from a forested granitic-regolith: Panola Mt., Georgia, USA: *Geoderma*, v. 91, p. 261-279.
- Schroeder, P. A., Melear, N.D., Bierman, P., Kashgarian, M., and Caffee, M.C., 2001, Apparent gibbsite growth ages for regolith in the Georgia Piedmont: *Geochimica et Cosmochimica Acta*, v. 65, no. 3, p. 381-386.
- Sherrill, J.H., 1987, Skidaway Island: Unpublished Manuscript in the "Skidaway Island" vertical file in the Georgia Room at the University of Georgia Library [as cited in Pluckhahn, 1995c; Georgia Room vertical file was checked during the course of this study, and the manuscript could not be found.].
- Soil Survey Laboratory Staff, 1992, Soil survey laboratory methods manual: United States Department of Agriculture-Soil Conservation Service, National Soil Survey Center, Soil Survey Investigations report 42, version 2.0, 400 p.
- Turck, J.A., and Alexander, C.R., 2013, Coastal landscapes and their relationship to human settlement on the Georgia coast, *in* Thompson, V.D., and Thomas, D.H., eds., *Life among the tides: Recent archaeology on the Georgia Bight: Anthropological Papers of the American Museum of Natural History*, no. 98, in press.
- Vanags, C.P., 2000. A pedological study of soil genesis on Skidaway Island [Master's Thesis]: Department of Crop and Soil Sciences, University of Georgia, Athens. 112 p.
- Vance, R.K., Bishop, G.A., Rich, F.J., Meyer, B.K., and Camann, E.J., 2011, Application of ground penetrating radar to investigations of the stratigraphy, structure, and hydrology of St. Catherines Island, *in* Bishop, G.A., Rollins, H.B., and Thomas, D.H., eds., *Geoarchaeology of St. Catherines Island, Georgia: Anthropological Papers of the American Museum of Natural History*, v.94, p. 209-236.
- Vento, F.J., and Stahlman, P.A., 2011, Development of a Late Pleistocene-Holocene genetic stratigraphic framework for St. Catherines Island: Archaeological implications, *in* Bishop, G.A., Rollins, H.B., and Thomas, D.H., eds., *Geoarchaeology of St. Catherines Island, Georgia: Anthropological Papers of the American Museum of Natural History*, v.94, p. 99-112.
- Wachecka-Kotkowska, L., and Kotkowski, P., 2011, Grain-size distribution analysis of Quaternary sediments from the southern part of the Lodz region in Poland: a computational methods approach: *Geologos*, v. 17, p. 205-219.
- Weems, R.E., and Edwards, L.E., 2001, Geology of Oligocene, Miocene, and younger deposits in the coastal area of Georgia: *Georgia Geological Survey Bulletin*, v.13, 124 p.
- Weinland, M.K., 1981, Assessment of cultural resources in Skidaway Island State Park: Georgia Archeological Site File Report No. 331.

Wells, L.E., 2001, Archaeological sediments in coastal environments *in* Stein, J.K., and Farrand, W.R., eds., *Sediments in archaeological context*: Salt Lake City, University of Utah Press, p. 149-182.

White, C.M., Alexander, C., and Robinson, M., 2010, A stratigraphic investigation of paleoshoreline position on Skidaway Island, Georgia [Abstract]: *Geological Society of America Abstracts with Programs* v.42, no.1, p.70-71.

## Appendix A

### X-ray Diffractograms with Prominent Peaks Labeled

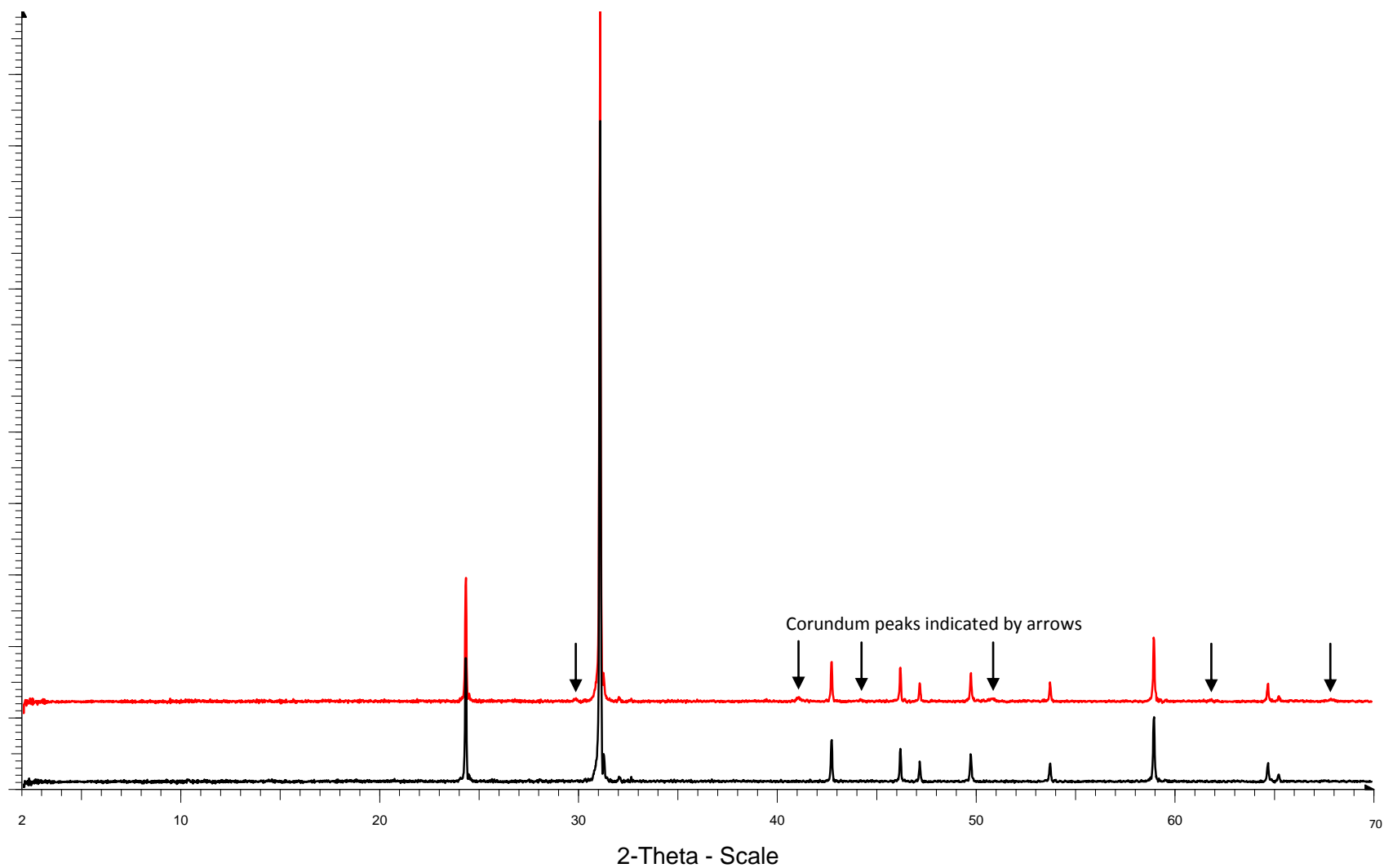


**Fig. A.1** Bulk XRD results for sample UGA P 286 cm; In the McCrone micronizing mill, the sample producing the red diffractogram was processed using corundum pellets, whereas the sample producing the black diffractogram was processed using agate pellets. Thus, corundum peaks in the red diffractogram are artifacts of processing using corundum pellets.

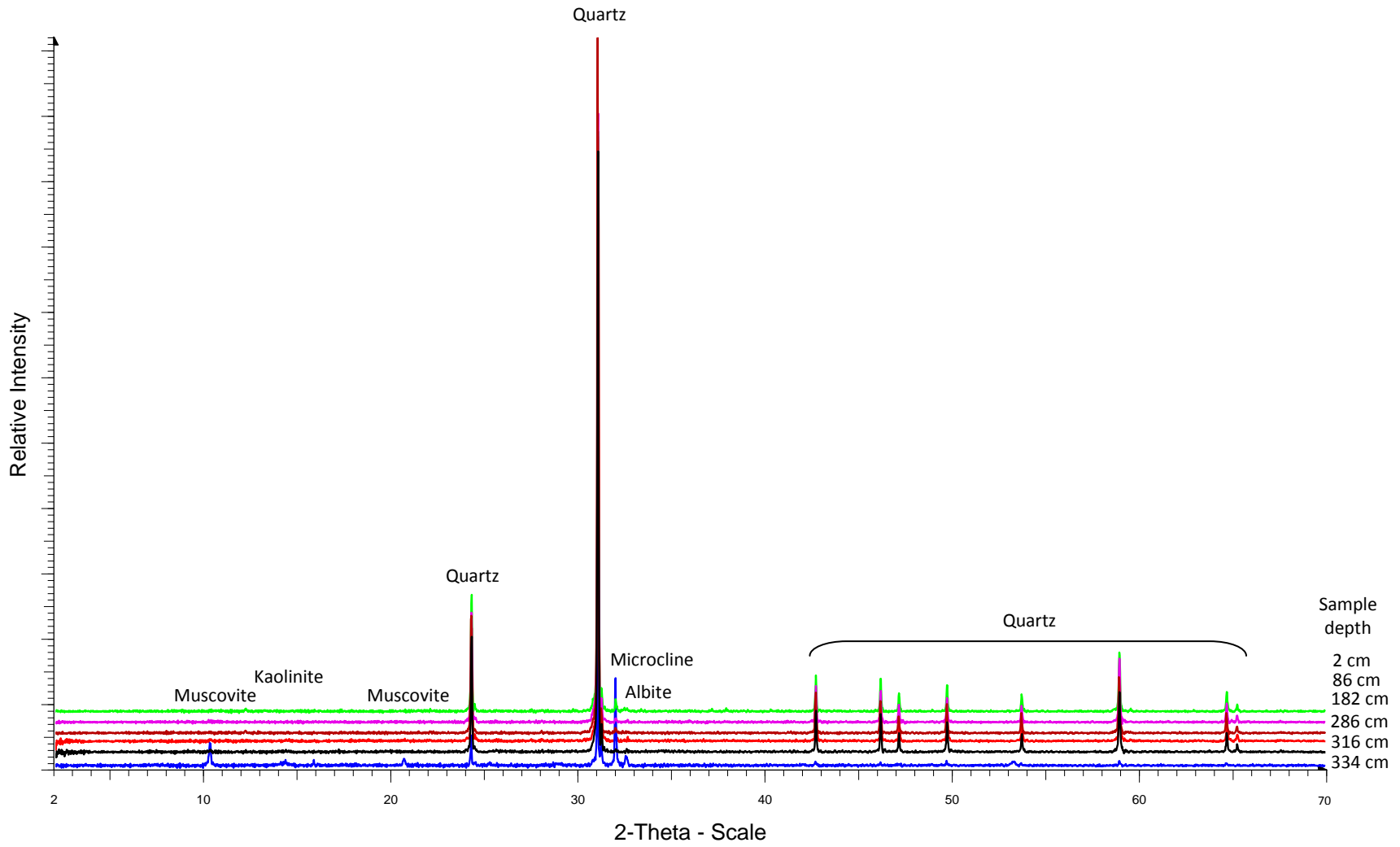


Fig. A.2 Bulk XRD results for core UGA P

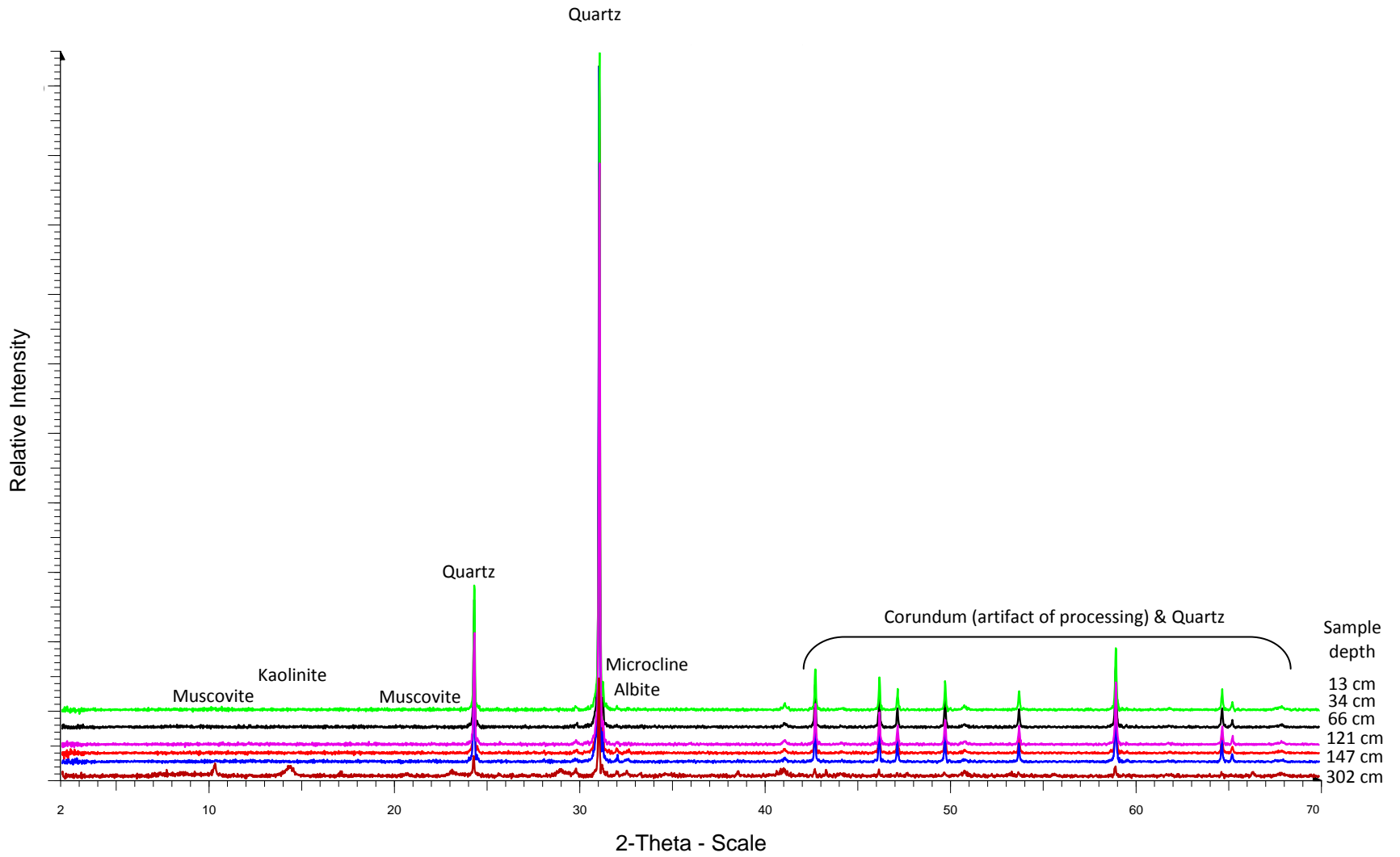
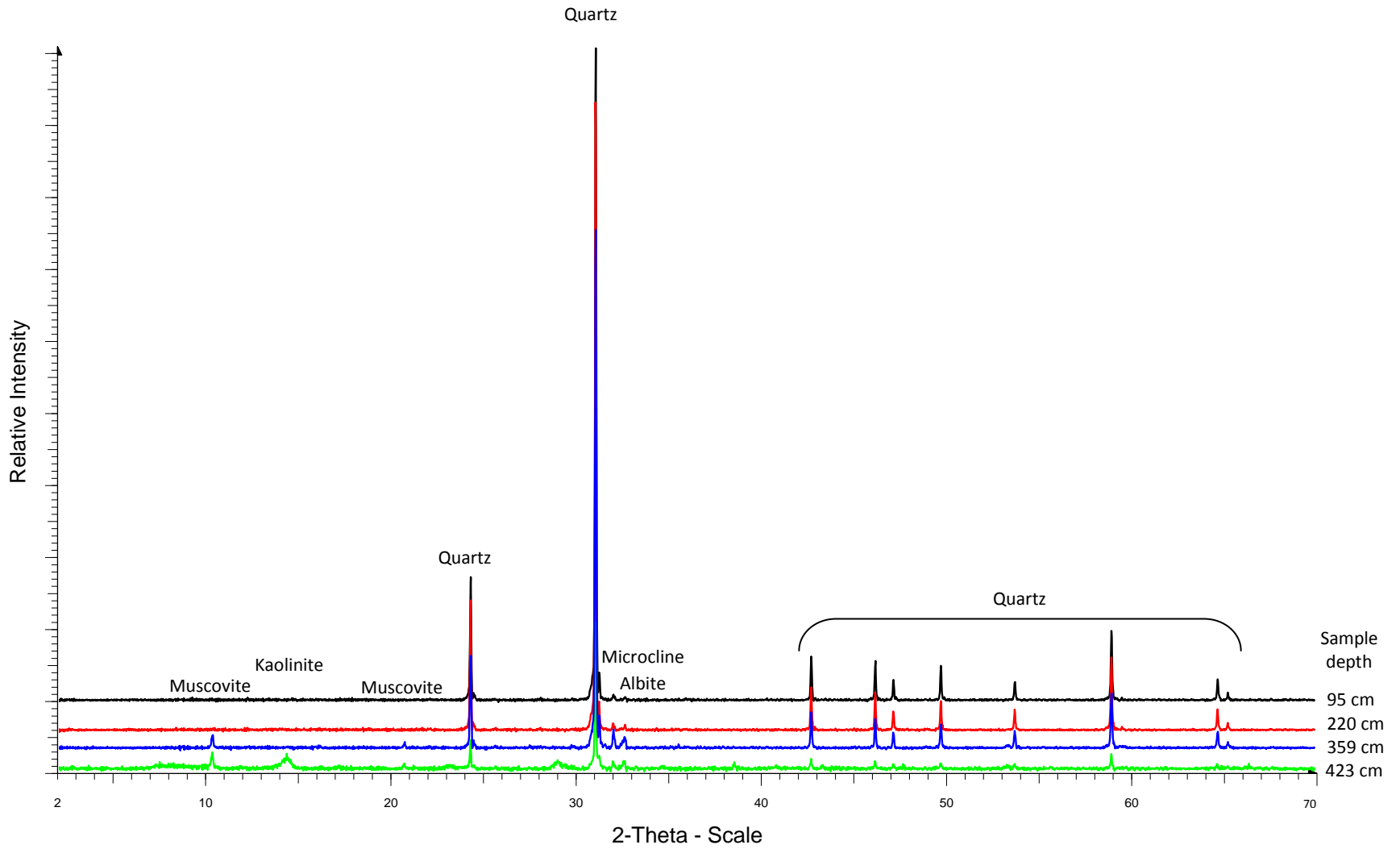
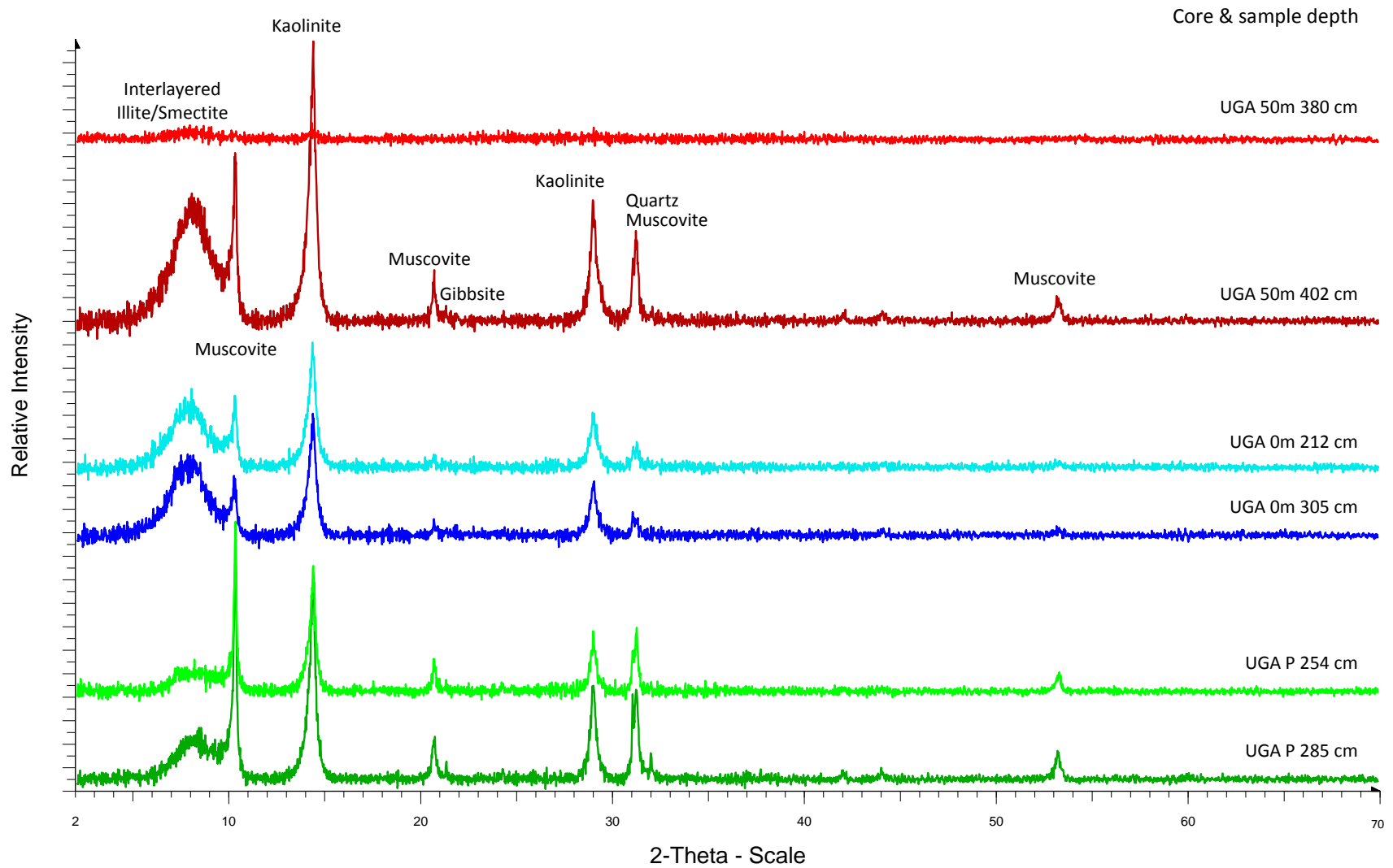


Fig. A.3 Bulk XRD results for core UGA 0m



**Fig. A.4** Bulk XRD results for core UGA 50m



**Fig. A.5** Clay fraction XRD results for all UGA cores

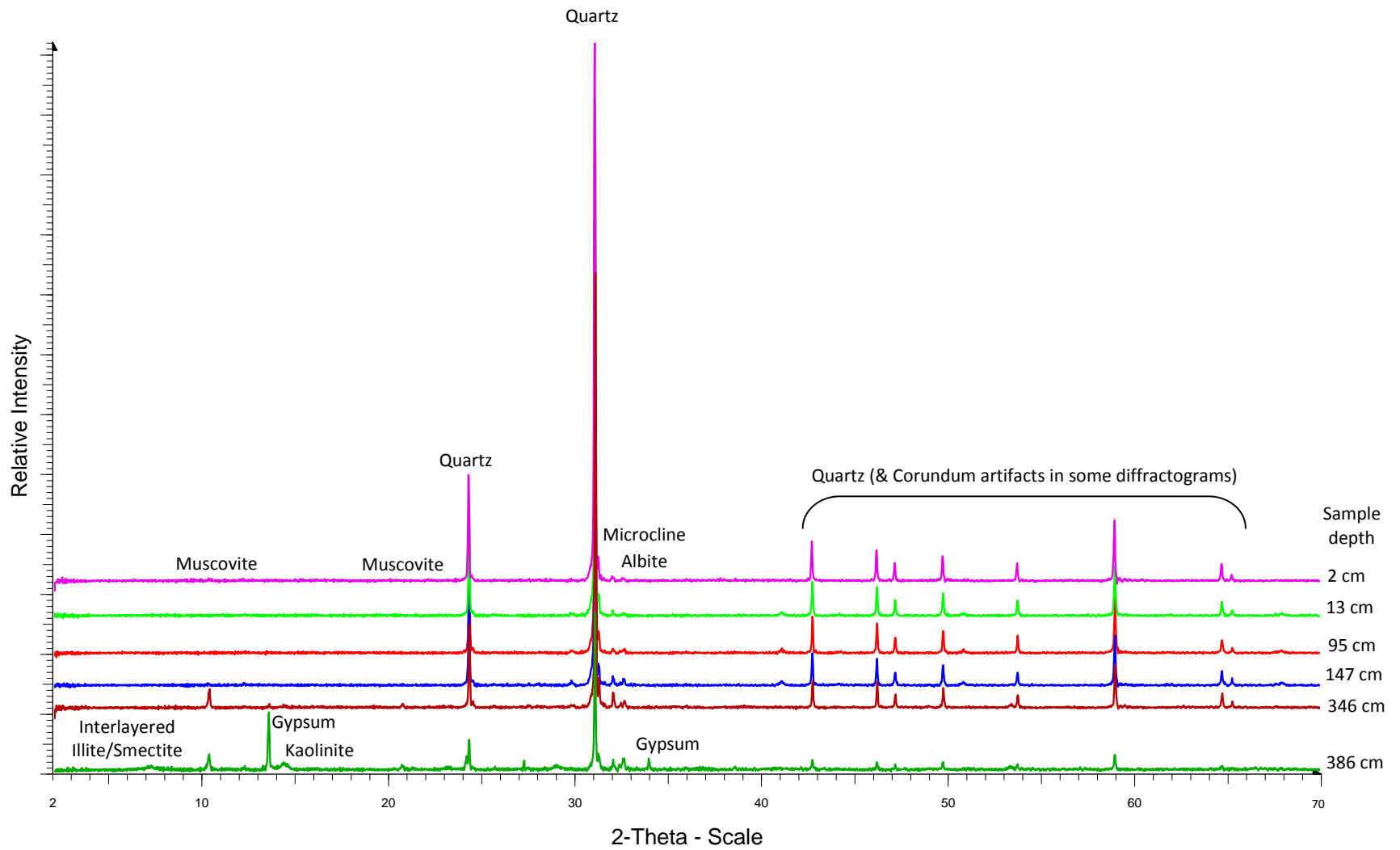
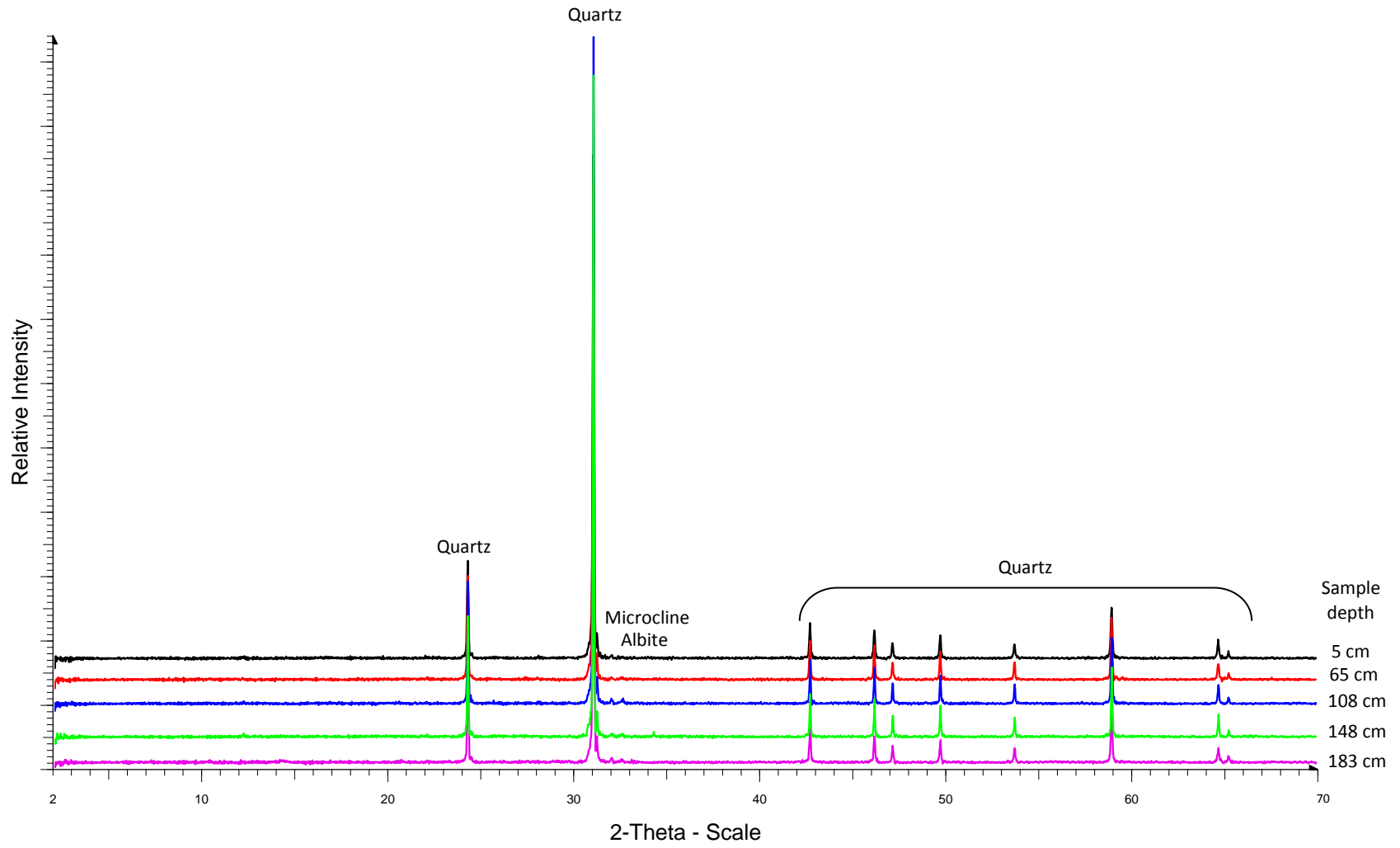
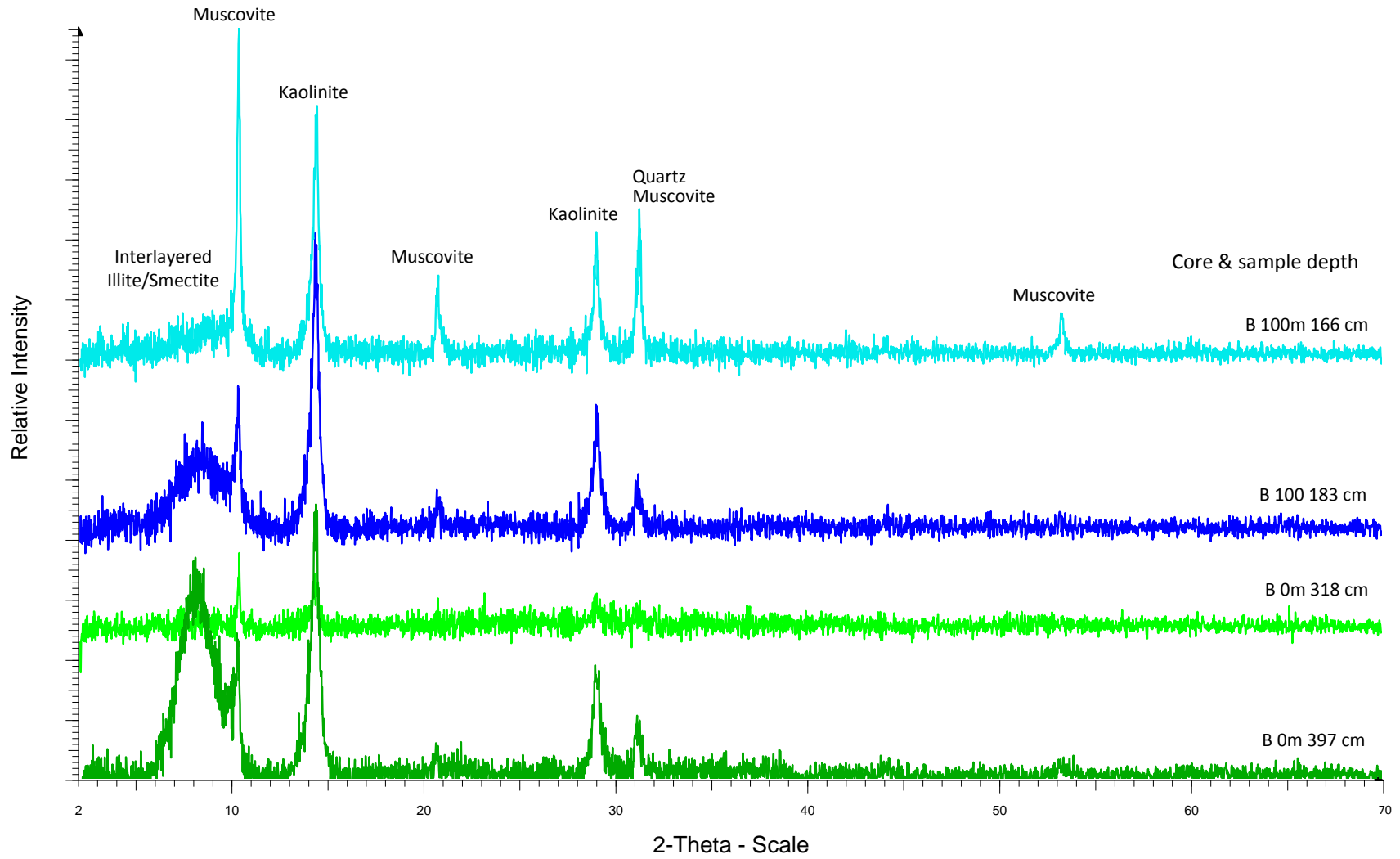


Fig. A.6 Bulk XRD results for core B 0m



**Fig. A.7** Bulk XRD results for core B 100m



**Fig. A.8** Clay fraction XRD results for both B cores

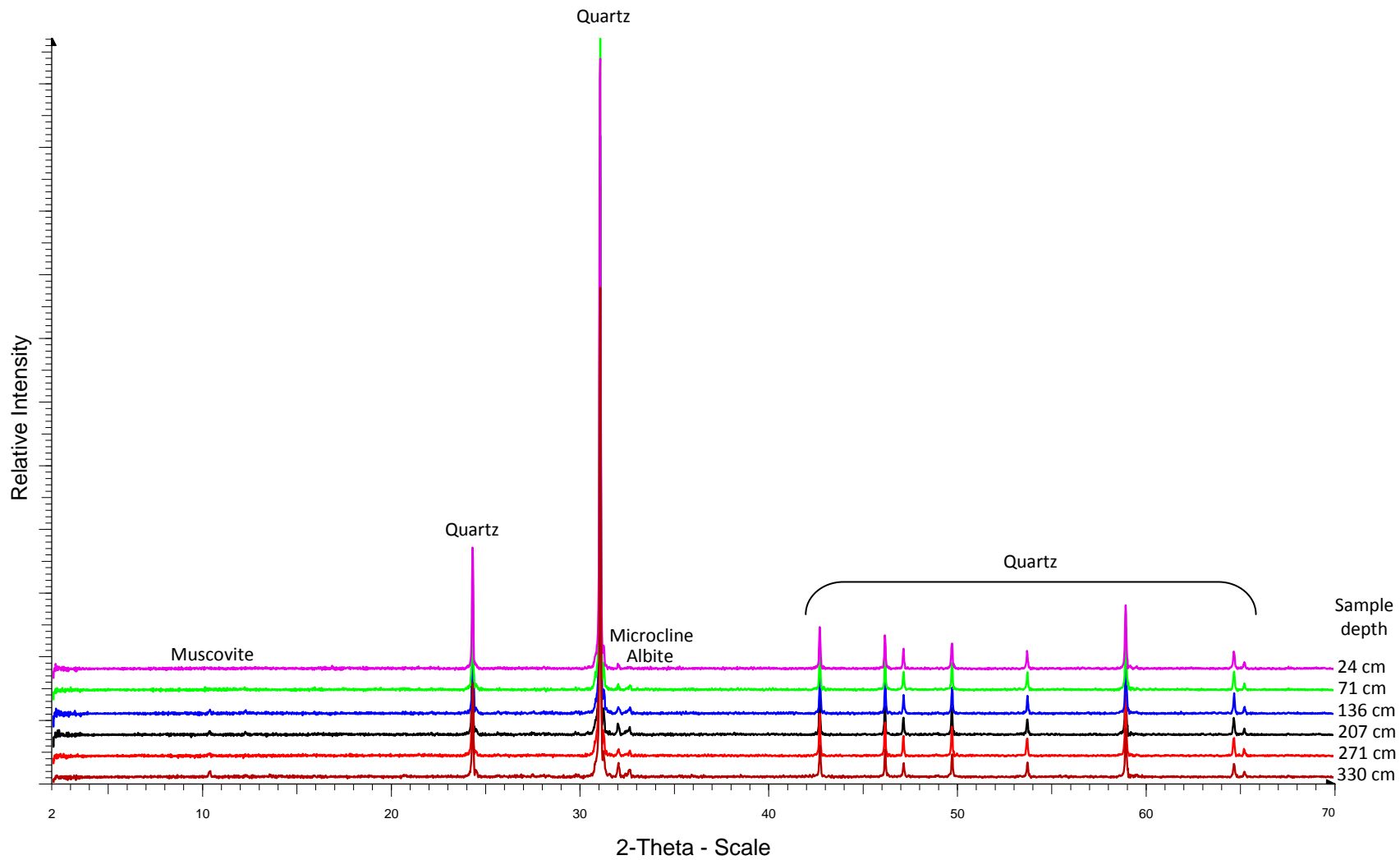


Fig. A.9 Bulk XRD results for core GCF 0m

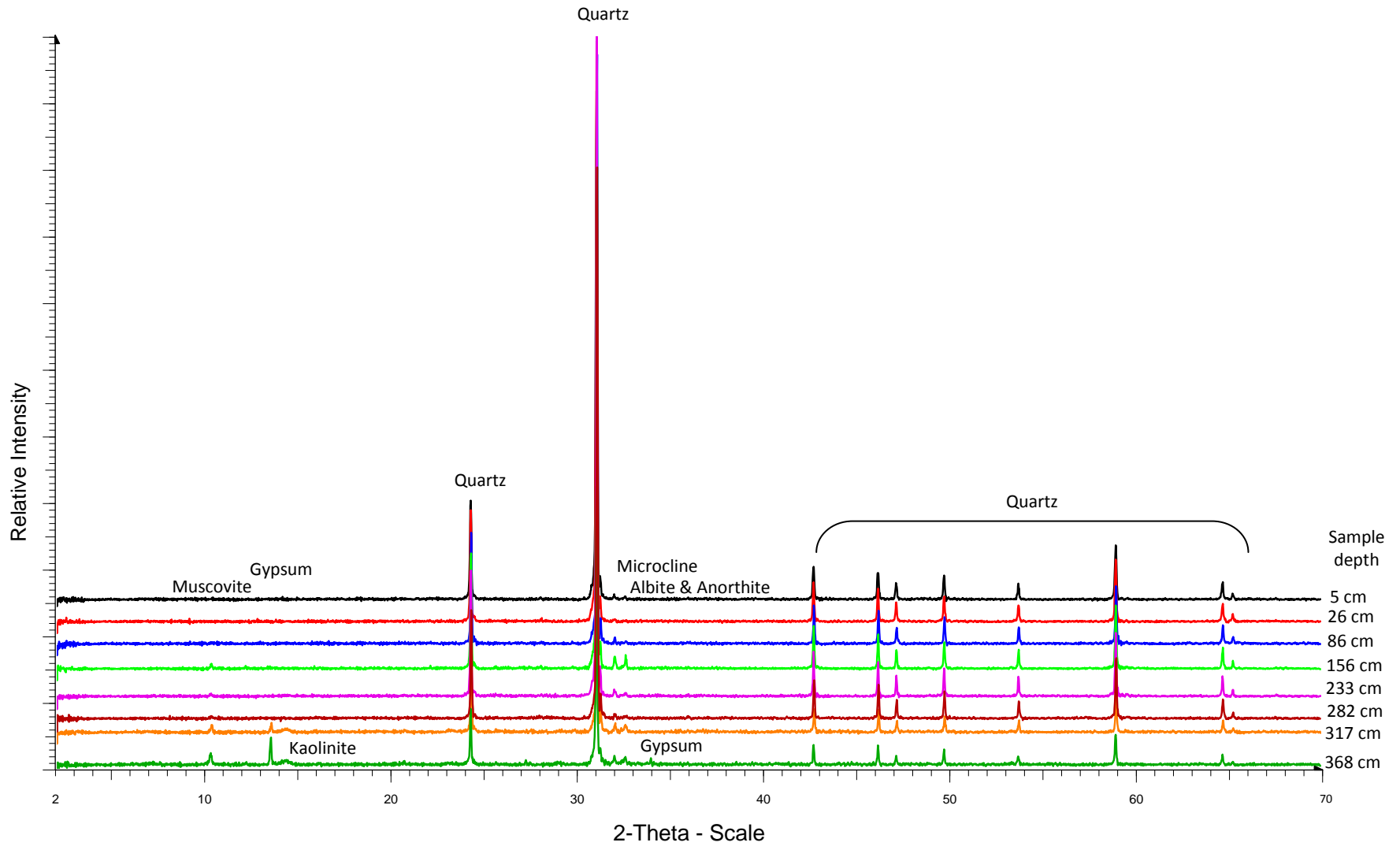
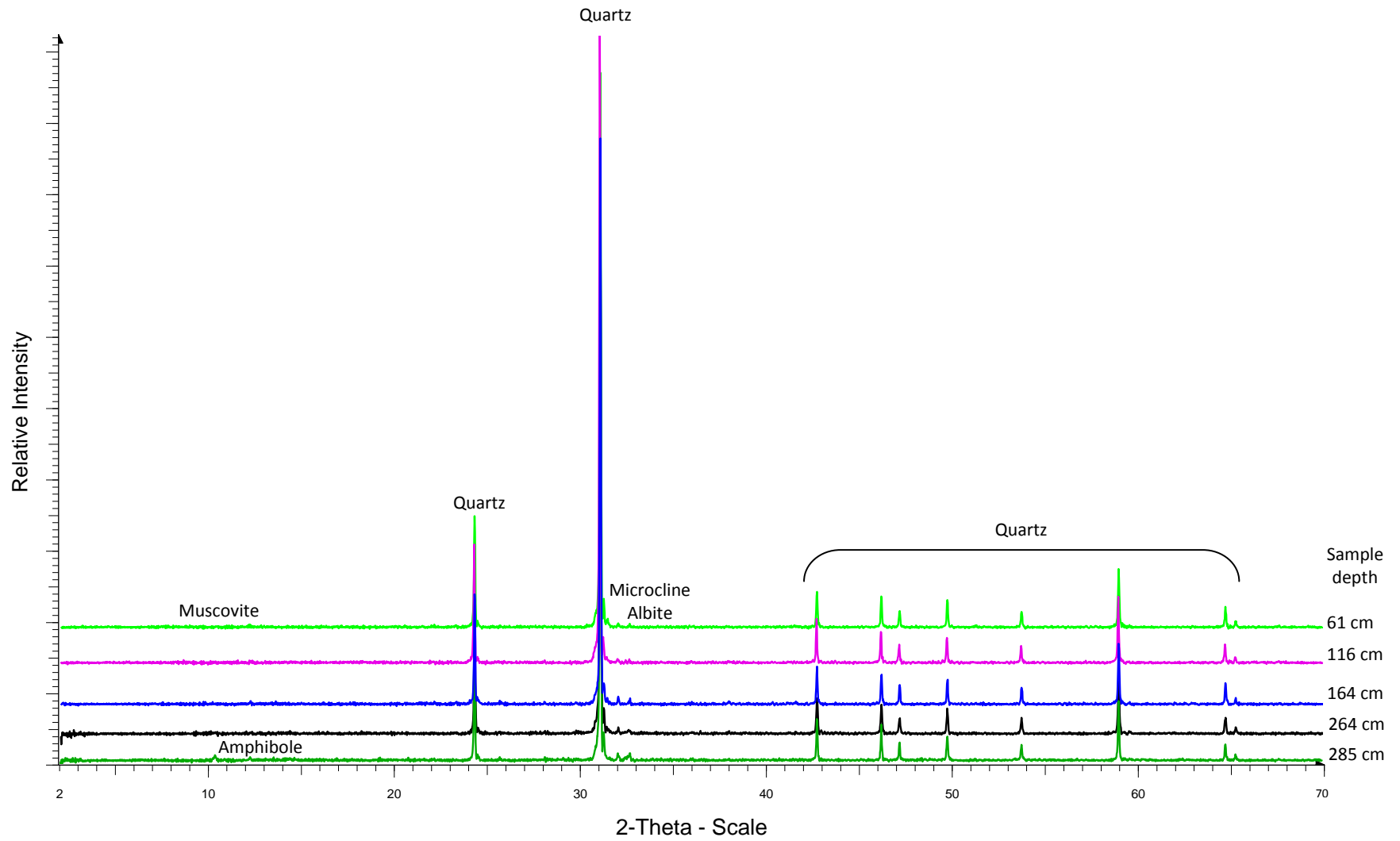
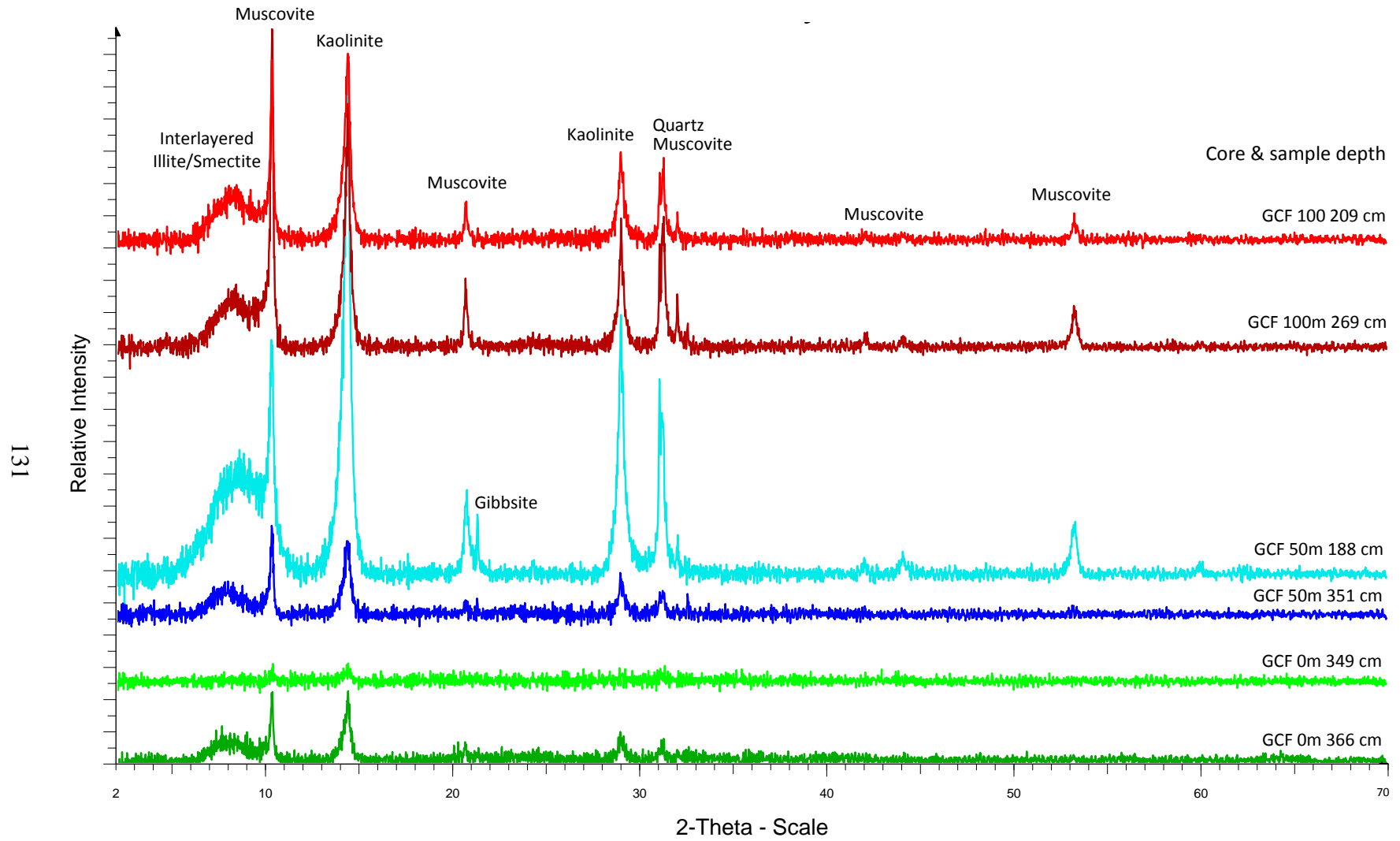


Fig. A.10 Bulk XRD results for core GCF 50m



**Fig. A.11** Bulk XRD results for core GCF 100m



**Fig. A.12** Clay fraction XRD results for all GCF cores

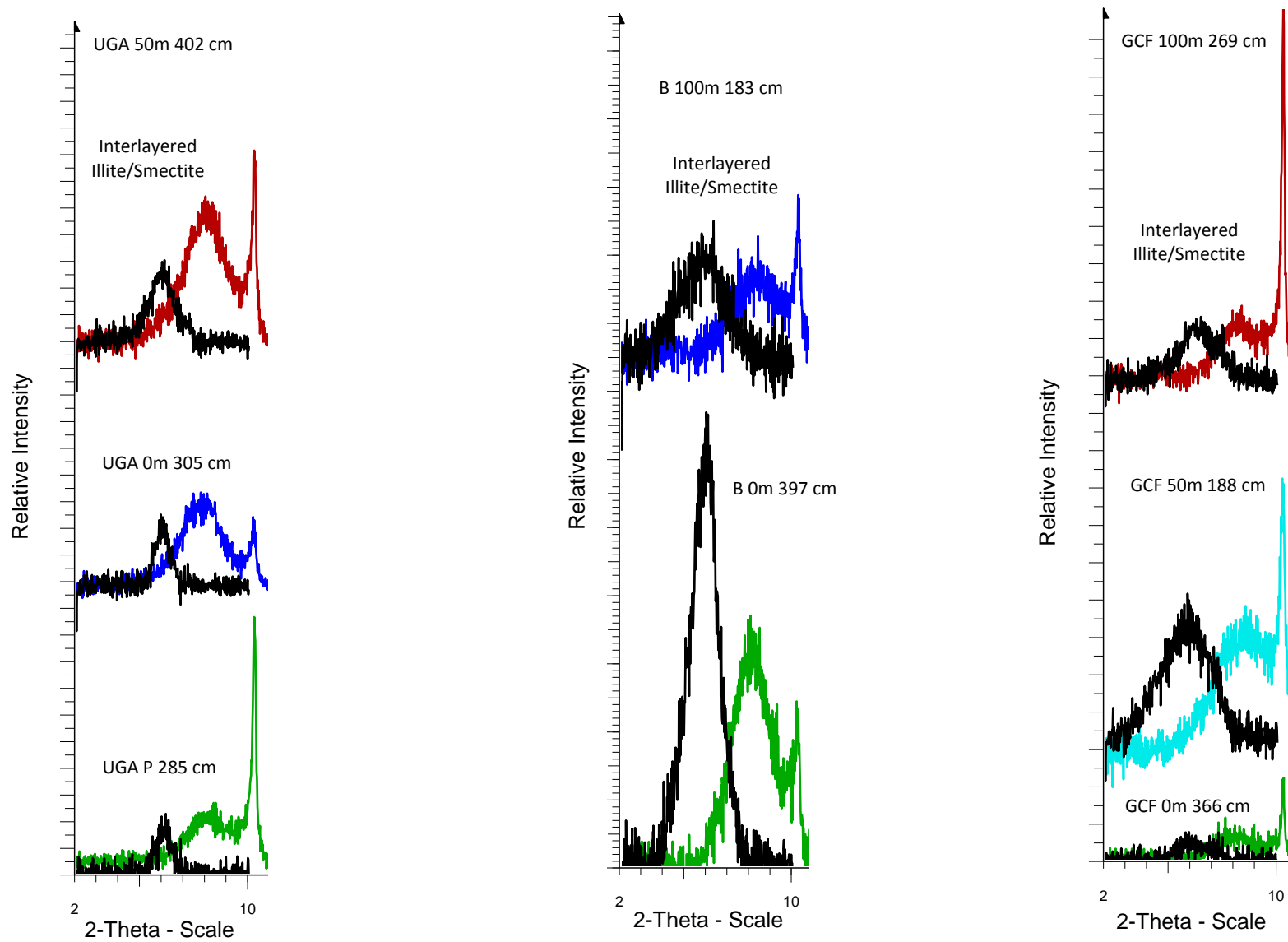


**Fig. A.13** Select ethylene glycol-solvated clay fraction XRD results; the black diffractograms collected from 2 to 10  $2\theta$  represent each ethylene glycol-solvated sample. One diffractogram from each core is presented here to provide a representative sample of the data.

## Appendix B

### Grain Size Percents and Statistical Data

**Table B.1** Core UGA P Grain Size Percents and Statistical Data

Depth	Percent coarse sand	Percent medium sand	Percent fine sand	Percent very fine sand	Percent silt & clay	Percent silt	Percent clay	Mean (µm)	Sorting	Skewness	Kurtosis
2.11	2.12	12.31	72.35	11.17	2.06	-	-	179.6	1.498	0.037	1.410
8.46	2.41	18.58	67.14	9.18	2.69	-	-	197.3	1.572	0.137	1.319
26.43	1.37	13.41	76.17	6.58	2.48	-	-	183.5	1.434	0.094	1.277
52.85	1.14	13.58	76.27	6.51	2.50	-	-	183.5	1.430	0.094	1.265
63.42	2.24	20.60	68.43	6.43	2.30	-	-	203.3	1.541	0.194	1.211
85.56	1.25	10.45	75.42	9.04	3.85	-	-	179.0	1.452	0.038	1.364
100.67	1.22	11.06	75.24	8.76	3.72	-	-	179.7	1.453	0.043	1.358
106.63	1.75	19.20	69.50	6.57	2.98	-	-	199.1	1.522	0.178	1.231
121.76	0.51	14.22	77.99	6.37	0.90	-	-	183.5	1.419	0.095	1.230
142.48	2.38	19.70	69.81	6.34	1.78	-	-	201.7	1.531	0.199	1.220
156.39	1.66	33.05	59.81	3.38	2.10	-	-	225.0	1.544	0.202	0.804
161.80	1.86	22.39	71.24	3.20	1.32	-	-	207.9	1.494	0.269	1.088
182.28	1.30	21.00	73.70	2.63	1.37	-	-	204.1	1.469	0.263	1.100
192.89	1.27	16.45	75.80	5.06	1.41	-	-	191.4	1.431	0.210	1.136
206.79	1.77	6.90	79.38	9.65	2.30	-	-	176.0	1.432	0.018	1.356
233.65	0.00	3.65	57.93	12.37	26.05	6.84	19.21	35.45	12.79	-0.856	2.263
244.35	0.05	3.53	39.50	7.72	49.20	21.8	27.4	16.42	19.53	-0.688	0.858
254.22	0.53	5.18	64.23	19.79	10.27	6.29	3.35	139.7	2.225	-0.491	2.250
274.80	0.00	10.32	76.40	8.63	4.65	4.65	0	174.4	1.511	-0.080	1.543
284.67	1.28	8.81	36.34	4.12	49.45	13.69	35.76	13.06	27.24	-0.666	0.700
295.37	0.82	7.67	45.49	5.55	40.47	11.91	28.56	20.31	22.01	-0.821	0.828
300.31	2.52	11.96	61.25	8.07	16.20	2.5	13.69	127.9	5.371	-0.644	6.155
315.95	2.66	13.02	63.90	8.81	11.62	2.36	9.26	156.1	4.018	-0.517	5.647
334.05	2.15	11.82	64.65	11.58	9.80	0.47	9.33	155.8	3.963	-0.509	5.700

**Table B.2** Core UGA 0m Grain Size Percents and Statistical Data

Depth	Percent coarse sand	Percent medium sand	Percent fine sand	Percent very fine sand	Percent silt & clay	Percent silt	Percent clay	Mean (µm)	Sorting	Skewness	Kurtosis
9.02	1.93	10.83	73.22	9.24	4.77	-	-	179.7	1.471	0.048	1.398
22.55	2.08	15.53	71.14	6.60	4.65	-	-	191.7	1.491	0.152	1.285
32.47	1.82	16.46	72.00	2.41	7.31	-	-	198.1	1.446	0.256	1.145
36.98	1.65	19.93	69.99	4.92	3.51	-	-	202.0	1.486	0.252	1.106
45.10	2.78	20.96	67.79	5.36	3.11	-	-	206.8	1.530	0.243	1.145
67.65	2.57	15.60	72.92	6.29	2.62	-	-	192.8	1.489	0.175	1.274
83.89	2.70	15.57	74.87	5.07	1.79	-	-	193.6	1.456	0.236	1.180
90.20	2.91	17.57	72.87	4.60	2.05	-	-	200.0	1.480	0.271	1.148
102.10	2.21	13.62	69.45	12.44	2.28	-	-	180.3	1.522	0.038	1.400
112.00	2.64	15.19	73.26	6.92	1.99	-	-	191.0	1.494	0.152	1.311
118.60	3.06	19.05	69.55	6.26	2.07	-	-	202.5	1.539	0.211	1.234
129.60	2.96	12.26	71.36	11.33	2.09	-	-	180.1	1.513	0.047	1.436
139.50	3.28	32.25	59.35	3.92	1.19	-	-	226.8	1.564	0.211	0.803
170.00	3.14	22.90	68.41	3.97	1.58	-	-	211.8	1.525	0.278	1.028
194.50	1.22	10.35	81.15	5.28	2.00	-	-	181.6	1.381	0.144	1.164
212.30	0.15	0.18	3.64	1.85	94.18	52.78	41.4	2.831	15.47	-0.381	0.826
217.92	0.00	0.00	2.47	0.38	97.15	43.96	52.95	1.661	15.64	-0.253	0.727
241.35	0.00	0.16	2.25	2.85	94.74	30.42	64.32	1.024	17.03	-0.002	0.740
264.77	0.00	0.00	4.85	4.49	90.66	45.84	43.25	2.759	17.66	-0.318	0.809
288.20	0.00	0.00	4.30	0.00	95.70	34.42	61.28	1.148	16.52	-0.064	0.725
305.06	0.00	0.00	1.15	0.87	97.98	41.86	56.12	1.405	15.56	-0.187	0.72

**Table B.3** Core UGA 50m Grain Size Percents and Statistical Data

Depth	Percent coarse sand	Percent medium sand	Percent fine sand	Percent very fine sand	Percent silt & clay	Percent silt	Percent clay	Mean (µm)	Sorting	Skewness	Kurtosis
6.68	1.16	9.09	76.84	10.77	2.15	-	-	176.4	1.453	0.013	1.370
15.74	1.90	12.25	69.83	12.71	3.31	-	-	178.0	1.510	0.027	1.405
20.03	0.00	6.53	78.59	11.12	3.76	-	-	173.2	1.399	-0.066	1.221
23.85	0.96	6.71	76.14	11.37	4.82	-	-	173.8	1.431	-0.023	1.317
33.39	0.90	8.46	80.25	7.09	3.30	-	-	178.5	1.400	0.052	1.258
47.70	0.63	7.37	79.04	9.17	3.80	-	-	175.9	1.410	-0.006	1.281
63.92	0.22	12.89	79.24	6.08	1.56	-	-	182.3	1.402	0.098	1.203
71.55	1.17	11.26	79.27	6.35	1.94	-	-	181.5	1.411	0.097	1.255
95.40	1.29	11.34	79.45	7.33	0.59	-	-	180.9	1.429	0.073	1.306
118.89	0.00	7.39	81.64	10.97	0.00	-	-	174.1	1.405	-0.046	1.246
119.88	0.73	8.72	79.85	9.81	0.90	-	-	176.5	1.429	0.008	1.324
130.80	1.09	15.39	73.00	9.66	0.85	-	-	183.9	1.491	0.056	1.346
144.71	1.18	6.58	77.20	14.13	0.91	-	-	171.8	1.446	-0.032	1.321
169.53	1.95	7.52	82.40	7.44	0.70	-	-	178.3	1.411	0.064	1.311
192.22	3.29	4.23	74.22	15.65	2.62	-	-	170.1	1.488	0.010	1.441
219.46	0.74	7.54	86.55	4.60	0.57	-	-	179.4	1.331	0.140	1.024
244.80	0.68	2.21	80.81	15.09	1.21	-	-	167.8	1.372	-0.164	1.099
269.55	0.87	2.13	80.12	16.14	0.75	-	-	166.5	1.381	-0.172	1.098
293.42	0.65	2.62	79.93	15.72	1.07	-	-	167.5	1.377	-0.164	1.097
303.88	0.60	1.98	83.20	13.18	1.04	-	-	169.1	1.359	-0.163	1.095
310.54	1.02	5.06	80.89	11.99	1.04	-	-	172.4	1.396	-0.079	1.209
316.61	0.78	2.88	79.94	14.84	1.57	-	-	168.4	1.374	-0.163	1.095
337.88	0.75	2.94	76.36	17.98	1.97	-	-	162.0	1.415	-0.210	1.087
359.16	0.00	0.91	50.82	43.14	5.12	4.72	0.00	125.3	1.566	-0.072	0.740
365.96	1.13	9.86	9.90	19.80	59.31	24.91	32.19	9.384	24.22	-0.432	0.827
380.43	0.50	0.40	13.98	75.23	9.89	3.74	1.93	92.54	1.533	-0.065	-0.663
388.94	0.52	2.84	25.12	34.18	37.35	20.04	14.59	40.52	8.574	-0.663	1.487

<b>Depth</b>	<b>Percent coarse sand</b>	<b>Percent medium sand</b>	<b>Percent fine sand</b>	<b>Percent very fine sand</b>	<b>Percent silt &amp; clay</b>	<b>Percent silt</b>	<b>Percent clay</b>	<b>Mean (µm)</b>	<b>Sorting</b>	<b>Skewness</b>	<b>Kurtosis</b>
393.20	0.04	0.07	0.40	0.05	99.44	40.75	55.96	1.285	15.16	-0.169	0.717
401.71	0.22	0.22	0.41	0.30	98.85	46.99	51.73	1.737	15.04	-0.302	0.730
422.98	0.23	0.32	2.19	1.12	96.14	45.27	48.36	2.031	15.65	-0.333	0.739

(Table B.3 Core UGA 50m Grain Size Percents and Statistical Data, continued)

**Table B.4** Core B 0m Grain Size Percents and Statistical Data

Depth	Percent coarse sand	Percent medium sand	Percent fine sand	Percent very fine sand	Percent silt & clay	Percent silt	Percent clay	Mean (µm)	Sorting	Skewness	Kurtosis
1.95	3.59	6.07	54.99	25.45	9.89	-	-	151.8	1.669	-0.024	1.241
10.73	2.41	6.33	57.60	21.83	11.82	-	-	155.4	1.612	-0.061	1.324
24.38	2.55	6.99	55.91	25.41	9.14	-	-	152.0	1.643	-0.049	1.191
35.10	3.21	11.06	57.66	26.07	2.00	-	-	156.7	1.675	-0.031	1.231
48.75	2.23	5.52	58.49	30.06	3.70	-	-	146.8	1.620	-0.068	1.055
58.50	2.95	10.65	64.25	20.03	2.12	-	-	165.0	1.607	-0.029	1.380
73.13	3.84	9.51	52.15	28.83	5.68	-	-	152.0	1.710	-0.003	1.139
86.21	3.25	9.83	64.16	21.22	1.54	-	-	162.7	1.619	-0.032	1.383
96.24	3.74	8.13	62.61	20.92	4.60	-	-	161.4	1.628	-0.025	1.418
109.92	2.08	3.07	49.74	42.56	2.54	-	-	133.6	1.571	-0.038	0.777
119.04	1.49	3.20	48.27	40.53	6.50	-	-	133.7	1.556	-0.067	0.747
130.90	2.13	4.34	51.88	38.01	3.64	-	-	138.2	1.617	-0.026	0.899
141.84	1.40	3.70	51.84	33.80	9.26	-	-	139.6	1.569	-0.107	0.835
164.82	1.56	7.12	60.65	28.95	1.71	-	-	149.2	1.613	-0.078	1.085
173.40	3.77	5.74	48.10	39.57	2.82	-	-	139.1	1.710	0.072	1.021
188.67	1.62	6.44	62.67	26.77	2.51	-	-	151.0	1.593	-0.094	1.140
197.25	2.45	3.32	45.16	46.65	2.42	-	-	130.1	1.609	0.077	0.833
212.52	1.88	2.28	39.55	49.96	6.34	-	-	124.2	1.558	0.113	0.743
223.01	3.48	4.15	48.89	36.61	6.88	-	-	139.3	1.682	0.037	1.017
236.37	14.52	16.47	45.15	20.00	3.85	-	-	214.7	2.088	0.208	1.052
263.16	2.87	3.27	34.43	52.55	6.87	-	-	122.8	1.647	0.256	0.917
287.69	4.25	3.72	35.97	48.22	7.85	-	-	127.4	1.739	0.267	1.044
309.56	3.24	3.78	39.18	45.36	8.44	-	-	129.3	1.685	0.184	0.958
318.31	1.75	1.63	17.78	65.87	12.98	2.87	8.20	98.52	3.311	-0.266	5.220
331.44	1.95	0.86	21.18	68.34	7.66	6.89	0.00	102.8	1.701	0.029	1.720
346.31	1.78	2.49	33.93	49.42	12.38	10.28	0.00	113.1	2.005	-0.137	1.505

<b>Depth</b>	<b>Percent coarse sand</b>	<b>Percent medium sand</b>	<b>Percent fine sand</b>	<b>Percent very fine sand</b>	<b>Percent silt &amp; clay</b>	<b>Percent silt</b>	<b>Percent clay</b>	<b>Mean (μm)</b>	<b>Sorting</b>	<b>Skewness</b>	<b>Kurtosis</b>
353.31	0.61	1.66	12.40	51.30	34.03	6.28	18.20	22.94	11.77	-0.796	2.482
375.19	2.63	0.04	1.56	9.64	86.13	58.77	20.32	8.605	9.989	-0.381	1.497
385.69	1.39	1.62	1.31	11.82	83.86	39.18	31.93	4.429	17.67	-0.363	0.827
397.06	2.12	0.18	3.19	13.15	81.36	42.62	33.85	4.716	17.94	-0.357	0.850

(Table B.4 Core B 0m Grain Size Percents and Statistical Data, continued)

**Table B.5** Core B 100m Grain Size Percents and Statistical Data

Depth	Percent coarse sand	Percent medium sand	Percent fine sand	Percent very fine sand	Percent silt & clay	Percent silt	Percent clay	Mean (μm)	Sorting	Skewness	Kurtosis
4.35	2.56	13.00	67.76	12.72	3.96	-	-	179.9	1.531	0.041	1.413
21.75	0.74	10.02	71.52	12.86	4.85	-	-	175.0	1.477	0.001	1.369
26.97	2.17	15.94	71.74	8.22	1.93	-	-	190.6	1.515	0.122	1.336
43.50	1.47	6.62	69.90	18.71	3.29	-	-	162.9	1.519	-0.079	1.318
65.25	1.14	8.07	71.77	16.57	2.45	-	-	168.9	1.495	-0.036	1.347
87.00	0.84	7.93	71.60	15.85	3.78	-	-	170.0	1.480	-0.032	1.334
94.68	1.53	5.83	59.75	29.94	2.96	-	-	146.9	1.599	-0.092	1.023
108.33	3.98	11.47	58.29	24.54	1.72	-	-	159.8	1.680	-0.023	1.317
129.65	4.13	20.07	64.38	9.40	2.02	-	-	204.8	1.625	0.163	1.311
147.73	1.94	8.46	73.67	13.88	2.05	-	-	173.9	1.488	0.013	1.412
165.91	0.00	2.45	67.92	15.12	14.51	7.84	6.67	131.2	3.145	-0.622	3.428
175.91	0.00	0.94	62.46	11.82	24.77	13.36	10.88	69.98	6.366	-0.805	2.800
183.18	0.06	2.43	54.97	9.55	32.99	12.56	20.43	31.40	13.86	-0.853	1.235

**Table B.6** Core GCF 0m Grain Size Percents and Statistical Data

Depth	Percent coarse sand	Percent medium sand	Percent fine sand	Percent very fine sand	Percent silt & clay	Percent silt	Percent clay	Mean (µm)	Sorting	Skewness	Kurtosis
14.15	1.42	6.65	70.82	16.94	4.17	-	-	166.5	1.496	0.056	1.334
23.58	0.66	4.51	75.77	15.96	3.10	-	-	167.4	1.404	-0.147	1.128
36.78	0.52	6.83	78.16	11.91	2.58	-	-	173.2	1.421	-0.042	1.281
47.15	0.37	6.80	77.44	13.36	2.04	-	-	171.9	1.426	-0.054	1.270
59.41	1.54	4.28	69.68	21.21	3.29	-	-	156.9	1.499	-0.160	1.177
70.73	1.03	3.41	69.39	24.44	1.73	-	-	151.8	1.482	-0.238	1.032
94.30	0.86	2.63	62.13	31.47	2.91	-	-	142.9	1.517	-0.206	0.834
105.62	0.47	3.67	70.72	24.28	0.85	-	-	152.1	1.478	-0.240	1.038
112.87	0.85	7.50	64.68	25.83	1.15	-	-	152.7	1.578	-0.107	1.170
116.00	0.86	8.85	54.45	33.54	2.29	-	-	145.1	1.644	-0.041	0.981
135.58	2.21	6.90	53.41	35.88	1.60	-	-	142.6	1.659	-0.010	0.988
155.08	1.20	5.92	48.20	37.82	6.85	-	-	137.8	1.630	-0.002	0.896
173.17	1.32	5.89	54.07	38.49	0.23	-	-	139.3	1.617	-0.036	0.899
183.52	0.79	5.24	68.58	24.07	1.33	-	-	153.4	1.518	-0.170	1.136
194.20	1.17	9.77	70.34	14.98	3.74	-	-	173.3	1.496	0.003	1.376
206.80	0.33	2.54	51.66	44.75	0.71	-	-	131.1	1.542	-0.058	0.742
209.48	1.87	5.75	54.26	35.45	2.67	-	-	141.7	1.630	-0.037	0.954
216.90	1.36	3.44	44.37	47.99	2.84	-	-	133.8	1.578	-0.029	0.791
221.36	2.02	5.51	44.17	40.98	7.31	-	-	134.8	1.659	0.071	0.915
228.03	3.13	12.58	50.53	30.68	3.07	-	-	153.2	1.723	0.002	1.063
249.22	7.15	31.63	41.14	16.71	3.37	-	-	219.2	1.881	0.049	0.968
270.78	16.16	37.74	30.55	14.23	1.32	-	-	261.5	1.999	-0.071	0.956
281.92	4.45	13.01	44.19	33.20	5.16	-	-	156.1	1.810	0.085	1.015
292.21	3.31	13.25	47.35	30.91	5.18	-	-	155.7	1.760	0.036	1.036
296.49	2.57	22.12	46.20	27.94	1.18	-	-	174.2	1.825	0.039	0.996
308.38	3.39	12.97	48.19	31.63	3.81	-	-	154.2	1.752	0.031	1.038

<b>Depth</b>	<b>Percent coarse sand</b>	<b>Percent medium sand</b>	<b>Percent fine sand</b>	<b>Percent very fine sand</b>	<b>Percent silt &amp; clay</b>	<b>Percent silt</b>	<b>Percent clay</b>	<b>Mean (μm)</b>	<b>Sorting</b>	<b>Skewness</b>	<b>Kurtosis</b>
312.06	5.25	15.57	43.91	31.37	3.89	-	-	165.9	1.874	0.107	1.034
319.41	2.73	15.46	55.97	25.03	0.81	-	-	166.0	1.716	0.005	1.218
330.43	0.00	1.58	31.00	61.80	5.62	5.62	0.00	109.7	1.615	0.101	1.033
338.52	0.00	1.44	20.10	71.13	7.32	6.91	0.41	99.75	1.659	0.003	1.738
348.61	2.44	6.59	35.21	51.24	4.53	0.67	3.35	123.3	1.720	0.248	0.933
365.86	0.00	2.38	36.15	52.76	8.72	6.27	2.45	112.8	2.028	-0.166	1.665

(Table B.6 Core GCF 0m Grain Size Percents and Statistical Data, continued)

**Table B.7** Core GCF 50m Grain Size Percents and Statistical Data

Depth	Percent coarse sand	Percent medium sand	Percent fine sand	Percent very fine sand	Percent silt & clay	Percent silt	Percent clay	Mean (µm)	Sorting	Skewness	Kurtosis
5.22	2.61	10.57	66.03	17.08	3.71	-	-	170.4	1.563	-0.006	1.406
8.34	2.35	11.40	68.24	16.96	1.04	-	-	172.0	1.551	0.000	1.398
17.73	1.44	11.79	69.41	15.71	1.64	-	-	174.6	1.518	0.013	1.379
26.08	1.67	10.98	68.26	16.60	2.49	-	-	171.5	1.535	-0.008	1.381
52.15	1.61	11.65	68.52	16.80	1.42	-	-	171.8	1.539	-0.008	1.375
78.23	1.35	11.93	72.15	14.04	0.52	-	-	176.1	1.503	0.015	1.388
85.53	1.10	11.35	67.67	18.97	0.92	-	-	166.4	1.559	-0.047	1.338
98.71	1.72	20.90	59.26	16.84	1.28	-	-	190.1	1.662	0.070	1.252
103.12	1.97	19.72	58.43	18.76	1.14	-	-	183.8	1.686	0.046	1.248
117.06	0.70	14.76	51.15	32.60	0.79	-	-	151.0	1.695	-0.019	0.992
135.41	6.07	10.38	52.63	25.33	5.60	-	-	162.9	1.791	0.064	1.332
156.34	1.04	4.63	50.92	40.22	3.19	-	-	135.8	1.585	-0.046	0.815
179.26	1.38	17.66	65.63	13.97	1.37	-	-	187.3	1.579	0.075	1.330
182.93	1.60	12.25	69.66	15.63	0.86	-	-	175.2	1.522	0.016	1.383
188.43	0.86	0.12	24.74	14.54	59.74	23.65	34.71	8.145	23.08	-0.456	0.719
196.69	0.00	0.00	55.65	32.73	11.62	5.08	6.55	123.8	3.024	-0.509	2.869
201.92	0.81	12.35	66.11	16.10	4.62	0.87	3.35	162.5	1.626	-0.116	1.417
211.34	0.31	13.17	65.26	10.72	10.54	3.54	6.69	155.5	3.239	-0.499	4.744
215.62	0.00	8.41	59.52	19.18	12.89	5.57	0.00	148.4	1.768	-0.274	1.530
223.32	1.01	6.35	53.96	29.75	8.93	4.98	3.34	134.6	2.238	-0.374	1.861
233.17	0.50	1.38	70.35	17.91	9.87	7.57	2.11	139.5	2.044	-0.521	2.221
238.73	0.82	0.32	69.25	19.84	9.77	6.11	3.07	138.1	2.102	-0.524	2.226
244.72	0.57	1.91	51.51	17.10	28.90	18.39	8.71	67.98	5.759	-0.758	1.880
261.00	1.07	0.82	64.17	19.30	14.64	11.52	0.34	132.7	2.085	-0.520	1.792
265.12	0.08	11.15	67.54	8.28	12.96	6.44	5.51	151.8	2.811	-0.506	4.161
282.27	0.00	12.63	69.58	11.35	6.43	6.43	0.00	167.2	1.747	-0.231	1.988

<b>Depth</b>	<b>Percent coarse sand</b>	<b>Percent medium sand</b>	<b>Percent fine sand</b>	<b>Percent very fine sand</b>	<b>Percent silt &amp; clay</b>	<b>Percent silt</b>	<b>Percent clay</b>	<b>Mean (μm)</b>	<b>Sorting</b>	<b>Skewness</b>	<b>Kurtosis</b>
299.42	2.06	4.78	50.73	12.84	29.59	12.91	13.00	59.18	8.372	-0.768	2.189
302.16	0.39	6.03	43.68	14.04	35.85	19.25	12.93	53.83	8.503	-0.753	1.461
316.57	0.78	4.89	53.41	6.70	34.22	16.62	15.35	50.44	9.573	-0.811	1.426
333.72	0.15	5.99	46.84	11.35	35.67	22.21	11.06	58.42	7.538	-0.756	1.411
338.52	0.55	2.07	10.33	10.33	76.73	35.35	35.28	5.132	21.79	-0.306	0.791
350.87	1.04	0.74	1.34	15.32	81.56	42.29	33.32	4.706	17.16	-0.380	0.831
357.04	0.35	4.94	26.41	13.74	54.56	27.16	22.93	17.20	16.93	-0.581	1.027
368.02	1.60	4.08	17.63	10.64	66.05	31.60	30.08	8.715	22.02	-0.374	0.822

(Table B.7 Core GCF 50m Grain Size Percents and Statistical Data, continued)

**Table B.8** Core GCF 100m Grain Size Percents and Statistical Data

Depth	Percent coarse sand	Percent medium sand	Percent fine sand	Percent very fine sand	Percent silt & clay	Percent silt	Percent clay	Mean (µm)	Sorting	Skewness	Kurtosis
2.44	4.60	13.52	62.55	16.11	3.22	-	-	184.0	1.640	0.099	1.417
11.37	1.82	9.65	71.21	15.93	1.39	-	-	172.7	1.510	0.008	1.397
20.30	1.20	9.16	71.02	16.27	2.35	-	-	170.6	1.503	-0.018	1.365
28.42	1.10	8.43	67.75	19.41	3.33	-	-	162.6	1.544	-0.073	1.321
40.60	1.08	8.12	68.34	19.44	3.01	-	-	159.3	1.498	-0.137	1.218
60.90	1.01	7.52	69.85	18.82	2.80	-	-	163.2	1.520	-0.080	1.308
81.20	1.15	7.42	70.99	16.63	3.81	-	-	167.8	1.494	-0.047	1.337
93.62	1.23	8.09	67.93	20.49	2.26	-	-	160.8	1.552	-0.080	1.311
96.23	1.09	7.80	67.29	21.05	2.77	-	-	159.4	1.553	-0.090	1.291
99.50	1.68	8.23	67.30	17.62	5.17	-	-	166.0	1.538	-0.043	1.367
115.85	1.97	10.14	66.64	19.56	1.69	-	-	164.8	1.576	-0.043	1.361
132.20	3.40	22.81	62.13	9.82	1.84	-	-	207.2	1.635	0.143	1.190
148.55	5.22	18.65	66.52	8.13	1.48	-	-	206.3	1.625	0.206	1.354
163.58	3.65	21.07	65.79	8.64	0.85	-	-	205.5	1.608	0.167	1.283
169.59	3.76	23.48	63.84	8.20	0.72	-	-	210.4	1.619	0.168	1.137
177.32	4.25	17.59	66.01	10.30	1.85	-	-	199.3	1.616	1.155	1.367
186.77	2.14	18.22	70.07	7.90	1.66	-	-	196.4	1.539	0.149	1.297
190.21	1.49	21.73	67.85	7.49	1.44	-	-	202.2	1.553	0.158	1.230
198.80	0.00	2.26	57.42	13.56	26.76	12.39	13.22	59.42	7.729	-0.813	2.462
217.64	0.21	9.26	66.41	9.52	14.60	13.86	0.74	138.6	2.349	-0.498	2.859
227.09	0.00	6.81	56.84	16.47	19.88	9.38	9.14	97.72	4.932	-0.704	3.214
227.88	0.00	6.45	68.76	10.77	14.02	7.10	6.92	137.8	3.300	-0.604	4.856
246.01	1.02	6.10	61.34	16.76	14.78	8.25	6.48	132.2	3.256	-0.561	3.122
250.73	0.04	1.61	44.18	12.26	41.91	20.41	21.08	26.30	14.31	-0.772	1.084
266.49	0.94	7.51	61.01	9.03	21.50	15.05	6.20	94.69	4.151	-0.690	2.539